An Ecosystem Model with Evolutionary Adaptive Trophic Structure

Philip J. Underwood

Doctorate of Philosophy
The School of Environmental Sciences
University of East Anglia

September 2013

"The physical laws governing evolution in all probability take on a simpler form when referred to the system as a whole than to any portion thereof. It is not so much the organism or the species that evolves, but the entire system, species and environment. The two are inseparable."

– *Alfred James Lotka, February 1925.*

Abstract

We live in an era of rapid change in ecosystems and their environments, that all scales up to the global. The contemporary view is that the interactions between life and the environment are bidirectional: the environment creates life and life creates the environment. However, most ecosystem models have an inbuilt rigidity such that the degrees to which they can mimic structural change in response to environmental cues is very limited. In an effort to capture the plasticity of life we present a new theoretical individual-based ecosystem model in the context of previous classical and experimental modelling approaches. The aim is to develop a deeper understanding of the factors determining trophic structure. The individual-based approach permits the inclusion of traits to model heritable attributes. Population-level models implement a mean-field approximation that led to the competitive exclusion principle. The addition of a trait to define specific feeding strategy permits the model exploration of this problem. Life history theory predicts that reduced juvenile mortality selects for delayed maturity and decreased reproductive effort, and reduced adult mortality will select for the opposite. Through the inclusion of a different trait to represent relative parental investment in offspring, we explore the predictions of life history theory and hypotheses for clutch size.

Contents

1 Introduction

In the 1920s, the predator-prey equations attributed to Alfred Lotka and Vito Volterra represented a major contribution to the emerging field of biomathematics (Israel, 1988). The biomathematical approach treats biology as a deterministic phenomenon in order that it can be described using classical mechanics (Israel, 1988). This is apparent when it is considered that the form of the Lotka-Volterra equations originate in work describing periodic chemical reactions (Lotka, 1910, 1920a,b). Volterra (1926b; 1926a) appropriated the work and applied the mathematical pattern to population interactions. Lotka (1925) doubted Newtonian dynamics in its potential to describe complex processes, suggesting that some of the missing detail could be essential to the result. In the absence of a better tool, the course of scientific development illustrates that Volterra's mechanistic view of biology was adopted (Israel, 1988).

1.1 Deterministic Approaches

1.1.1 Riley

During the 1940s, Gordon A. Riley and colleagues collected data on factors that affected the phytoplankton population on Georges Bank; an area of shallow ocean between the United States of America and Canada (Riley, 1941a,b, 1942, 1943). Using the data Riley and Bumpus (1946) defined a set of explicitly simple assumptions in order to permit the mathematical derivation of relationships between observed quantities. This led to a differential equation describing the rate of change of the phytoplankton as a function of the physical environment, and the zooplankton that graze on them. In the absence of a computer, results were integrated by hand and were found to correlate with the data.

Riley and Bumpus (1946) highlighted some limitations of the work. The model assumed zooplankton feed at a constant rate, despite the presence of different feeding strategies. Earlier studies had also shown a non-linear relationship between temperature and zooplankton metabolic rate, implying a correlating non-linear change to the rate of feeding. In later work, other seasonal cycles were examined with the model (Riley, 1963). It was found to depict the general trend of the regional differences in phytoplankton abundance across seasons,

and years, in the case of one data set.

Riley's (1963) work represented a method for marine ecosystem modelling, but he called for more development to be done. The assemblage of species into broad categories required that physiological trait values were framed in average terms. Riley (1963) was concerned that critical species detail may be lost in the process of species aggregation. He (Riley, 1963) considered the alternative of explicitly representing species to be "impossibly laborious", and would likely introduce unsolvable theoretical problems. It was also pointed out that progress towards models that explicitly represent physiological detail was restricted by lack of data.

1.1.2 NPZD-type

Starting with rigorous theoretical analysis of ecosystems in general, John H. Steele (1974) discussed what he considered the most important marine ecosystem components. The vertical mixing of the water brings nutrients to, and takes phytoplankton away from the euphotic zone. The nutrient cycle in the upper mixed layer balances supply from mixing and production from zooplankton waste. Grazing by herbivorous zooplankton was considered the main factor behind reduction of the phytoplankton. This implied the importance of the determinants of the zooplankton population. Using data from the North Sea, Steele (1974) aggregated the ecosystem components into just three groups; nutrient, phytoplankton and zooplankton. He produced a set of coupled differential equations to describe their dynamics. The premise for the work was to start with the most simple description, to discover if it were necessary to introduce more complex ecosystem processes.

Following earlier work, Steele (1974) made some idealised assumptions between the components of the model. The thermocline depth was fixed, and there was a constant rate of mixing between the upper and lower layers. A constant stoichiometric ratio permitted the elemental content of living matter to be derived from the amount of any element. The zooplankton were assumed to be ammonotelic, so that excreted nitrogen was immediately available to the phytoplankton. Like Riley (1946), Steele (1974) included a single zooplankton type, but based it on data regarding the life cycle of *Calanus* copepods. Unlike Riley (1946) however, Steele (1974) used a variable feeding rate. This was implemented using a Holling (1965) type 2 functional response, ensuring the

consumption rate correlated to changes in the zooplankton and phytoplankton populations (Steele, 1974). There was no explicit representation of carnivorous heterotrophs. Instead Steele (1974) applied a constant rate of grazing on the zooplankton to close what was acknowledged to be an open system.

Steele (1974) explained his reservations with the approach. The decision to interact a single phytoplankton, and a single herbivorous zooplankton type was considered the fundamental defect of the model. He also highlighted the importance of developing an understanding of the complexities of the ocean system. His practical concern was with the fraction of photosynthetically produced energy that goes through us. Steele (1974) called for more data to further refine his approach. The model provided proof of concept for extension to a more realistic food web. It became known as a nutrient-phytoplankton-zooplankton or NPZ (NPZD-type) model.

Nitrogen was regarded the main limiting factor on primary production (Fasham et al., 1990). Earlier work had shown the importance of vertical mixing of the water, and grazing by herbivorous zooplankton in determining the nature of the phytoplankton spring bloom (Eppley and Peterson, 1979). This is because phytoplankton are able to assimilate nitrogen brought into the system as a result of vertical mixing and in the various forms produced within the system as waste products of various metabolisms. Eppley and Peterson (1979) termed the ratio between these as the f ratio. Such that f would be the probability that consumed nitrogen came from outside the system, and $(1 - f)$ would be the probability that it was being recycled.

In an effort to describe the annual cycle at station "S" near Bermuda, (Fasham et al., 1990) extended the NPZD-type approach to include the dynamics of additional ecosystem processes. The aim of the work was to balance simplicity and complexity. The marine ecosystem was represented using seven state variables to characterise the natural system. These were phytoplankton, zooplankton, bacteria, nitrate, ammonium, dissolved organic nitrogen, and deteritus. The seperation of the inorganic, dissolved organic, and particulate organic forms of nitrogen permitted distinction between new and regenerated production.

Eppley and Peterson (1979) had discussed the rate that material sinks from the upper mixed layer. In the absence of any data for this, Fasham et al. (1990) assumed a constant rate. This permitted experimentation with different

parameter values. It was also assumed that the elemental content of biogenic material followed a constant Redfield ratio. Despite these limitations the model results reasonably matched observations at the study site, and it was suggested that more data could improve them. Critiquing the work, Fasham et al. (1990) pointed out that the model was still highly aggregated, and suggested that future models may be multi-elemental and differentiate organisms on the basis of size.

In order to more realistically include some missing physical processes, the nitrogen-based model was later coupled to a spatial general circulation model (Fasham et al., 1993; Sarmiento et al., 1993). The results were in broad agreement with the data, and supported the theory that cessation of vertical mixing initiates the spring bloom. However, this interpretation has since been questioned (Behrenfeld, 2010). One of the difficulties of the approach was distinguishing erroneous results that could be attributed to the ecosystem model from those that could be attributed to the physical model (Fasham et al., 1993). Overestimates of spring bloom were attributed to deficiencies in the zooplankton representation due to the lack of available data.

1.1.3 Plankton Functional Types

Jorge L. Sarmiento and Corinne Le Quéré (1996) performed experiments with coupled models of the atmosphere and oceans with a focus on carbon uptake by the ocean. The model was configured to describe analogue scenarios for more and less carbon productive worlds. Life was not explicitly represented, except by the representation of simple chemical and physical processes. Sarmiento and Le Quéré (1996) stated that uncertainty in the mechanics of biological oceanic processes could have put their results out by as much as 1000 petagrams of carbon in the 350 year scenario. They highlighted the lack of consensus on what determines regional differences in efficiency of primary production and advocated continued research and long-term satellite observation to improve the understanding of biological processes in the ocean.

By the early 2000s, projects such as the Joint Global Ocean Flux Study (JGOFS) and Sea-viewing Wide Field-of-view Sensor (SeaWiFS) began to produce an abundance of data (Moore et al., 2002). These gave a much clearer picture of the dynamic interplay between chemistry and biology in marine ecosystems across the globe. It was at that time that Doney (1999)

highlighted the debate surrounding biological representation in models. It was known that under certain conditions, the elemental content of biogenic material could depart significantly from the often assumed constant Redfield stoichiometric ratio. It was still unclear whether explicit species representation was necessary, or whether the effects of life on global biogeochemical cycles could be encapsulated by describing life in terms of its functional characteristics.

It was thought that chlorophyll concentrations correlated positively with those of nitrate and phosphate in the euphotic zone (Aumont et al., 2003). However, there were data from three major oceanic regions that challenged this commonly accepted view. These findings supported the hypothesis that iron and silicate may also limit the growth of large phytoplankton cells. Earlier NPZD-type models were not suitable for exploring this hypothesis. To address this, Aumont et al. (2003) produced a model that split the general phytoplankton and zooplankton groups into two distinct size-classes, and described them in terms of their affinity for iron and silicate.

The work of Baretta et al. (1995) on the European Regional Seas Ecosystem Model (ERSEM) represented a major development for ecological representation in models. Both this and the work of Aumont et al. (2003) contributed to a plan for an entire marine ecosystem model that grouped species less arbitrarily, based on their ecological function (Quéré et al., 2005). Initially there were definitions for ten "key" Plankton Functional Types (PFTs), each representing species that performed a similar biogeochemical function. For example, large organic particles sink more readily and so contribute more to export, whereas smaller particles can be remineralised at the surface (Quéré et al., 2005; Bopp et al., 2003). This logic provided a basic framework for differentiating species based on size.

Further distinctions were based on specific nutrient affinities and biochemical function. Calcifying phytoplankton species assimilate carbon to biogenically produce calcium carbonate (Quéré et al., 2005). As dense organisms they are a major sink of atmospheric CO_2. Nitrogen fixing phytoplankton can assimilate atmospheric nitrogen, but can only outcompete other species in warm, nitrogen poor waters. Silicifing phytoplankton outcompete other species in colder waters. Dimethyl sulfide producing phytoplankton are major contributors to the sulfur cycle. There was also the definition of micro-, meso-, and macrozooplankton types. Their grazing on the phytoplankton and subsequent fecal

pellets provide an indirect route by which small species are exported to the deep.

Like marine ecosystem models before it, the PFT approach was seen as a balance between intended simplicity and necessary complexity (Quéré et al., 2005). Representation of the ten PFTs required an enormous amount of observational and laboratory data. While a lot of new data were becoming available, there were still many other ecosystem processes that were not fully understood. Initially only five of the ten PFTs were implemented. The work of Le Quéré et al. (2005) better framed ecosystem models in a global biogeochemical context. As well as providing proof of concept for describing species based on traits.

Despite the increased model complexity, the work has been criticised as an oversimplification (Anderson, 2005). Anderson (2005) pointed out that species aggregation still occurs, and that in many cases the choices regarding the PFTs to include and exclude are arbitrary. Anderson (2005) attributed decisions like this to a "poorly understood ecology". He also stated that many models have parameterizations tuned to fit regional data, but that they are then not able to respond equally well to new scenarios. It was also noted that much of the plankton altering physical activity takes place on spatial scales that are thousands of times smaller than those represented in the models. This led to an appeal for more to be done to improve the accuracy of model parameterisations and the physicochecmical environment of Ocean General Circulation Models (OGCMs). He stated that current modelling approaches embrace a reductionist philosophy, whereby the true emergent properties of the complex systems they seek to describe are ignored.

1.2 Emergent Approaches

1.2.1 Follows

Follows et al. (2007) introduced a new type of emergent marine ecosystem model. Species were also aggregated based on ecological function However, instead of basing the trait values on species descriptions, they were drawn randomly from ranges guided by known ecological trade-offs. This was seen as an explicit attempt at being unbiased about what species to include. The model was initialised with 78 phytoplankton strains that were uniquely identifiable by their particular physiological details and coefficients. Each was given the

same starting biomass value, and the model was integrated forward in time for ten years allowing the ecosystem structure to emerge. Despite each individual run having a completely unique set of species it was found that the general ecosystem patterns were similar between all ten ensemble runs. Follows et al. (2007) identified from the range of species broad categories of functional types and analogues for extant species. The model data was then compared with empirical data for *Prochlorococcus* collected along the cruise track of the Atlantic Meridional Transect 13 (AMT13) and there was found to be general correspondance.

1.2.2 Bruggeman

Bruggeman and Kooijman (2007) presented a prototype example of an entirely new approach to representing phytoplankton in marine ecosystem models. Phytoplankton species differed in their affinity for nutrient and light. This was captured by two traits describing relative investment in either nutrient, or light harvesting cellular machinery. Trait-space was discretised and the full range of trait values were represented, resulting in populations that maximised assimilation of both light and nutrients. The total biomass for each species was partitioned into nutrient harvesting, light harvesting, and structural biomasses. Each biomass pool represented cellular machinery that required maintenance. While the trait values could enhance resource availability, it was assumed that the cellular machinery responsible for this would carry an increased cost for maintenance. Strains that maximised assimilation of both light and nutrients would have a proportionally higher metabolic rate than those that maximised assimilation of one or the other. Instead of predefining the trade-off in the allocation of trait values, it was an emergent property of the model.

By representing phytoplankton strains with every combination of traits, the approach was referred to as a System of Infinite Diversity (SID) (Bruggeman and Kooijman, 2007). The model was proof of concept for extension to an n-trait system describing any number of biological systems. However, the 2-trait system was found to be computationally expensive and was not considered a practical implementation. For this reason Bruggeman (2009) developed an approximation that represented the populations as distributions across continous trait-space. These were characterised by distributional moments. Changes to the populations resulted in corresponding changes to the moments that ap-

proximated them.

1.2.3 Individual-Based Model

So far, all of the work cited has referred to Population Level Models (PLMs). The choice of this approach is to aggregate species detail into a single group with average trait values, or to represent a chosen number of the trait combinations in multiple groups. Woods (2005) offered an agent-based plankton modelling approach as an alternative. This later become known as the Individual-Based Modelling (IBM) approach, due to the explicit representation of individuals (Woods et al., 2005; Hellweger and Kianirad, 2007). IBMs permit the simulation of complete life-cycles, life sustaining mechanisms, and selective events (Hellweger and Bucci, 2009). Species can evolve from discrete changes at the level of the individual, making it a promising avenue for exploration of population heterogeneity, behavioural adaptation, and genomic evolution. The approach often includes the explicit representation of processes that take place on scales that are often overlooked (Woods, 2005; Woods et al., 2005). Spatial heterogeneity at the level of the individual has been shown to influence the state of the entire system (Woods et al., 2005).

The computational expense of modelling discrete individuals and their environments increases as the population and model complexity increases (Woods, 2005; Hellweger and Kianirad, 2007). Techniques have been developed to overcome this. Woods (2005) linked a series of "metamodels" together to describe a planktonic system at different scales. The output from one model informed the computation of another. In this way, a complete description of the study system required more than one model to compute. Another technique combined individuals with the same or similar trait values, potentially permitting the simulation of millions of individuals with the computational expense of only a few thousand (Rose et al., 1993). Such model agents were later referred to as "super-individuals" (Hellweger and Kianirad, 2007; Hellweger, 2008; Hellweger and Bucci, 2009). This technique has been implemented in IBM models of phytoplankton cells (Hellweger and Kianirad, 2007; Hellweger, 2008; Hellweger and Bucci, 2009; Clark et al., 2011).

The IBM approach has also been applied to representations of higher trophic levels. Huse and Giske (1998) used neural-networks and a genetic algorithm to evolve the spatial movements of individual model fish. The work was used to

build predictions about predator-prey interactions between and spatial movements of cod (*Gadus morhub*) and capelin (*Mallotus villosus*) (Huse et al., 2004). A later extension was used to predict changes to the spawning behaviour of capelin in the Barents Sea as a result of climate change (Huse and Ellingsen, 2008). Shin and Cury (2001) implemented an IBM designed to simulate the effects of exploitation on commercial fishing stocks. The populations were age- and size- structured, and were comprised of super-individuals, where entities were seen to represent an aggregated group of fish with similar attributes.

Experiments showed that growth of *Pavlova lutheri* does not depend directly upon external nutrient concentration (Droop, 1968). Algal cells take-up nutrients and store them internally to fuel growth as required. This work led to a deterministic, PLM describing growth as a function of this internal nutrient store (Burmaster, 1979; Burmaster and Chisholm, 1979). As with other PLMs, the parameters controlling growth were constant in any single run; the population was homogeneous. Clark et al. (2011) published details of an IBM implementation of this earlier PLM. It was seen as an explicit attempt to model the genomic evolution of a phytoplankton population. Individuals carried a "genome" that was passed to clonal offspring, subject to potential mutation (Clark et al., 2011). It described rates of extracellular and intracellular nutrient uptake, minimum and maximum levels for the internal nutrient store, and the rate of mutation for each individual. Based on a PLM by Grover (1991), trade-offs were captured in the assigned trait values (Clark et al., 2011). To reduce computational costs the model also implemented a version of Rose et al.'s (1993) super-individual approach.

The IBM model developed by Clark et al. (2011) has been extended and more recently implemented in a General Circulation Model (GCM) (Clark et al., 2013). This work adds support to the IBM approach for use in global models, and forms the core of the the EVolutionary Ecosystem (EVE) model (Lenton, 2012). The aim of EVE is to improve the model representation of marine ecosystems in order to improve understanding of their role in biogeochemical cycles. EVE forms an extensible framework of trait-based IBMs. This thesis concerns the development of a model designed to represent heterotrophic life within the EVE framework.

1.2.4 This Project

The model developed as part of this project and presented in this thesis is a trait-based IBM of heterotrophic life. As an individual-based model, selective events can be explicitly resolved. This permits the evolution of individuals' heritable attributes. Model development initially focusses on size as the only evolvable trait in order that the outcome of predator-prey interactions can be determined mechanistically as a function of size. The intent is to produce a model that exhibits Evolutionary Adaptive Trophic Structure. This is the reason for the acronym EATSM.

Chapter 2 explains the detail of the model construction. Chapter 3 tests the model sensitivity to the input parameters. This is where the adaptive nature of the model will be demonstrated. No particular hypothesis will be under test. However, many results will be presented and comparisons with the literature made where appropriate.

Life history theory predicts that reduced juvenile survival will select for delayed maturation and decreased reproductive effort, and reduced adult survival will select for the opposite (Reznick et al., 1990). The comparative ease with which data on bird clutch sizes can be collected has resulted in a number of complimentary and competing hypotheses to explain the mechanisms behind it. Chapter 4 will review some of the literature on reproductive strategies and life history theory. The model will be modified to include an additional evolutionary trait that represents the adult investment in offspring. Model results will be compared with the literature in order to answer the question *do the predictions of life history theory completely explain the evolution of reproductive effort?*

Planktonic ecosystems contain diverse communities of species that compete for the same resources (Hutchinson, 1961). The search for the mechanisms behind the coexistence of plankton began with the work of Hutchinson (1961). However, there still remain some questions. Pelagic ciliates and heterotrophic dinoflagellates are observed to occupy a similar ecological niche, yet the mechanisms behind their coexistence remain largely unexplored. Unpublished data suggests a trade-off in their feeding strategy that may yield a clue. EATSM will be modified to capture this trade-off in the assignment of trait values that determine individuals' prey size selectivity. Model results will be discussed in

an attempt to answer *what mechanisms can explain the coexistence of pelagic ciliates and heterotrophic dinoflagellates?*

Chapter 6 summarises the work and draws some overall conclusions.

2 Method

2.1 Matter

EATSM is materially closed. The material with which the model is initialised is conserved throughout every model run. All biotic and abiotic material in EATSM is assumed to be the same density and stoichiometric ratio. This simplifies the material representation by making volume proportional to mass, and dispenses with the need for explicit chemical representation. Measures of volume do not need units, as their magnitude is only relative to others in the model.

There are two global values representing volumes of pools of matter; nutrient and phytoplankton. For simplicity detrital organic matter is not explicitly represented. Instead it is assumed that detritus is instantly remineralised. The nutrient pool (N) is completely passive and simply serves as a material buffer between the phytoplankton and heterotrophic population. At every time step the volume of the phytoplankton pool (P) is inspected. If it is less than its initial volume (P_{init}), a growth volume (P_{grow}) is calculated and added to the pool.

$$P = P + P_{grow} \tag{2.1.1}$$

The growth volume is calculated as below:

$$P_{grow} = \begin{cases} P_{init} - P & \text{if } (P_{init} - P) \leq N \\ N & \text{else} \end{cases} \tag{2.1.2}$$

In this way, the initial phytoplankton volume also serves as its maximum. To approximate the effect of the volume of phytoplankton (P) being comprised of a large number of small individuals, the volume of a single phytoplankton cell is assumed to take the smallest possible position in volume trait space (v_{small}).

The rest of the matter in EATSM is in the bodies of individuals that make up the population of heterotrophs. Matter enters the heterotrophic population from the consumption of phytoplankton by secondary producers. This matter is recycled within the population from consumption by higher trophic levels (tertiary, quaternary, quinary, etc). To close the material loop, waste and dead

matter from the population is added directly to the nutrient pool.

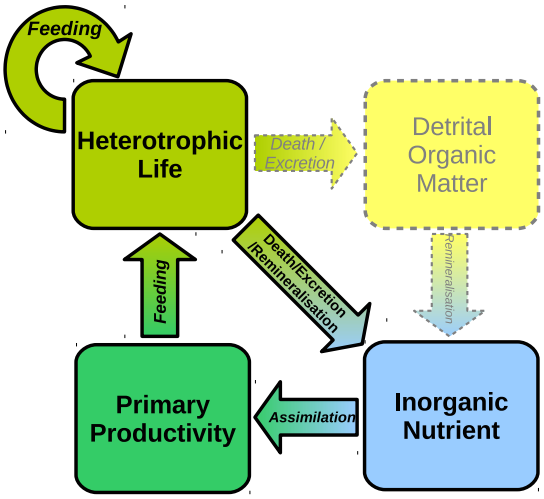

Figure 2.1.1: A schematic highlighting the represented pools and fluxes of material in EATSM. Detrital organic matter and the fluxes to and from it are approximated by the flux of material from the heterotrophic population directly to the inorganic nutrient.

The total volume in the model (V) is defined by summing the initial heterotrophic population volume (H_{init}), the initial phytoplankton volume (P_{init}), and the initial nutrient volume (N_{init}).

$$V = H_{init} + P_{init} + N_{init} \tag{2.1.3}$$

2.2 Individuals

Individuals carry with them a set of heritable traits that do not change for the duration of their lifespan, but are passed to offspring subject to potential mutation at reproduction. An unprocessed heritable trait (g) takes a value between 0 and 1. This is mapped onto an appropriate linear scale to define a processed heritable trait. The individuals that make up the heterotrophic population all have size, as equivalent spherical volume (ESV) (Jennings and Parslow, 1988). In this version of the model, the only heritable trait is an individual's heritable volume (v_h). This can be anywhere between the smallest (v_{small}) and the largest (v_{large}). The unprocessed trait value is mapped onto the logarithm of the range of possible volumes in the system to base 10. Accordingly, the heritable volume of an individual is defined as:

$$v_h = 10^{\left[g \cdot (log_{10}(v_{large}) - log_{10}(v_{small})) + log_{10}(v_{small})\right]} \tag{2.2.1}$$

Individuals have an actual volume (v) set initially to the heritable volume (v_h). The actual volume increases with food consumption, and decreases with metabolic losses and reproduction. Upper and lower volume thresholds are set, by reference to v_h. If v reaches the upper threshold (v_{max}), reproduction occurs. While at the lower threshold (v_{min}), starvation occurs.

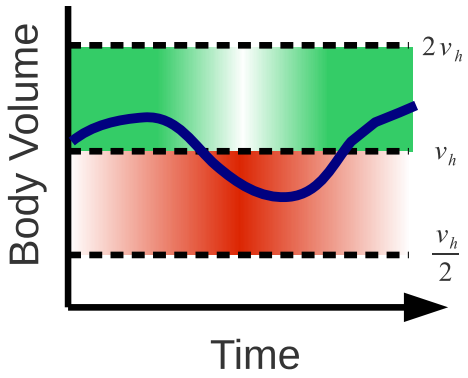

Figure 2.2.1: An idealised plot of an individual's actual volume over time (blue line) when compared to its heritable volume (v_h) and its reproduction and starvation thresholds. In this example v_{max} is set to v_h multiplied by 2, and v_{min} is set to v_h divided by 2.

The change of an individual's actual volume (v) over time is therefore defined by the additive effect of food assimilated (v_a), and the deductive effects of metabolic loss (v_l) and the amount passed to offspring at reproduction (v_r).

$$\frac{dv}{dt} = v + v_a(v_c) - v_l(v) - v_r(v) \tag{2.2.2}$$

2.3 Feeding

The only term from equation 2.2.2 that allows the volume of an individual to increase is the volume of food assimilated, which is a function of the volume consumed (v_c). The volume consumed is a function of the individual, the rest of the population, and the environment. Before food can be consumed, it must be located. The relationship between the rate at which an organism assimilates and the concentration of its substrate is a well observed ecological principle (Holling, 1959, 1965; Dowd and Riggs, 1965). Depending on the

particular context there are three basic forms this response can take. The general trend of each shows that the rate at which an individual feeds will go up with the concentration of its food, and will reach a theoretical limit when the rate of ingestion cannot increase any further. Holling (1965) referred to this phenomenon as a functional response.

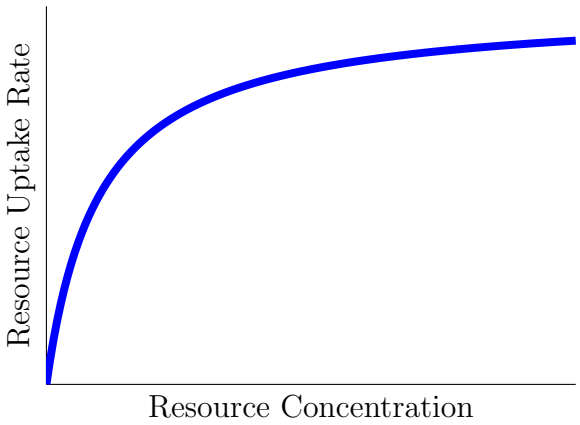

Figure 2.3.1: An general plot of a functional response showing the basic relationship of resource uptake rate (feeding) to resource (food) concentration.

Population-level models represent life and its food using state variables that allow the relationship between the two quantities to be easily handled using an appropriate mathematical function. In this context a functional response is used to calculate the quantity of food that is consumed by the entire population per unit time. The individual-based phytoplankton models of Clark et al. (2011; 2013) handle the relationship between food supply and rate of consumption in a similar way. Here nutrients are represented using state variables, making the numerical interface between a single individual and its food equivalent to a population and its food. In EATSM, individuals are required to find and eat others. A value representing the consumption amount cannot be directly applied in this context. Since the model is not spatially resolved, individuals do not literally move around and find their prey. This introduces subtle, but non-trivial problems.

The difficulties of using a functional response in an individual-based model of this type can be summarised by the following three questions:

Question 1 What defines prey for a given predator?

Question 2 When feeding, how do individuals select a prey individual?

Question 3 How does the prey population affect the rate of consumption?

The answers to these questions are collectively addressed with the encounter algorithm.

2.4 Encounter Algorithm

2.4.1 Preference Function

Following another well observed ecological principle, EATSM uses the volume of an individual to mechanistically define its relationship to predators and prey (Brooks and Dodson, 1965; Peters, 1983; Werner and Gilliam, 1984). This is encapsulated by the use of a preference function, that takes one of two forms. The first is a log-normal function:

$$\phi(v, v_p) = a \cdot exp\left[\frac{-\left(ln\left(\frac{\beta v_p}{v}\right)\right)^2}{2c^2}\right] \tag{2.4.1}$$

The second is an inverse log-parabolic function, taken from Hartvig et al. (2011):

$$\phi(v, v_p) = max\left[0, a \cdot 1 - \left(\frac{log_{10}\left(\frac{v/\beta}{v_p}\right)}{c}\right)^2\right] \tag{2.4.2}$$

Each is a function of predator/grazer volume (v) and prey volume (v_p), and produces a value for the predator preference for the prey. The maximum height of the function is intended to be no greater than 1, but can be controlled by the constant a. The constant β defines the preferred prey volume ratio. This is the distance in volume trait space between a predator and its maximally preferred prey. There is also a constant to control the width of the function (c).

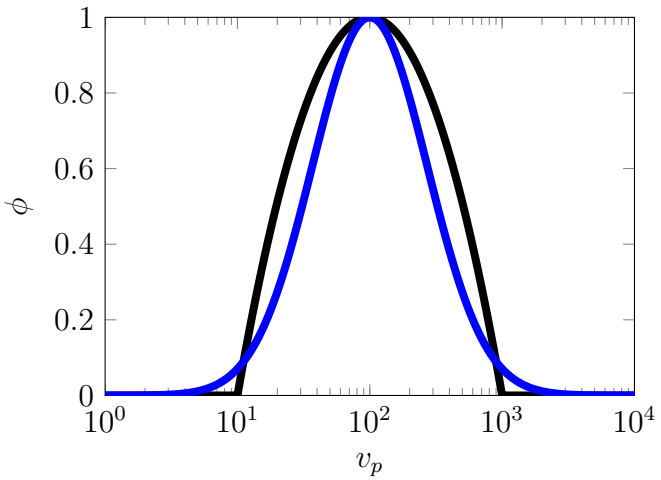

Figure 2.4.1: The predator preference (ϕ) as a function prey equivalent spherical volume (v_p), using the inverse log-parabolic (black), and the log-normal (blue) functions. In both the predator/grazer volume (v) is 10,000, the preferred prey volume ratio (β) is 100, the function height (a) is 1, and width (c) is 1.

The preference functions determine what is prey for a given predator, and thus answer question 1 above. The use of either function is mutually exclusive, as they both serve the same purpose. The reasons for implementing two functions, and the results that can be achieved with each can be seen in chapter 3.

Questions 2 and 3 are answered as part of the same mathematical process. EATSM uses a functional response, but instead of calculating the amount an individual will consume, it produces a probability that an individual will feed. The feeding probability is determined by the difference between the possible prey volume, and the volume of prey to which a predator would realistically respond, hereafter the effective prey volume. The effective prey volume is a summation of the coupling strengths between a predator and the available prey items. This can be achieved using a one-dimensional population structure, but prey selection becomes complicated if more than one predator are coupled to the same individual. To facilitate the process of prey selection, individuals were grouped into discrete size classes. This permits an individual to be coupled to the size class that contains the most viable prey.

2.4.2 Discrete Size Classes

Trait space between v_{small} and v_{large} was divided into a number (d) of discrete locations to define the volume mid-point for each size class. This necessitated

values to define the boundary values for each size class.

A vector of d size class mid-point values was created:

$$\mathbf{v}_m = (v_1, v_2, v_3, \ldots, v_d) \tag{2.4.3}$$

The value of the ith mid-point is defined by:

$$v_m(i) = 10^{\left[log_{10}(v_{small})+(i-0.5)\frac{log_{10}(v_{large})-log_{10}(v_{small})}{d}\right]} \tag{2.4.4}$$

A vector of $d+1$ boundary values was created:

$$\mathbf{v}_b = (v_1, v_2, v_3, \ldots, v_{d+1}) \tag{2.4.5}$$

The value of the ith boundary is defined by:

$$v_m(i) = 10^{\left[log_{10}(v_{small})+(i-1)\frac{log_{10}(v_{large})-log_{10}(v_{small})}{d}\right]} \tag{2.4.6}$$

These vectors are used to give every individual a size class index (i) based on their volume (v) such that:

$$v_b(i) \leq v < v_b(i+1)$$

An individual's size class index value (i) is the same as the size class mid-point that approximately equals their volume.

$$v \approx v_m(i)$$

If an individual's volume increases such that:

$$v \geq v_b(i+1)$$

Its size class index (i) is incremented. If its volume decreases such that:

$$v < v_b(i)$$

Its size class index (i) is decremented.

These rules permit the creation of a two-dimensional matrix ($\mathbf{M}$) of individuals that contains d separate size classes where individuals are grouped according to the volume mid-point (v_m) that is nearest their own (v). It is assumed that the number of individuals in a size class i is given by $M(i)$. Individuals are moved between each size class as their volume changes. The size classes are static, the individuals are dynamic.

2.4.3 Effective Prey Volume

In a general sense, either preference function can be used to calculate the coupling strength (s) between a predator (v) and a potential prey item (v_p) as a function of their volumes.

$$s(v, v_p) = \phi(v, v_p) \cdot v_p \tag{2.4.7}$$

This general concept permits the coupling strength to be used in determining whether an individual will feed from the phytoplankton pool, or whether it will consume another individual. The coupling strength (s_h) an individual with volume v has for consuming a heterotroph from size class i is given by:

$$s_h(v, i) = \sum_{j=1}^{M(i)} s(v, v(j)) \tag{2.4.8}$$

Since the phytoplankton pool is comprised of individuals that take the smallest volume in trait space (v_{small}), they are assumed to occupy the first size class. The coupling strength calculation for the first size class therefore includes the preference the grazer would have for a single phytoplankton cell, and the volume of the phytoplankton pool.

$$s_p(v, P) = \phi(v, v_{small}) \cdot P \tag{2.4.9}$$

Equations 2.4.8 and 2.4.9 can be used to determine the coupling strength an individual has to each of the d size classes. The size class that produces the highest single coupling strength is the one that the individual is coupled to.

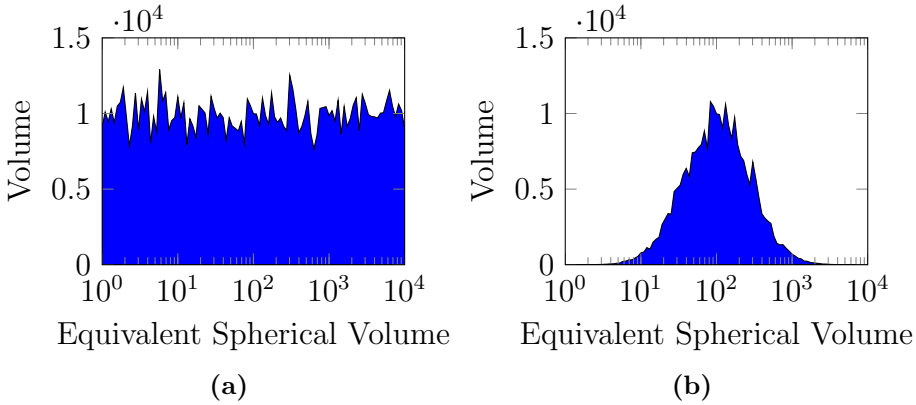

Figure 2.4.2: Plots show: **(a)** a hypothetical volume distribution across trait space, and **(b)** the result of applying equation 2.4.8 to each of the d size classes, where v_{small} is 1, v_{large} and the predator volume (v) are 10,000, the preferred prey volume ratio (β) is 100, the function height (a) is 1, and width (c) is 1.

In order to produce a single value that is used for the calculation of effective prey volume, the coupling strengths to each of the populations are added together.

$$v_e(v, P) = s_p(v, P) + \sum_{i=1}^{d} s_h(v, i) \tag{2.4.10}$$

This method explicitly determines the relationship a potential predator has to each individual within each size class. For this reason it is computationally expensive. Since individuals are grouped by size, the probability of feeding can be approximated by combining the preference function with the volume mid-point and the size of each size class. The approximation starts by assuming a constant size-based relationship (ϕ) set by the input parameters. The preference size class i has for size class j is therefore defined by:

$$\hat{\phi}(i, j) = \phi(v_m(i), v_m(j)) \tag{2.4.11}$$

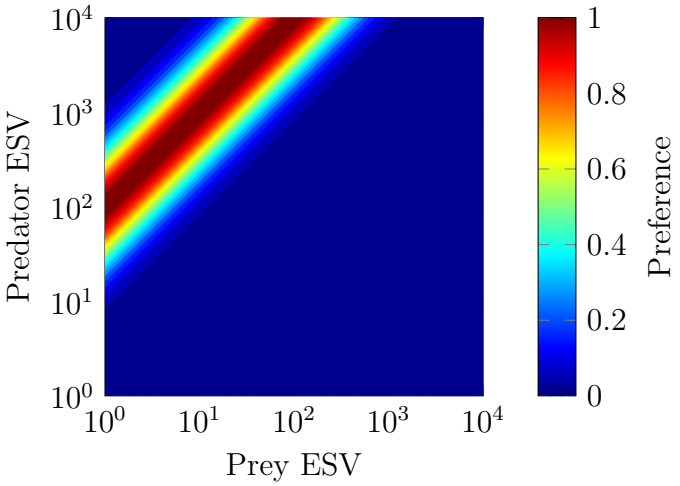

Figure 2.4.3: A plot of the preference matrix; the preference of every size class i, for every size class j using the log-normal preference function (blue line) in figure 2.4.1.

The coupling strength size class i has for consuming a heterotroph from size class j can be approximated by the product of the preference it has for size class j, the mid-point volume (v_m), and the number of individuals in it ($M(j)$). The approximation is in the assumption that the mean size class volume is matched by the mid-point values.

$$\hat{s_h}(i,j) = \hat{\phi}(i,j) \cdot v_m(j) \cdot M(j) \tag{2.4.12}$$

The approximation also assumes that phytoplankton cells take the smallest volume in trait space (v_{small}). The coupling strength between size class i and the first size class also includes an approximation for the effect of the phytoplankton:

$$\hat{s_p}(i,P) = \hat{\phi}(i,1) \cdot P \tag{2.4.13}$$

The coupling strengths are added together to produce the approximate effective prey volume experienced by size class i.

$$\hat{v_e}(i,P) = \hat{s_p}(i,P) + \sum_{j=1}^{d} \hat{s_h}(i,j) \tag{2.4.14}$$

The approximated method for calculating the effective prey volume also per-

mits the size class with the highest coupling strength to be determined.

2.4.4 Feeding Probability

Section 2.4.3 describes the calculation of an actual and approximate effective prey volumes (v_e and $\hat{v_e}$). This section describes how these are converted into a probability that an individual or size class will feed. Since the approximation is used to generate the majority of the results, this section will refer exclusively to that version. At this stage the reader is asked to assume that both the actual and approximate effective prey volumes can be used interchangeably in the equations that follow. This will be referred to again in chapter 3.

In order that the rate of consumption correlates with the changes to the number of prey, the effective prey volume is used as part of a functional response to calculate the probability that an individual or size class will feed. For this a second value is needed as an upper limit, and to provide context to the first. Since material is conserved in EATSM, this value is taken to be the total volume in the system (V). There are two types of functional response, both are used as probability functions that calculate the likelihood that an individual or size class will feed (P_f). The first follows the linear form of a Holling (1965) type 1 functional response.

$$P_f(i,P) = \frac{\hat{v_e}(i,P)}{V} \tag{2.4.15}$$

The second follows a non-linear form of a Holling (1965) type 2 functional response.

$$P_f(i,P) = \frac{\hat{v_e}(i,P)}{V \cdot K_{frac} + \hat{v_e}(i,P)} \tag{2.4.16}$$

Here K_{frac} is a half-saturation constant fraction, which takes a value between 0 and 1. The product of this parameter and the upper limit (V) produces a value for the effective prey volume that would result in a fifty percent chance of and individual drawn from size class i of feeding.

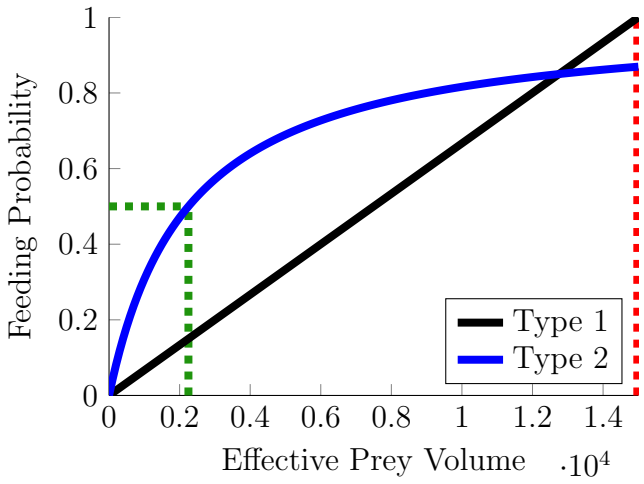

Figure 2.4.4: Example plots of the linear type 1 (black), and non-linear type 2 (blue) functional responses. The half saturation constant fraction (K_{frac}) is set to 0.15 (green), and the maximum volume (V) is set to 15000 (red).

As with the preference functions, only one of the two functional responses can be used at a time. The results that can be achieved with both will be explored in chapter 3.

By grouping similarly sized individuals and calculating the feeding probabilities for each size class, the approximation for the encounter algorithm is more computationally efficient by several orders of magnitude. Its accuracy can be quantified by the amount the mean volume of a size class deviates from the mid-point (v_m).

2.5 Initialisation

The initial population volume (H_{init}) sets a maximum budget from which to build the first population of individuals. There is little computational difference between individuals at either end of trait space. Since more small than large individuals can be built from the same volume, applying a fixed initial volume to the smallest end of trait space would produce a very large, computationally expensive population. The preference matrix (2.4.3) shows that individuals at the smallest end of trait space would be unlikely to consume anything.

Currently there is no implementation of Rose et al.'s (1993) method for combining similar individuals to reduce computational expense. As a way of reducing

computation at the beginning of the model run, the smallest size classes are not initialised with individuals. The first size class to be initialised is the one whose mid-point is closest to the product of the smallest volume and the preferred prey volume ratio. Members of this size class have the highest preference for the phytoplankton. We shall refer to the index of this size class is i_{first}.

$$v_m(i_{first}) \approx \beta \cdot v_{small}$$

The number of size classes that are initialised is therefore given by the following calculation.

$$d_{init} = d - i_{first} \tag{2.5.1}$$

The initial population volume is divided between the number of size classes that will be initialised. The volume budget for each initialised size class is therefore given by:

$$H_{class} = \frac{H_{init}}{d_{init}} \tag{2.5.2}$$

For reasons that are explained in chapter 3, the largest individuals in the system should be a significant distance from the largest volume in trait space (v_{large}). The parameter configuration should therefore meet the following condition:

$$V \ll v_{large}$$

Because of this condition, initialisation of the size classes begins at the largest end of volume trait space and works towards the smallest end. At each size class the system attempts to create individuals with a heritable and an actual volume that matches the mid-point for that size class (v_m). This continues until the volume budget for the size class (H_{class}) is less than the mid-point. The remaining volume is then carried over to the next smallest size class, and the process repeats. If there is any volume from the initial population volume (H_{init}) remaining at the end, it is added to the nutrient pool to ensure the system always starts with the precise amount configured by the input constants. By sharing the initial heterotrophic volume between as many size

classes as possible, this initialisation method effectively forces a trophic system to occur even if the parameter values result in its subsequent collapse.

2.6 Functions

The model is run forward in time for a specified number of real seconds, and computes as many abstract time steps (t) as possible. At every time step growth is calculated and added to the phytoplankton pool, and the matrix of size classes ($\mathbf{M}$) is updated according to and in order of the four activities mentioned below.

1. May consume food.
2. Should experience a metabolic loss.
3. May starve.
4. May reproduce.

2.6.1 Size Class Subset

The approximate effective prey volume ($\hat{v_e}$) is calculated based on a snapshot of the state of the size classes at the beginning of each time step. During the round of feeding individuals are consumed and are removed from the matrix ($\mathbf{M}$). This should technically alter the probability of subsequent individuals feeding. A correct update of the approximated feeding probabilities would result in d^2 calculations for a change in any single individual. Updating the feeding probabilities every time an individual is consumed would be computationally expensive. To reduce the need to perform this update, only a subset of each size class are allowed to feed. The size of the subset is controlled by the subset fraction parameter (α), which essentially acts as a coefficient on the number of individuals in the size clas ($M(i)$). The initial size of the subset from size class i ($\hat{m}(i)$) is given by:

$$\hat{m}(i) = \alpha \cdot M(i) \tag{2.6.1}$$

On the condition that:

$$0 < \alpha \leq 1$$

However, the subset size is defined by an integer value. The size class would have to contain a number of individuals that was at or above a threshold in order to produce a subset that was greater than zero. If equation 2.6.1 was truncated the threshold would be:

$$M(i) \geq \frac{1}{\alpha}$$

If it was rounded conventionally, the threshold would be:

$$M(i) \geq \frac{1/\alpha}{2}$$

Size classes higher in volume trait space will generally fall well below both of these thresholds for reasonable values of α. This is why equation 2.6.1 has been extended so that the integer subset size from size class i is given by:

$$m(i) = \begin{cases} \lceil \hat{m}(i) \rceil & \text{with probability} = \hat{m}(i) - \lfloor \hat{m}(i) \rfloor \\ \lfloor \hat{m}(i) \rfloor & \text{else} \end{cases} \tag{2.6.2}$$

This makes use of a probability-based rounding algorithm. The subset size is rounded up with a probability defined by the initial size of the subset ($\hat{m}(i)$) with the floored $\hat{m}(i)$ value subtracted. In short, only the fractional part of the $\hat{m}(i)$ value. Calculating the subset size in this way ensures that size classes that fall below the thresholds will eventually be permitted to feed. It also ensures that fewer of the individuals feed in that time step. This reduces the theoretical difference between the feeding probabilities at the beginning and the end of feeding, when this is calculated using the approximate effective prey volume ($\hat{v_e}$).

2.6.2 Food Consumption

Starting at the first size classes, a subset from each (defined by equation 2.6.2) are selected with a uniform probability to feed. Individuals in the subset feed with a probability (P_f) defined by equation 2.4.15 or 2.4.16. If an individual is coupled to feed from the first size class it is initially assumed to feed from

the phytoplankton. While phytoplankton is available the volume of a single phytoplankton cell (v_{small}) is subtracted from the pool and consumed by the individual. If the phytoplankton pool is less than the volume of a single phytoplankton cell or if the predator is coupled to feed from any other size class, it consumes the volume (v) of an individual drawn with a uniform probability from the size class to which it is coupled. If there are no prey items available nothing is consumed and the feeding attempt is over. Although under realistic parameter configurations this is an extremely infrequent event. In both cases the volume assimilated (v_a) is function of the consumed volume (v_c), and the assimilation efficiency coefficient (γ):

$$v_a(v_c) = \gamma \cdot v_c \tag{2.6.3}$$

At this stage it would be possible to consider more complex internal dynamics, such as absorption rates (e.g. Atkinson et al. 2012). To simplify the representation of individuals, assimilated food is added directly to the individual's volume:

$$v = v + v_a \tag{2.6.4}$$

Food consumption produces waste. For material conservation the volume that is lost during assimilation (v_w) is added to the nutrient pool.

$$v_w(v_c) = (1 - \gamma) \cdot v_c \tag{2.6.5}$$

Feeding continues for every individual in the subset. Once each individual has been given an opportunity to feed the process repeats for the next size class in the same way. When every size class has been handled in the same way, the round of feeding is over. Please see figure 2.6.1 for a flowchart that illustrates diagramatically the process of feeding.

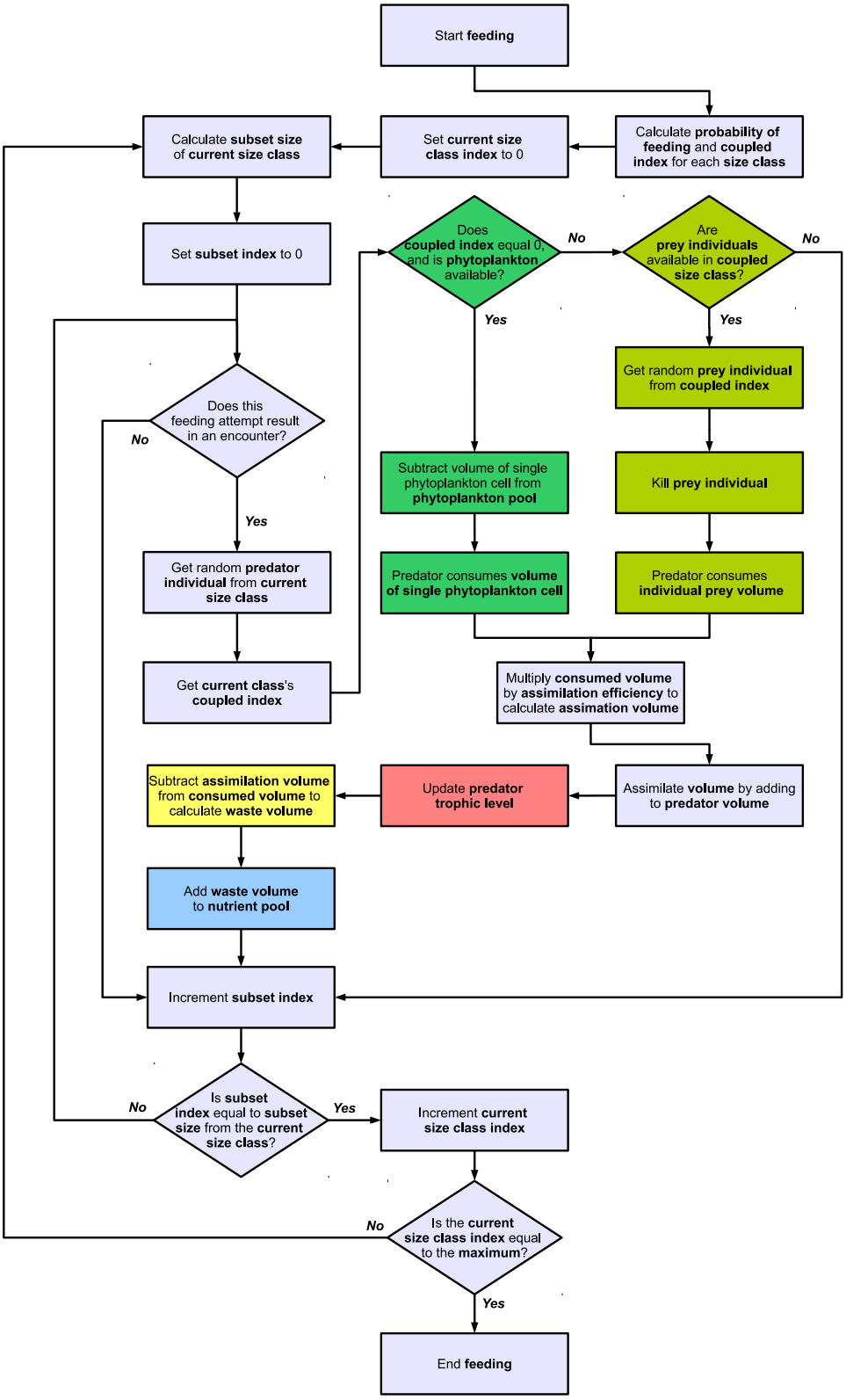

Figure 2.6.1: A flowchart depicting the model logic and decisions during a round of feeding. Some boxes are colour-coded according to the pools of matter in figure 2.1.1. See section 2.7.1 for a description of the trophic level update (pink box).

2.6.3 Metabolisation and Starvation

Metabolic losses are applied to every individual by subtracting a fraction of their actual volume and adding it to the nutrient pool at every time step. The volume subtracted (v_l) is a function of the somatic volume (v) of the individual and a parameter to define the fractional metabolic expense per time step (ϵ). A power-law relationship is assumed between v and ϵ (Kleiber, 1947; Glazier, 2005). The metabolic scaling exponent (k_m) specifies the value of the power.

$$v_l(v) = \epsilon \cdot v^{k_m} \tag{2.6.6}$$

Not all individuals will consume food. Such individuals would continue to shrink by metabolic loss unless a threshold for starvation were established. It's certainly possible to consider the literature on experiments on zooplankton under conditions of starvation. A preliminary review suggests that starvation is a complex process that is intimately related to age (Threlkeld, 1976) and metabolism (Mayzaud, 1976). For simplicity, a constant threshold for starvation is used that scales with the individuals heritable volume (v_h). Individuals starve if their actual volume (v) is reduced to or below their minimum volume (v_{min}). The value of v_{min} is set at half their heritable volume.

$$v_{min}(v_h) = \frac{v_h}{2} \tag{2.6.7}$$

In addition to this, starvation is probabilistically applied to a subset of individuals from each size class. The subset is created in the same way as the subset that feed (equation 2.6.2). When an individual's volume (v) is at or above its heritable volume (v_h) its probability of starving is 0. For simplicity, this increases linearly to 1 as its volume approaches its minimum volume (v_{min}).

$$P_s(v, v_h) = 1 + \frac{v_{min}(v_h) - v}{v_h - v_{min}(v_h)} \tag{2.6.8}$$

The volume of starved individuals is added to the nutrient pool.

2.6.4 Reproduction

The reproduction threshold (v_{max}) sets the level an individual's volume needs to reach in order for reproduction by binary fission to occur. The value of v_{max} is set at twice the heritable volume.

$$v_{max}(v_h) = 2 \cdot v_h \tag{2.6.9}$$

Offspring are clones of the parent, subject to potential mutation of the heritable volume trait. Following the work of McDonald-Gibson et al. (2008) mutation occurs with probability P_μ per heritable trait. It is modelled with the addition of a random number drawn from a normal distribution with a mean of 0 and standard deviation of σ to an unprocessed trait value (g). This ensures that a mutation of the same value is relatively the equivalent at any point in trait space. If a mutation would result in a heritable trait (g) being less than 0 or greater than 1, then the amount outside the trait interval is reflected about the upper or lower bound respectively. This keeps the trait values within the allowable range, and ensures that a random mutation results in a change to the heritable trait.

A fraction of the parent's volume (v_r) is used to initialise its child. The calculation for this takes one of two forms. If the child has a mutation of the heritable volume trait that does not exceed its parent's volume, the child is initialised with a volume that matches its heritable volume (v_o).

$$v_r = v_o \tag{2.6.10}$$

If the heritable volume of the child is greater than the volume of the parent or if the child is a clone of the parent, the volume of the parent is shared evenly between the parent and child.

$$v_r(v) = \frac{v}{2} \tag{2.6.11}$$

2.7 Trophic Classification

2.7.1 Tau Attribute

Individuals carry with them an attribute that defines their trophic level (τ). Since the trophic structure of EATSM is not prescribed, the uninitialised value of this attribute is zero. Every time food is consumed it is initialised or updated based on its existing value and the source of food. Consumption from the phytoplankton pool results in a different calculation from consumption of another individual. The calculations produce real values, to account for individuals that may consume from multiple trophic positions during their lifetime (see tables 2.7.1 and 2.7.2). The τ attribute has no effect on the model functions, it is used only as a means of visualising the emergent trophic structure.

At the base of every ecosystem are the primary producers. In the context of EATSM, they are assumed to occupy the first trophic level, denoted by a value 1. This concept is extended to higher trophic levels, where the second is denoted by 2, etc. Individuals may survive between trophic levels by for example, consuming phytoplankton and other individuals. Such individuals would have a trophic level value (τ) greater than 2 and less than 3. Since the individuals in EATSM are exclusively heterotrophic, the value for the first trophic level is not used, but its position is reserved.

Table 2.7.1: Grazer trophic level update after consuming from the phytoplankton.

Grazer (τ)	0	$\tau = 2$
	Not 0	$\tau = \frac{\tau+2}{2}$

Individuals that consume phytoplankton for the first time occupy the second trophic level (top row, table 2.7.1). An individual with a previously initialised trophic level value may have previously consumed another heterotroph. An existing τ value is added to the value for the second trophic level, and divided by two (bottom row, table 2.7.1). This ensures that a mixed feeding strategy is reflected by the τ value. It also means that some aspect of the individual's feeding history is preserved, but is potentially altered by its current feeding activity.

Table 2.7.2: Predator trophic level update after consuming another heterotroph.

		Prey (τ_p)	
		0	Not 0
Predator (τ)	0	$\tau = 3$	$\tau = \tau_p + 1$
	Not 0	$\tau = \frac{\tau+3}{2}$	$\tau = \frac{\tau+\tau_p+1}{2}$

An individual that consumes another individual potentially has its own (τ), and the trophic level value of its prey (τ_p) to use in the calculation. An uninitialised predator consuming an uninitialised prey individual is assumed to occupy the third trophic level (top left, table 2.7.2). An uninitialised predator, consuming an initialised prey is set to occupy the trophic level above the prey (top right, table 2.7.2). For an initialised predator consuming an uninitialised prey, the trophic level value tends towards the third (bottom left, table 2.7.2). Initialised predators consuming initialised prey tend towards the trophic level above their prey (bottom right, table 2.7.2). Children inherit their parent's trophic level value, although it will change independently.

When the data are collected, the individuals' τ values are rounded to the nearest integer value to assign them to a discrete trophic level (τ_d).

$$\tau_d = \|\tau\| \tag{2.7.1}$$

Grouping the τ values in this way permits data about the volume and frequency of each trophic level to be collected more easily.

2.7.2 Trophic Level Count

The number of trophic levels of the artificially evolved system is a useful metric in drawing comparisons with natural trophic systems. While this can be determined by observation of the model outputs, the process is time consuming and largely subjective. Many parameter configurations produce result sets that are qualitatively similar to others, while differing in ways that may not be immediately obvious. In order to avoid the potential to make mistakes it was necessary to construct an algorithm that counts the number of trophic levels in any result set in the same way.

As mentioned in section 2.7.1, individuals start a new model run with an uninitialised τ value of 0 and can be said to occupy the 0th trophic level (τ_0). For every parameter configuration there is a period at the beginning of each run where uninitialised τ values disappear from the system. If the model starts at t_0 and the finishes at t_{max}, uninitialised τ values disappear by t_τ.

$$t_0 < t_\tau < t_{max}$$

In the period of model time (t) that comes after t_τ, all extant individuals have either consumed food or are children of those who have. The rest have been consumed or have died of starvation. Despite this the highest trophic level does not begin to appear until around $2 \cdot t_\tau$.

The population size of each trophic level is sampled at fixed intervals of model time (t). The data are converted into a boolean matrix where non-zero populations are represented with 1 to indicate the presence of that trophic level, and 0 indicate its absence. Depending on the parameter configuration some result sets can be more oscillatory than others. Under these conditions the number of individuals in each trophic level fluctuates, and some (usually the top) trophic levels can phase in and out of existence. A trophic level is therefore counted as wholly present if it observed to exist for more than a fixed fraction (0.75) of sampled time between $2 \cdot t_\tau$ and t_{max}.

Counting of the trophic levels only concerns heterotrophic individuals, and starts with the secondary producers. When a trophic level is found to exist, 1 is added to a running total. This continues for higher trophic levels until one is found to be absent. The algorithm then adds the fraction of sampled time that it was present to the running total and stops counting. Any trophic levels higher than this that may occur transiently are not counted. This is because trophic levels are found to be generally more unstable than the one that precedes them. This observation applies to all viable model configurations.

The counting algorithm therefore preserves the information about the most stable trophic levels, and the point at which the trophic system becomes unstable. For example, a count of 3.5 would indicate the presence of secondary, tertiary, and quaternary producers for over 75 percent of sampled time, and the presence of quinary producers for 50 percent of sampled time. This count would disregard any individuals in a senary trophic level. Model configurations

that do not reach any kind of stable or consistent state collapse in a very short space of time, and therefore produce a trophic-level count of zero.

3 Sensitivity Analysis

In this section a default or baseline configuration of the model is illustrated and the basic dynamics of the model are analysed. The results from this are used to validate the approximate method for calculating the effective prey volume (equation 2.4.14). In addition the sensitivity of the outputs to the most important parameters is investigated. The trophic level counting algorithm is used as a high-level view of the system to compare results. Discussion takes place as the results are presented.

3.1 Default Configuration

EATSM takes a number of input parameters and control switches. A parameter controls the length of the model run (in seconds), and another adjusts the rate (in time steps) at which the data are sampled. Three control switches select either of the two preference functions (see equations 2.4.1 and 2.4.2), either a type 1 or type 2 (see equations 2.4.15 and 2.4.16) functional response, and whether or not the model uses the approximated encounter algorithm (see equation 2.4.14). The default model configuration uses of the log-normal preference function, the type 2 functional response, and makes use of the approximate calculation of effective prey volume. Beyond these controls there are 16 constants that have configurable values. The default values for these can be seen in table 3.1.1 below.

Table 3.1.1: The default parameter values for the current EATSM model.

Symbol	Value	Description
d	100	Number of heterotrophic size classes.
N_{init}	0	Initial nutrient volume.
P_{init}	1e+06	Initial phytoplankton volume.
H_{init}	1e+06	Initial heterotrophic population volume.
v_{small}	1	Smallest individual volume.
v_{large}	1e+10	Largest individual volume.
β	15	Preferred prey volume ratio.
c	0.75	Feeding kernel width.
a	1	Feeding kernel height.
α	0.01	Size class subset fraction.
K_{frac}	0.15	Half-saturation constant fraction.
γ	0.5	Assimilation efficiency.
ϵ	1e–05	Fractional metabolic expense per time step.
k_m	0.67	Metabolic scaling exponent.
P_μ	0.001	Probability of mutation.
σ	0.01	Standard deviation of mutation distribution.

Using the default parameter values in table 3.1.1 the following results were generated. Note that plots that show cumulative quantities between times the data are sampled, whereas others show quantities at the time of sampling.

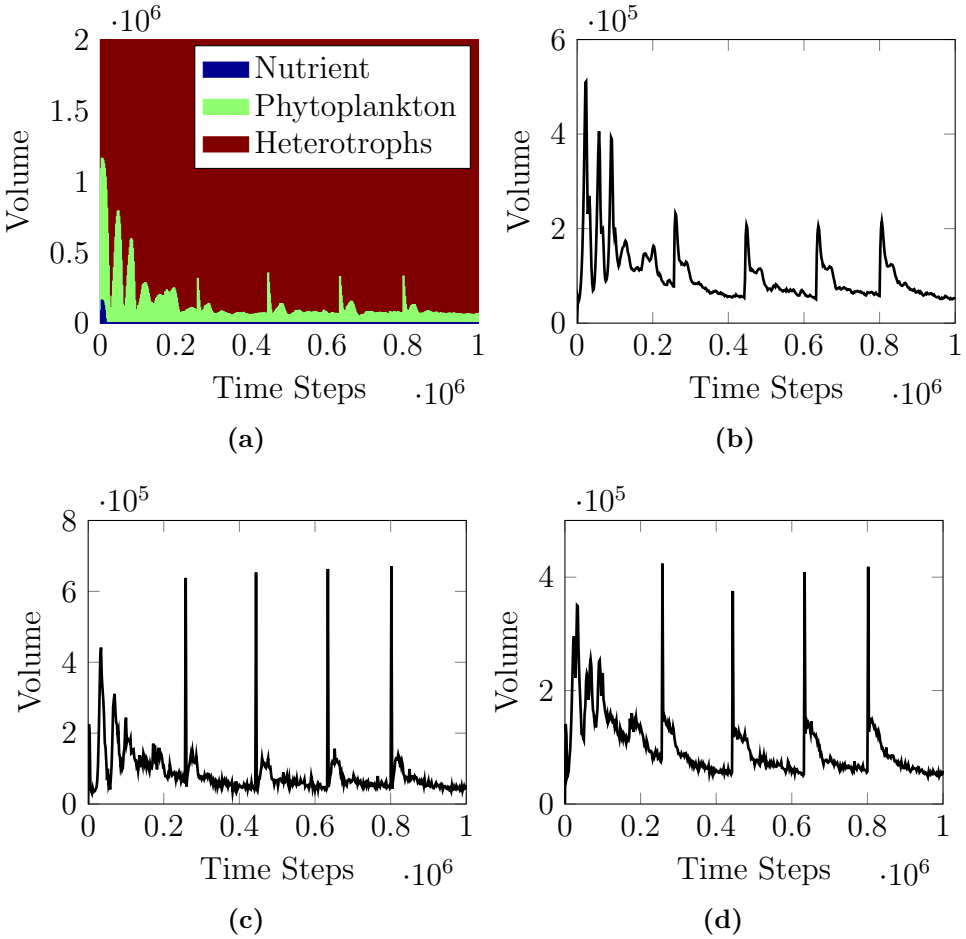

Figure 3.1.1: The changes in volumes of and fluxes between the pools of matter over time on the x-axis. Plots show: **(a)** a stacked bar chart showing the volumes of each of the pools of matter, **(b)** the volume fluxes from consumption of phytoplankton by the herbivores, **(c)** from consumption of prey individuals by carnivores, **(d)** and from the heterotrophic population to the nutrient pool through waste production, assimilatory losses, and death by starvation.

As described in section 2.1, EATSM is a materially closed system. The total volume is preserved, but is moved between the pools of matter. The way in which the volumes of the pools of matter change over time can be seen in figure 3.1.1a. These changes are determined by the fluxes between the pools (figures 3.1.1b, 3.1.1c, and 3.1.1d).

In this version of EATSM the growth of the phytoplankton is implemented simply to close the material loop. The most influential factor in determining the volumes of and fluxes between the pools of matter is the population of individual heterotrophs that can eat, be eaten, reproduce, and starve. This is

evident by the plot of the total number of heterotrophic individuals over time in figure 3.1.2 below.

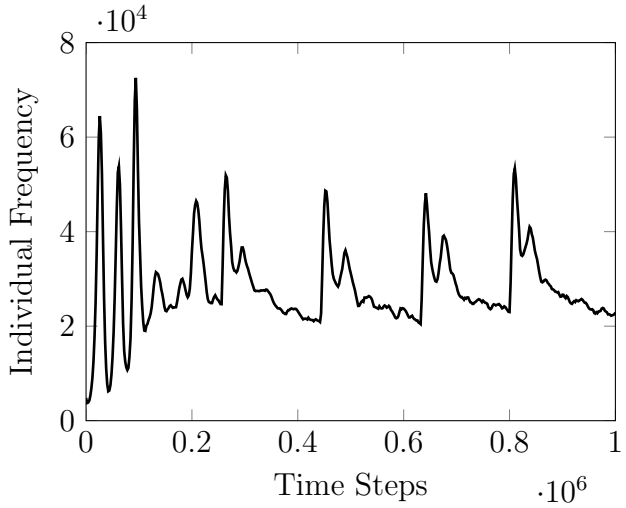

Figure 3.1.2: The total number of heterotrophic individuals over time.

The spikes in both pool volumes and fluxes directly correlate with the total number of heterotrophic individuals. Each individual from figure 3.1.2 is a member of one of the d size classes. Figure 3.1.3 illustrates this correlation in more detail by showing the evolution of the size classes of heterotrophs over time.

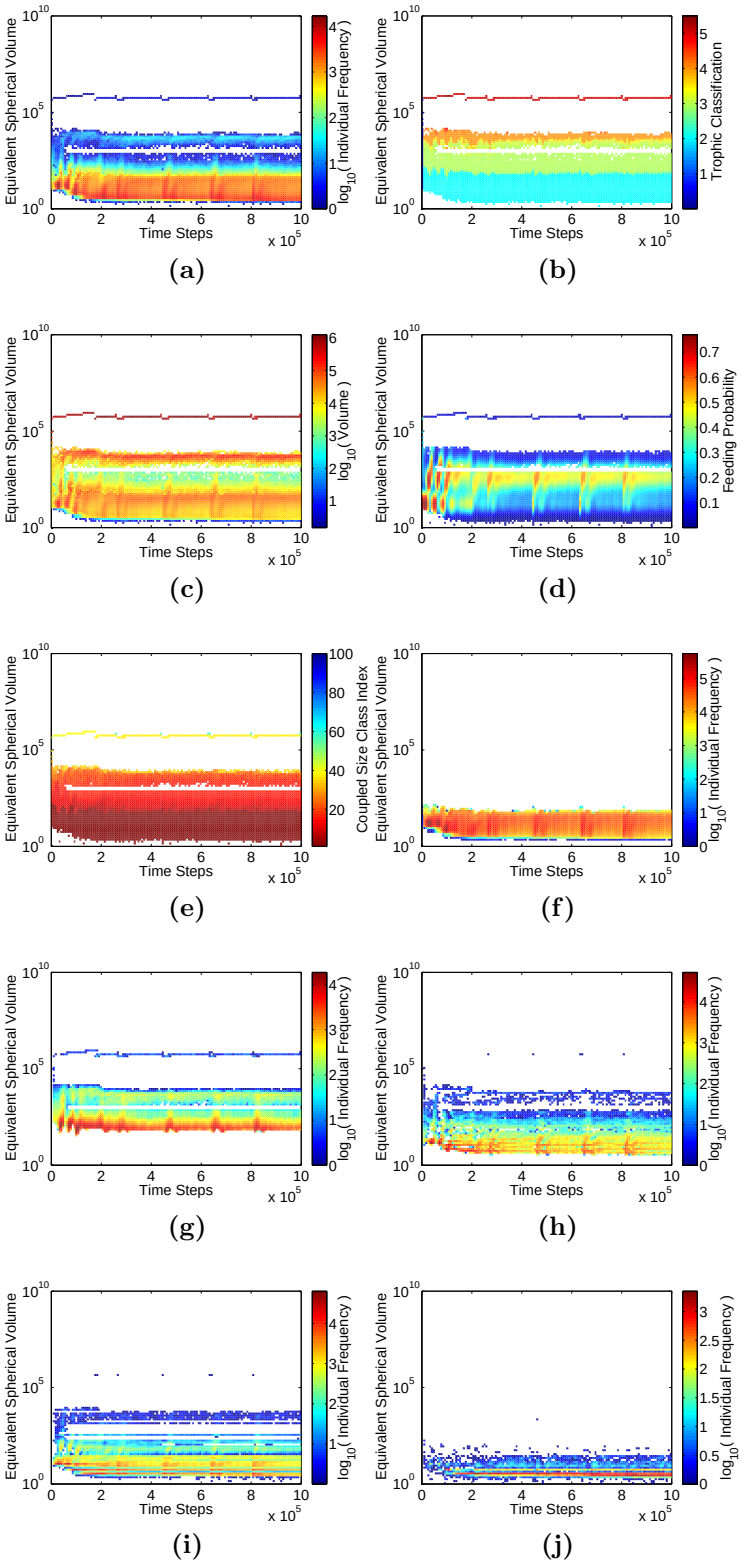

Figure 3.1.3: The evolution of the d size classes on the y-axis, over time on the x-axis. Plots show: **(a)** the number of all individuals, **(b)** the mean trophic classification, **(c)** the volume, **(d)** and the feeding probability of each size class, **(e)** the index to which each size class is coupled, and the **(f)** numbers of herbivores, **(g)** carnivores, **(h)** corresponding prey individuals, **(i)** children, **(j)** and starved individuals.

The calculation of approximate effective prey volume ($\hat{v_e}$) leads to each size class being coupled to consume from their preferred size class (fig. 3.1.3e). This means that some size classes behave as herbivores by feeding from the phytoplankton (fig. 3.1.3f), and others behave carnivorously (fig. 3.1.3g) by consuming other individuals as prey (fig. 3.1.3h). Those who consume enough food to reach twice their heritable volume produce children (fig. 3.1.3i). Those individuals who are not able to cover their metabolic expense fall below their heritable volume and may starve (fig. 3.1.3j).

It can be seen from figure 3.1.3a that the trophic structure finds a stable state that reproduces Charles S. Elton's "pyramid of numbers" (Elton, 1927). Elton's general observation was that individuals at the base of a trophic system will be more numerous when compared to those at the top. He described this as a consequence of a "system of territories", whereby individuals will have an area that is sufficiently large to supply their food requirements. EATSM has no explicit representation of space, but the treatment of volume implies it. This introduces the possibility that the classical trophic pyramid may be a result of a mechanistic size-based predator-prey relationship, and allometrically scaled metabolic rate. The system of territories may therefore be a consequence of lower-level processes.

The rate at which each size class consumes correlates with the rate at which they reproduce. This can be seen by the number of children over time (fig. 3.1.3i). The rates of both consumption and reproduction correlates negatively with individual size. This again reinforces the comparision with the Eltonian ecological pyramid, as this implies that smaller individuals are able to increase faster than larger ones (Elton, 1927). This permits a stable system where a certain fraction of smaller size classes serve as food for larger ones.

Individuals' trophic level attribute (τ) values were averaged for each size class and plotted in figure 3.1.3b. They were also rounded to the nearest integer value to assign each to a single trophic level (τ_d) (equation 2.7.1). This permitted the data to be viewed in terms of individual contributions to a discrete trophic level.

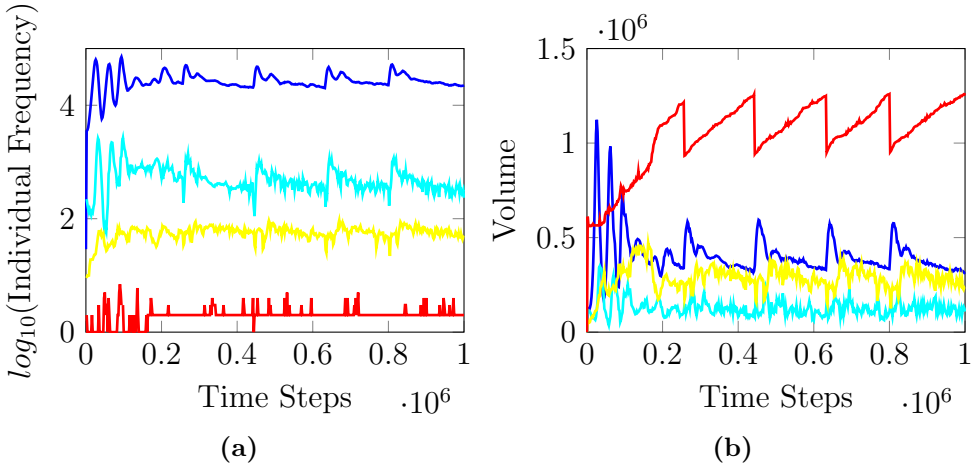

Figure 3.1.4: Plots show: **(a)** the numbers and **(b)** the volumes of the secondary (blue), tertiary (cyan), quaternary (yellow), and quinary producers (red) over time.

The results above show a population cycling between the trophic levels that is characteristic of Lotka and Volterra's work (Lotka, 1920b; Volterra, 1926a). Pimm and Lawton (1977) make the assumption that organisms occupy a discrete trophic level. When comparing these to the results in figure 3.1.3b, it can be seen that the trophic levels are roles that individuals can dynamically fulfil. This reflects the suggestion made by Shurin (2006); that the lines between trophic levels are blurred.

Model configurations that start with a high initial phytoplankton volume all show a rapid reduction of the phytoplankton when faced with a productive population of heterotrophic individuals. After the reduction in phytoplankton, some configurations do not show any oscillations. All of the plots in this section show a period of damped oscillations, leading to a consistent periodic oscillation. It is concluded that both are influenced by the parameter configuration, and can be attributed to two distinct mechanisms within the model.

3.1.1 Damped Oscillation

A sufficiently high initial volume of phytoplankton provide size classes with low v_m values an immediately high probability of consuming. These individuals rapidly assimilate phytoplankton, converting it to heterotrophic volume. This is evident in figure 3.1.4b where the volume of secondary producers peaks at 2,600 time steps, by which time it comprises over 56% of the total volume. This is the cause of the commonly observed reduction in phytoplankton (fig.

3.1.1a). The rate of phytoplankton consumption slows as the reduction of its volume impacts the probability of herbivores feeding (fig. 3.1.3d).

As described in section 2.5, the initialisation method divides the initial heterotrophic volume between as many viable size classes as possible. If the model was initialised with only small initial heterotrophic volume there would not be many individuals higher in volume trait space. The phytoplankton would be grazed and the system would transition smoothly to steady state. Since the default model configuration uses a high initial heterotrophic volume, a wide range of size classes are initialised with individuals occupying viable positions higher in the trophic system. In this situation the number of secondary producers is reduced shortly after their probability of feeding drops. This is because their high volume results in potential tertiary producers having a high probability of feeding.

This dynamic produces population cycles that continue higher in the trophic system until they reach the top-level carnivore. Larger individuals require more volume, and assimilatory and metabolic losses ensure that there is less volume available to the higher trophic levels each time. This is confirmed by figure 3.1.1b that shows the flux from consumption by herbivores to be generally larger than the flux of consumption by carnivores (figure 3.1.1c). The large spikes in figure 3.1.1c exceed the input to the heterotrophs from the phytoplankton. This must mean they are the result of volume recycling by higher trophic levels. Figure 3.1.4b shows that the volume of the quaternary producers is greater than the others. This is believed to be a consequence of the heterotroph initialisation method (see the experiments with H_{init} in section 3.3.5).

Waste volume is put back in to the nutrient pool, which drives phytoplankton growth. The secondary producers grow. The population cycle repeats, and is intense enough that the fluxes drive subsequent cycles. Each time the cycle occurs, the amplitude is reduced as volume is assimilated and redistributed throughout the size classes. The initial set of damped oscillations can be understood as a consequence of the method by which the size classes are initialised and the high initial heterotrophic volume. A reduced initial/maximum phytoplankton volume also serves to reduce the amplitude of the oscillations by reducing the rate of the secondary production, potentially to the point of a collapse of the trophic system. If the system does not collapse during this

phase, the system transistions into steady state. Following the definition of Steele (1974) this represents the point at which the form or pattern of the trophic structure remains consistent.

3.1.2 Periodic Oscillation

The periodic oscillation is related to the initialisation method and the high initial heterotrophic volume, but they are not present in all result sets. The four spikes in volumes and fluxes that form part of the periodic oscillation correlate with the times one of the largest individuals is consumed as prey. This can be seen in figure 3.1.3h as the four blue dots. The predator for these large prey individuals is an individual that is very similar in size. This can be seen in figure 3.1.3e that show five cyan dots, indicating the times when the highest trophic level was coupled to feed from a size class very near its own. It can also be seen that this process has a relationship to the number of times the highest trophic level reproduces. This is shown as the five blue dots in figure 3.1.3i. Figure 3.1.4b illustrates that during the initial period of damped oscillations the rate of assimilation in quinary producers gain exceeds that of metabolism. This permits them to reproduce for the first time at around 173,000 time steps. Beyond this point, the model dynamics are significantly altered.

When reproduction occurs, the parent's volume is divided and shared evenly between parent and child. This results in both parent and child occupying a slightly lower position in trait space. This provides them with an increased probability of consuming from the quaternary producers. By 200,000 in model time the largest quaternary producers have been consumed. This is evidenced by the drop in the quaternary volume and an increased rate of quinary volume growth between around 173,000 and 200,000 time steps. The quinary producers continue to grow until around 259,000 time steps when they reproduce for a second time.

By the next time step and in the face of reduced prey, the largest quinary producers are coupled to the size class containing their most recent parent and child. Having to share the food supply means the parent and child are not able to grow sufficiently quickly to escape their new predators, and either one of them is inevitably consumed. This event can be seen as the large spikes in the fluxes from consumption by carnivores (figure 3.1.1c) and waste added to the

nutrient pool (fig. 3.1.1d). It is also visible as the sharp drop in quinary volume 3.1.4b. From this point onwards the volumes and fluxes oscillate periodically.

The removal of a quinary producer causes a trophic cascade throughout the entire system. With predation reduced, the population of quaternary producers recovers slightly. This allows the remaining quinary parent or child to assimilate more quickly and grow to rejoin its counterparts. The quinary individuals are recoupled to a quaternary population, and resume a steady consumption that exceeds their metabolic rate. This allows them to grow until they reproduce again.

Different parameter configurations can produce varying results. Those that allow the largest individuals to assimilate in excess of their metabolic rate show a pattern of consumption and reproduction. The constants in table 3.1.1 were selected as the default due to the periodicity with which this cycle occurs. The initial heterotrophic volume and initialisation method populates the system with individuals that permit the trophic cascades to occur. However, it is concluded that the primary driver behind the periodic oscillation are the parameters that control the rate of assimilation and metabolic deduction.

3.2 Unapproximated Configuration

The results in all other sections of this chapter make use of the approximate calculation of effective prey volume (see section 2.4.3). To validate this approach, this section presents results from a model configuration that uses the actual calculation of effective prey volume.

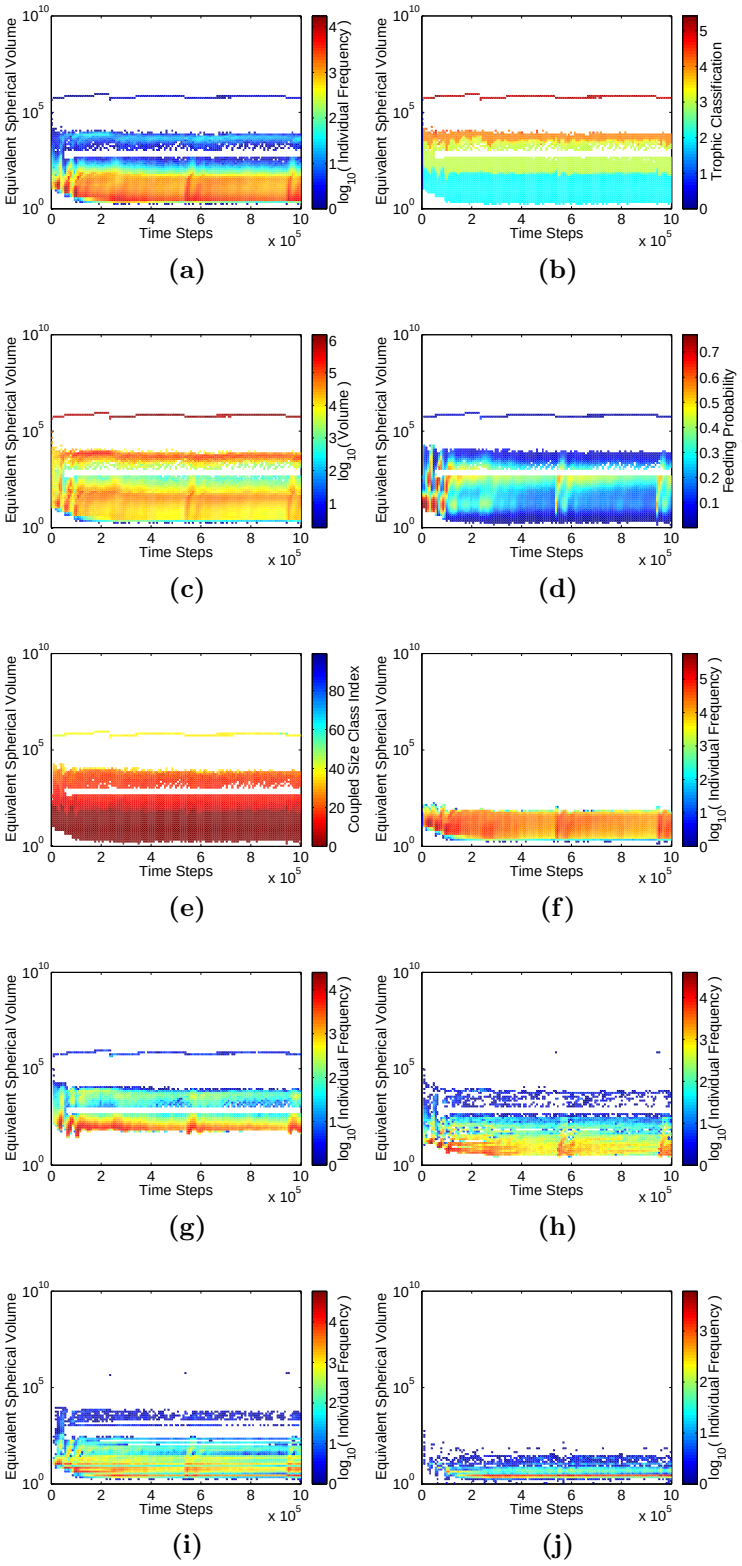

Figure 3.2.1: The evolution of the d size classes on the y-axis, over time on the x-axis. Plots show: **(a)** the number of all individuals, **(b)** the mean trophic classification, **(c)** the volume, **(d)** and the feeding probability of each size class, **(e)** the index to which each size class is coupled, and the **(f)** numbers of herbivores, **(g)** carnivores, **(h)** corresponding prey individuals, **(i)** children, **(j)** and starved individuals.

The results in figure 3.2.1 took more than 3 weeks to produce, whereas the approximated model took around 2 hours 30 minutes. They show that the periodic oscillation discussed in section 3.1.2 has a lower frequency. Figure 3.2.1i shows that the largest individuals are not reproducing as quickly. This is likely due to fact that in this configuration the feeding probability of each individual is calculated before it feeds. This means that the probability of an individual feeding slightly decreases as the smaller individuals are eaten. However, in general there is broad correlation with the results in figure 3.1.3. For this reason the approximated calculation for effective prey volume is considered to be valid.

3.3 Ensemble Configuration

3.3.1 Parameter Evaluation

Altering the parameter values can produce significantly different results. In order to better understand in what ways, some of the parameters have been selected for experimentation. Not all of the parameters will be subject to experimentation. Under certain parameter configurations it may be possible for the system to produce a top-level predator whose volume is the same or very near to v_{large}. This can produce a situation where the growth of the largest individuals is limited by the width of trait space and not by the dynamics of the model. This is the reason for the initialisation condition mentioned in section 2.5; the total volume in the system should be much less than the largest individual volume ($V \ll v_{large}$). The default width of trait space is wide enough to prevent the condition from being broken, even under high volume configurations. The parameters controlling trait space (v_{small} and v_{large}) will therefore not be investigated. This has the added benefit of making the results from each experiment directly comparable.

The model includes a half-saturation constant fraction (K_{frac}) parameter that is used with a type 2 functional response (equation 2.4.16). Since the model also includes the use of a type 1 functional response (equation 2.4.15) for comparison, K_{frac} will remain fixed at its default value. In addition, the model makes use of a size class subset (α) parameter that helps define the subset of individuals that will feed, and those that will be subject to a probabilistic starvation mortality (see equation 2.6.2). Because of this α has a relation-

ship to the metabolic rate (by operating in equivalence to a coeffcient on the feeding probability). As mentioned in section 2.6.1 the α value is kept sufficiently low to reduce the theoretical difference between feeding probabilities at the beginning and the end of feeding, when these are calculated using the approximate effective prey volume. For this reason it is not considered to be an experimental parameter.

The number of heterotrophic size classes (d) was tested and the number of trophic levels in the system were not found to be sensitive to its value. However, different values of d were found to affect the frequency of reproductive events for the highest trophic level over the same period of model time. A lower number of size classes increases the variance of individual volumes in each. Overall this was found to have a similar effect on the outputs as running the model with slightly lower β values. In both cases the rate of reproduction for the highest trophic levels is reduced. Since varying the value of d has no obvious experimental merit, it will remain fixed at its default.

The parameters that are left for experimentation are those that directly alter the rate at which individuals gain and lose volume (γ, ϵ, and k_m), those that control the shape and relative position of the preference function (β, c, and a), those that determine the rate and degree of mutation of heritable traits at reproduction (P_μ, and σ), and those that determine the amount and distribution of volume when the model is initialised (N_{init}, P_{init}, and H_{init}). In addition to these, the model has three switches: one to select either the log-normal or inverse parabolic preference function, one for the type 1 or type 2 functional response, and one to select between the actual or approximated calculation of effective prey volume. Since the unapproximated calculation for effective prey volume has been evaluated against the default model configuration (section 3.2), all experiments hereafter will make use of the approximate calculation of effective prey volume. Experiments will therefore include the four permutations of preference function and functional response.

Table 3.3.1: Tested control switch combinations

Figure Label	Preference Function	Functional Response
a	Log-normal	Type 1
b	Log-normal	Type 2
c	Inverse parabolic	Type 1
d	Inverse parabolic	Type 2

For each parameter that is being investigated, a range of values have been chosen with minimum and maximum values that straddle the default. Each experiment will focus on just two of the parameters and will run the model with every combination values from its prespecified range. The trophic level count, detailed in section 2.7.2 has been chosen as the high-level metric for the model outputs. As a stochastic model, EATSM can produce slightly different results each time (see section 7.2.3). To smooth out stochastic effects on the trophic level count, each experiment will be run three times and averaged to produce the final result.

Isolating and testing just two of the parameters permits the creation of two-dimensional plots, where the x and y-axes represent the range of tested parameter values, and the colour scale will show the mean number of trophic levels from the three sets of results. All other parameter values will be kept at their default. Each experiment will be run for about ten times longer than is required for the initial period of damped oscillation to subside (section 3.1.1). This allows enough time for the system to approximate steady state.

3.3.2 Metabolism

This set of experiments investigate the effect of altering the rates at which individuals gain and lose volume. These are controlled by the parameters that change the flows of energy with an individual, irrespective of food consumed. They are the assimilation efficiency coefficient (γ), the fractional metabolic expense per time step (ϵ), and the metabolic scaling exponent (k_m). Since ϵ uses very small values, it is the only parameter that is tested across a logarithmic range. All others use a linear range of values.

The first set of experiments alters the values of ϵ and γ.

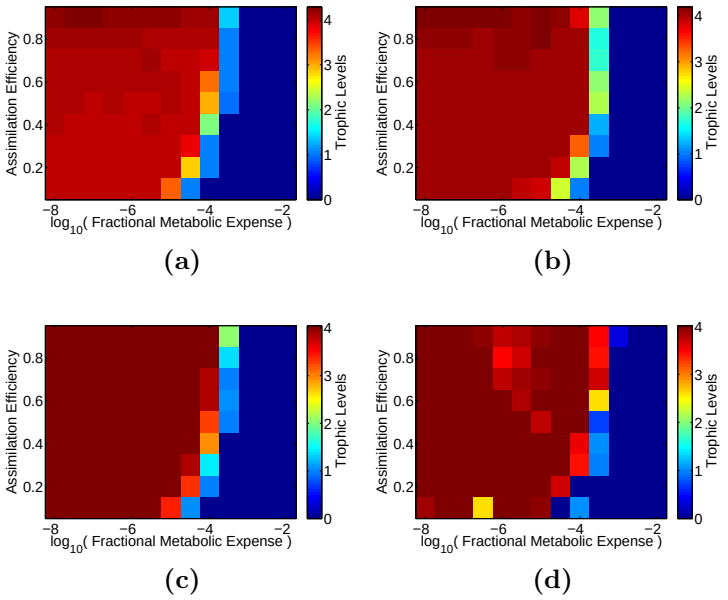

Figure 3.3.1: The mean number of trophic levels from an ensemble of three runs, varying the fractional metabolic expense (ϵ) against the assimilation efficiency (γ) across a range of values. The top two plots use a log-normal preference function with **(a)** a type 1 and **(b)** a type 2 functional response. The bottom two plots use an inverse parabolic preference function with **(c)** a type 1 and **(d)** type 2 functional response.

From the results it is clear that for all combinations of preference function and functional response there are combinations of ϵ and γ values that produce a productive trophic system, and others that cause it to collapse. All plots illustrate that ϵ has the greatest influence on the stability of the system. Despite the small default for ϵ, there is still a narrow range of values that produce stable systems with less than four trophic levels. In general it can be seen that the system either produces four trophic levels, or none at all. Very low epsilon values have no continued additive effect on the number of trophic levels. This suggests that metabolism can permit a stable system, but has a limited effect on the number of trophic levels.

The probability of an individual feeding in a given time step is approximately given by:

$$\alpha \cdot P_f$$

The probability of an individual or size class feeding (P_f) is always going to

be less than one, so individuals will never feed every time step. The default α value means that even with a certain probability of feeding and abundant prey, individuals would still consume only once every 100 time steps. The slight vertical structuring in the plots from figure 3.3.1 can be explained by the fact that individuals generally consume prey whose volume is many orders of magnitude larger than the volume that is lost by metabolism. Metabolic losses are taken at every time step, whereas the assimilatory loss is applied only when food is consumed. The number of trophic levels therefore has a weak positive correlation with the assimilation efficiency, but it only has a major influence in the region of parameter space where it is balanced against metabolisms, i.e. where ϵ is $\sim 10^{-4}$ timestep^{-1}.

When the metabolic rate is high, less energy is available to individuals higher in the trophic system. Even though larger individuals have a proportionally lower metabolic rate, too much energy is lost by the metabolisms of the individuals lower in the food chain. This can be seen in figure 3.3.2 that show the volume fluxes from herbivory and carnivory from one of the three runs using ϵ set at 3.1623e–04 and γ set at 0.5 in figure 3.3.1b above.

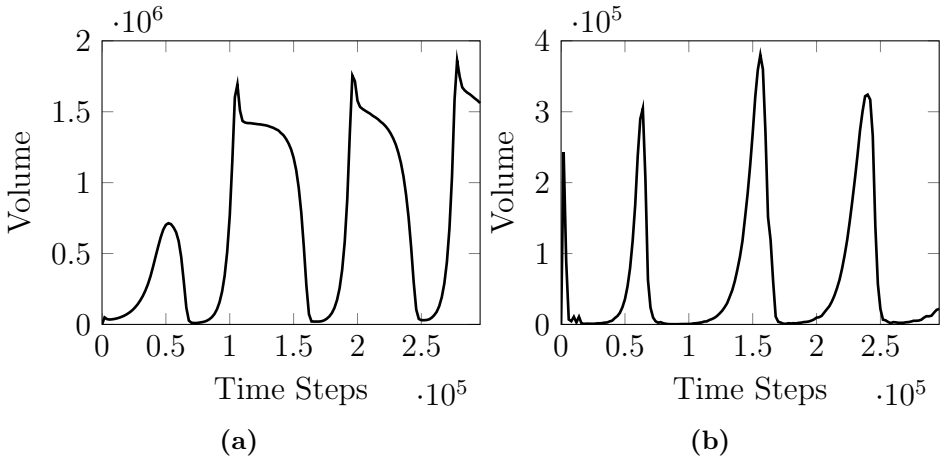

Figure 3.3.2: The volume fluxes from **(a)** consumption of phytoplankton by herbivores and from **(b)** consumption of prey individuals by carnivores, from a single run configured with a log-normal preference function, a type 2 functional response, ϵ set at 3.1623e–04 and γ set at 0.5.

All of the three runs for the parameter combination used for the plots in figure 3.3.2 above show a similar pattern of fluxes from consumption by herbivores and carnivores. When these are compared to those for the same fluxes using the default parameter values (figures 3.1.1b and 3.1.1c) the flux from herbivory

is much greater, and disproportionate to the flux from carnivory. The fluxes here are much more oscillatory and have periods of stopping almost entirely. The configuration produces a two-tier trophic system comprised of secondary and tertiary producers (see figure 3.3.1b). The fluxes in figure 3.3.2 correlate with strong population cycles.

To better compare the results in figure 3.3.2 some additional plots show the same fluxes in a model that uses slightly lower ϵ value of 1e–04 and γ set to 0.5. These are shown in figure 3.3.3 below:

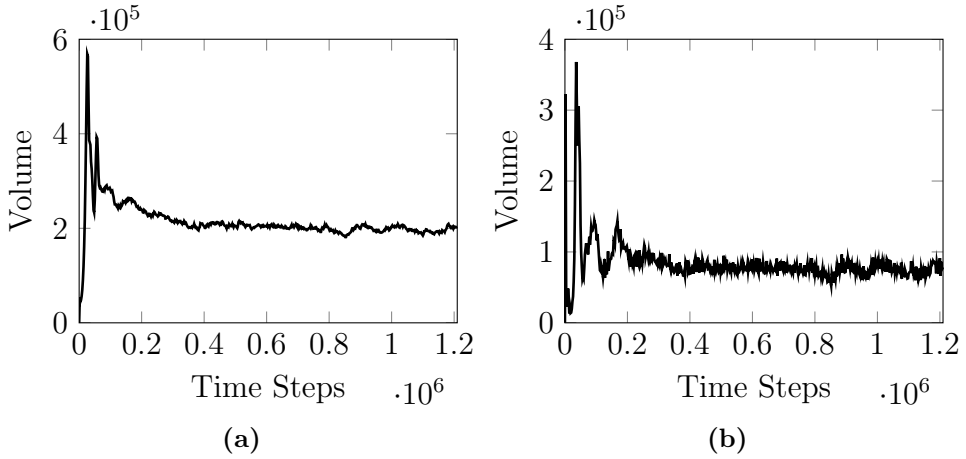

Figure 3.3.3: The volume fluxes from consumption of phytoplankton by herbivores **(a)** and from consumption of prey individuals by carnivores **(b)**. from a single run configured with a log-normal preference function, a type 2 functional response, ϵ set at 1e–04 and γ set at 0.5.

This plots in figure 3.3.3 show the same fluxes as before, in a configuration that produced four trophic levels (see figure 3.3.1b). Comparison with those in figure 3.3.2 emphasises that they are in proportion with each other. If cycling occurs, it is too small to appreciate at the scales of volume shown. Around a third of the assimilated phytoplankton volume is lost to the higher trophic levels. The metabolism is low enough to permit the quaternary and quinary producers to survive, but too high for the largest individuals to reproduce. The dynamics of reproduction that caused the periodic oscillation in the default configuration are not present here. Some configurations in this set supported slightly more than four trophic levels.

The next set of metabolic experiments vary the values of ϵ and k_m.

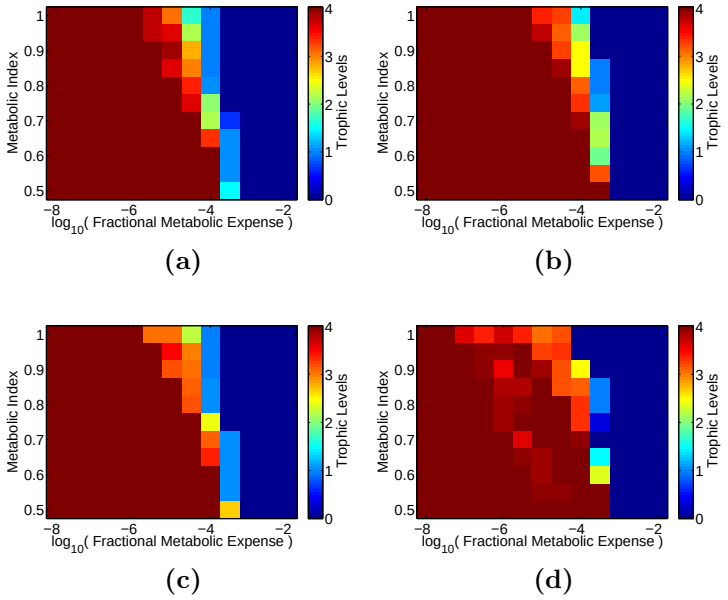

Figure 3.3.4: The mean number of trophic levels from an ensemble of three runs, varying the fractional metabolic expense (ϵ) against the metabolic scaling exponent (k_m) across a range of values. The top two plots use a log-normal preference function with **(a)** a type 1 and **(b)** a type 2 functional response. The bottom two plots use an inverse parabolic preference function with **(c)** a type 1 and **(d)** type 2 functional response.

These results are similar to those in figure 3.3.1. The fractional metabolic expense per time step (ϵ) again has the greatest influence in determining whether the trophic system survives or not. Lower values of k_m give larger individuals a smaller metabolic cost. This promotes the emergence of more trophic levels, but figure 3.3.4 illustrates that it is less effective than ϵ. The efficacy of ϵ at promoting more trophic levels is attributed to the comparatively large range of values tested. However, the results show that there is a significant range of viable k_m values. This is an observation reflected in the contemporary literature on the topic (Glazier, 2005, 2006). Four trophic levels is again the highest for this configuration.

The next set of experiments vary the values of k_m and γ.

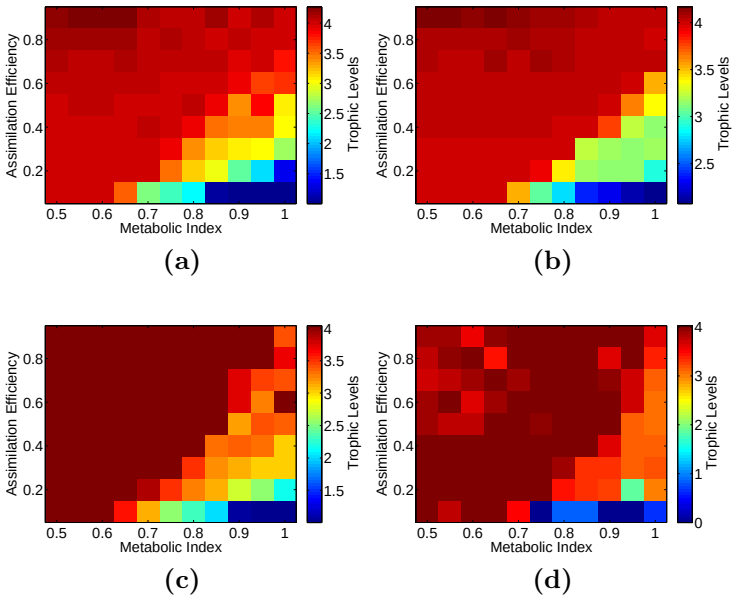

Figure 3.3.5: The mean number of trophic levels from an ensemble of three runs, varying the the metabolic scaling exponent (k_m) against the assimilation efficiency (γ) across a range of values. The top two plots use a log-normal preference function with **(a)** a type 1 and **(b)** a type 2 functional response. The bottom two plots use an inverse parabolic preference function with **(c)** a type 1 and **(d)** type 2 functional response.

From the results in figure 3.3.5 it appears that k_m and γ have a proportional power to determine the number of trophic levels in the system. Both of these parameters were shown to have a weak influence on the number of trophic levels in the earlier experiments. This observation is reinforced by the results in figure 3.3.5d as this was the only one of the four sets of configurations that caused the system to collapse. All of the others at least had a population of secondary producers. Despite this, just over four trophic levels was again the highest.

Four trophic levels is about the maximum for all the combinations of parameters in this section. This suggests that the number of trophic levels inversely correlates with metabolism to a limit, and that this upper limit cannot be exceeded by only reducing the metabolic rate.

3.3.3 Preference Function

These experiments test the effect of altering the parameters that control the size, shape, and relative position of the preference function. These are the preferred prey volume ratio (β), and the width (c) and the height of the feeding function (a). The first set of experiments vary β and c.

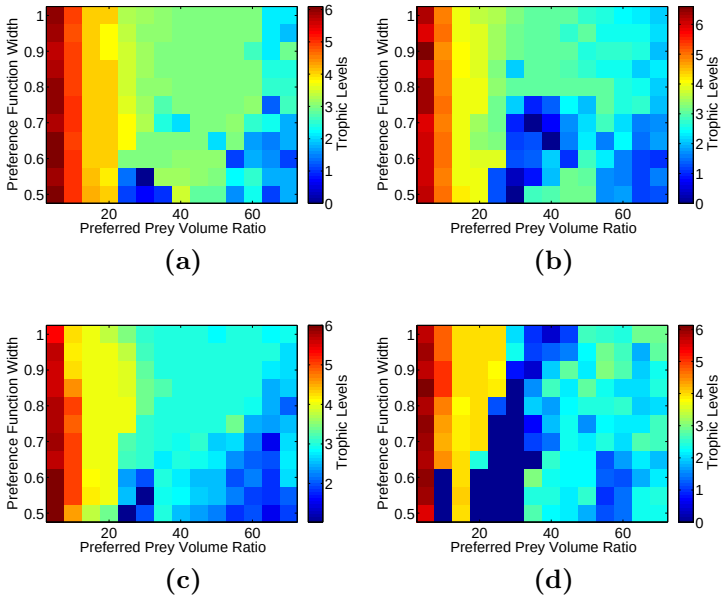

Figure 3.3.6: The mean number of trophic levels from an ensemble of three runs, varying the preferred prey volume ratio (β) against the preference function width (c) across a range of values. The top two plots use a log-normal preference function with **(a)** a type 1 and **(b)** a type 2 functional response. The bottom two plots use an inverse parabolic preference function with **(c)** a type 1 and **(d)** type 2 functional response.

Figure 3.3.6 shows that the number of trophic levels in the system is strongly determined by the value of β. This is reinforced by the empirical results of Jennings and Warr (2003) who found longer food chains in systems where predator-prey body size ratios were smaller. There is some structure to the results that change with different values of c. For certain model configurations there are combinations of β and c values that cause the system to collapse entirely. To examine this further, two of the three runs for a single parameter combination were isolated. The first plots show the numbers of individuals from each of the d size classes over time.

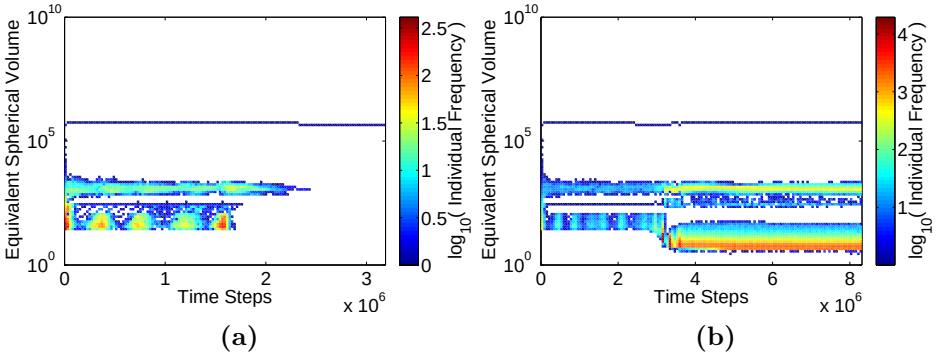

Figure 3.3.7: The number of individuals from each size class over time from two of the three runs configured with a log-normal preference function, a type 2 functional response, β set at 35, and c set at 0.75.

The second set shows the numbers of individuals from each trophic level over time.

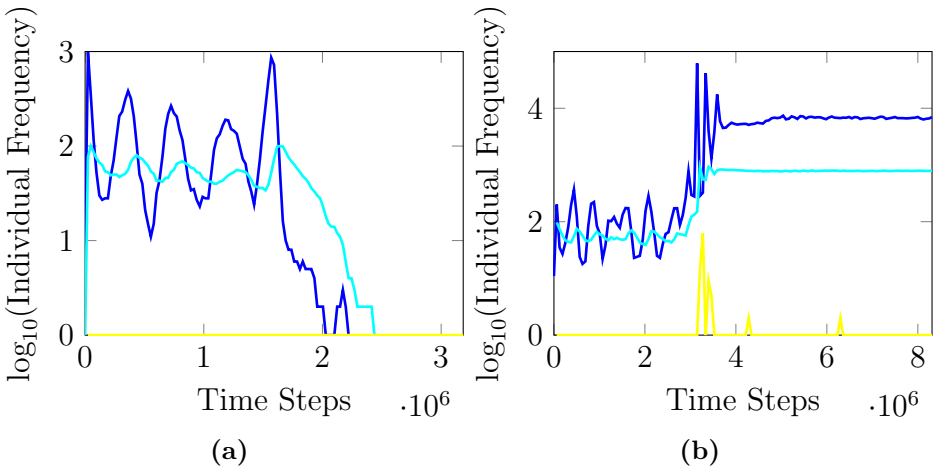

Figure 3.3.8: The numbers of the secondary (blue), tertiary (cyan), and quaternary producers (yellow) over time from two of the three runs configured with a log-normal preference function, a type 2 functional response, β set at 35, and c set at 0.75.

In both cases the system initially exhibits a strong population cycling. The largest individuals in figures 3.3.7a and 3.3.8a are largely inactive. This leaves just the secondary and tertiary producers locked in a boom bust population dynamic. The results in figures 3.3.7b and 3.3.8b illustrate a stochastic variation where the boom bust cycle continues for longer. This allows enough time for the largest individuals to reduce in volume as a result of their metabolic rate and establish their role as quaternary producers before the system col-

lapses. This reduces the grazing on the secondary producers allowing them to reproduce more rapidly. Mutant secondary producers appear that are farther away in volume trait space and are therefore less grazed by the tertiary producers. This ultimately stablises the system. Because the system collapsed after a short space of time, the first set of results have a trophic level count of 0 and the second has 3. The third in the set was much like the first, accounting for the count of 1 in figure 3.3.6b.

Certain β and c values introduce intense population cycling that destabilises some runs. Identical configurations from this section are subject to striking differences in trophic structure as a result of stochastic variation. The results shown in figure 3.3.6 indicate that some parameter combinations are ultimately less stable than others. This instability appears to be a function of both the preferred prey volume ratio and preference function width.

The next set of experiments varies the values of c and a.

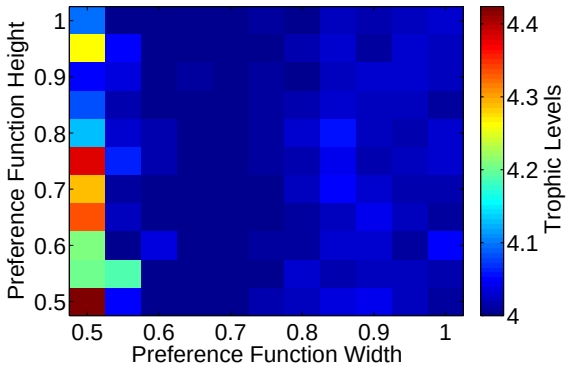

Figure 3.3.9: The mean number of trophic levels from an ensemble of three runs, varying the preference function width (c) and height (a) across a range of values in a model configuration that uses a log-normal preference function and a type 2 functional response.

While varying the height of the preference function changes the character of the trophic system, it can be seen that there appears to be no relationship between the number of trophic levels and the preference function height (a). There is a slight relationship between the c values and the number of trophic levels. This shows that the highest number of trophic levels come from configurations that use the lowest c values.

The preference function alters the effective prey volume experienced by the individual or size class, and therefore affects the probability of feeding. Figure

3.3.9 implies that the metabolic rate is low enough that a reduced probability of feeding has no significant effect on the survival of the trophic levels. However, the turnover in the model is slower. While the higher trophic levels do occasionally consume food they only assimilate enough to cover their metabolic expenses and so do not reproduce. Their reduced grazing also affects the lower trophic levels. This allows smaller individuals to grow more before they are consumed, and appears to create a more competitive element of predation in the system.

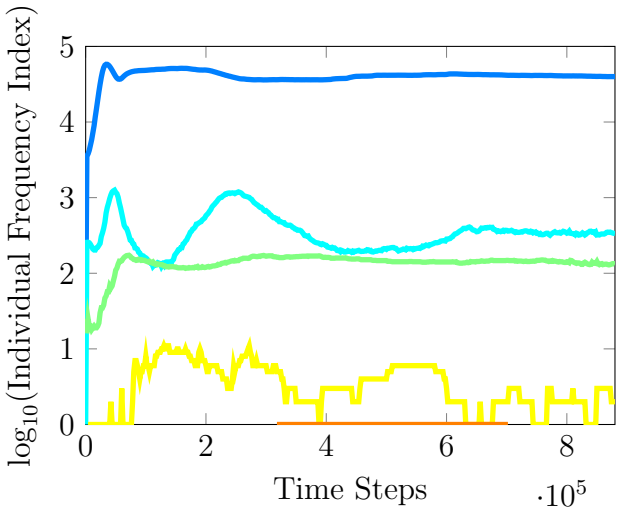

Figure 3.3.10: The numbers of the secondary (blue), tertiary (cyan), quaternary (green), quinary (yellow), and senary producers (orange) over time in a model configured with a log-normal preference function, a type 2 functional response, c set at 0.5, and a set at 0.5.

Figure 3.3.10 shows a run in which largest individuals barely consume at all. The quinary producers are comprised of individuals that are grouped with the quaternary and tertiary producers in volume trait space. Eventually one of the largest individuals consumes a quinary producer, and is calculated to be a senary producer. This senary trophic level persists until the individual that established it consumes from the quaternary trophic level. Since varying the value of a appears to contribute nothing to the model, it will not be investigated any further in this chapter.

3.3.4 Mutation

These experiments test the effect of varying the parameters that control the rate (P_μ) and degree (σ) of mutation of the heritable volume trait.

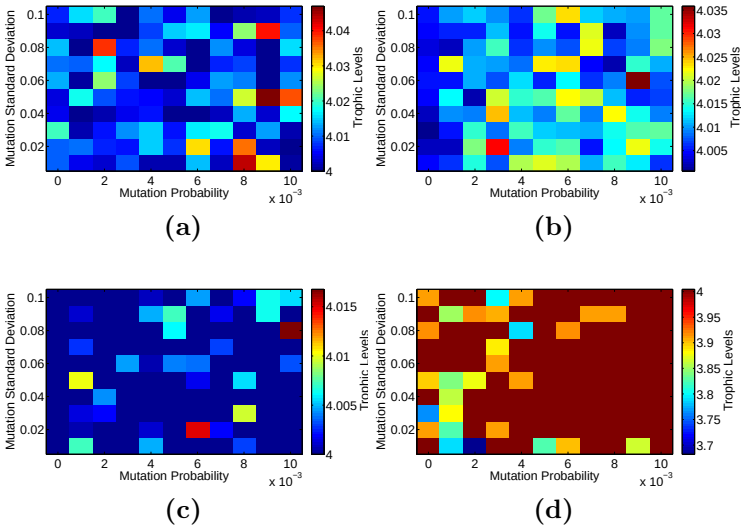

Figure 3.3.11: The mean number of trophic levels from an ensemble of three runs, varying the probability of mutation (P_μ) against the standard deviation of the mutation distribution (σ) across a range of values. The top two plots use a log-normal preference function with **(a)** a type 1 and **(b)** a type 2 functional response. The bottom two plots use an inverse parabolic preference function with **(c)** a type 1 and **(d)** type 2 functional response.

It appears from figure 3.3.11 that changing the rate and degree of mutation has little effect on the number of trophic levels. The results show a lot of noise, and the range of trophic level counts is very narrow when compared to the other results in this section. As with the discussion of the results in figure 3.3.7, it is likely that the rate and degree of mutation may only make a difference when the system is stressed. When pushed to the edge of stability, a mutant can make a substantial difference to the number of trophic levels in the system. In the absence of any such stress, most mutations are probably not viable.

3.3.5 Volume

These experiments test the effect of altering the parameters that control the initial, and therefore total volume in the system. Any individual that exists

in a configuration of EATSM is ultimately comprised out of a fraction of this initial volume. For this reason the trajectory of the system evolution is considered to be very sensitive to the values that determine the initial nutrient volume (N_{init}), the initial and maximum phytoplankton volume (P_{init}), and the initial heterotrophic volume (H_{init}). Higher initial volumes can produce larger populations, which is more computationally expensive. For this reason the model configurations in this section were run for just under 24 hours. Also, In the previous examples different parameter values were varied one against the other. This set of experiments will perform a higher resolution space search of each parameter in isolation.

The first set experiment with the N_{init} value.

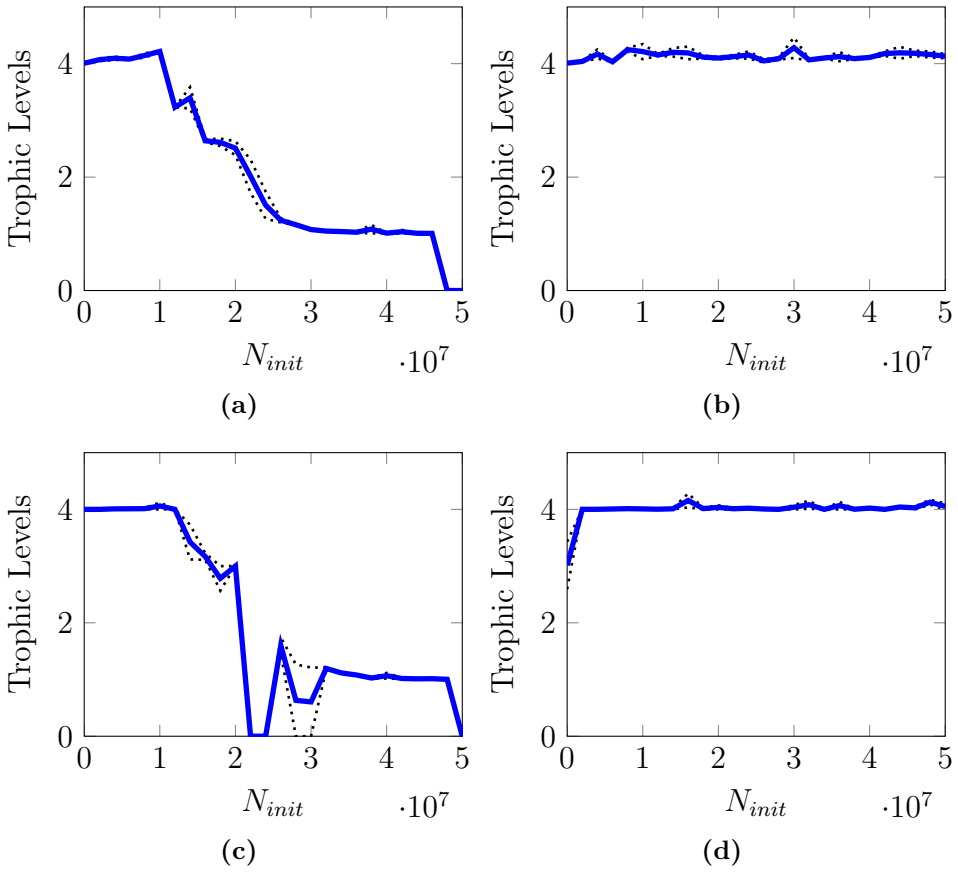

Figure 3.3.12: The minimum, maximum, and mean (blue line) number of trophic levels from an ensemble of three runs, varying the initial nutrient volume (N_{init}). The top two plots use a log-normal preference function with **(a)** a type 1 and **(b)** a type 2 functional response. The bottom two plots use an inverse parabolic preference function with **(c)** a type 1 and **(d)** type 2 functional response.

The results from these experiments highlight an important aspect of the calculation of the feeding probability (P_f). Both the linear (equation 2.4.15) and non-linear (equation 2.4.16) probability functions use the total volume in the system to provide context to the effective prey volume ($\hat{v_e}$). High initial nutrient volumes have no immediate impact on the probability of individuals consuming because N is not counted during the calculation for effective prey volume. However, both equations 2.4.15 and 2.4.16 use the total volume in the system (V) to add context to $\hat{v_e}$ and so P_f decreases with higher values of N_{init}. For this reason the system becomes unstable or collapses completely. The results in figure 3.3.12 therefore contribute to a deeper understanding of the model performance when using the different combinations of preference function and functional response types.

The most stable combination of model functions appears to be the log-normal preference function and the type 2 functional response (figure 3.3.12b). It is the only configuration that does not produce less than 4 trophic levels. Figure 3.3.12d illustrates that the inverse parabolic preference function with the longer run time is enough to see the system become unstable. The log-normal preference function produces an extremely small possibility that individuals will consume others that are near their own volume. This occurs (see section 3.1.2) if the 'preferred' prey is not available. Since the only thing that distinguishes one individual from another is volume, this can be seen to represent cannibalism. Vijendravarma et al. (2013) published evidence for predatory cannibalism when populations of fruit fly experienced a reduction in food availability. This experimental result suggests that cannibalism could be a mechanistic response to food availability. The use of the inverse parabolic function and the default parameter values prevent 'cannibalism', and that ultimately causes increased rates of starvation in some model configurations.

These results also illustrate the differences between the type 1 and 2 functional response. Figure 2.4.4 shows a direct comparison of each functional response. The type 1 functional response generally provides a lower relative chance of feeding, except for higher effective prey volumes. Both figures 3.3.12a and 3.3.12c show a point between N_{init} values of 2e+7 and 3e+7 where the probability of consuming becomes low enough to push the system to the edge of stability. Higher nutrient volumes provide enough volume for the system to sustain itself when it is later converted to heterotrophic volume. However, the period when that volume was unavailable to the heterotrophs reduces the

number of trophic levels exhibited by the system. The rigid mechanisms of this version of EATSM mean that once a trophic level collapses, it is very unlikely to return.

These experiments vary the P_{init} value.

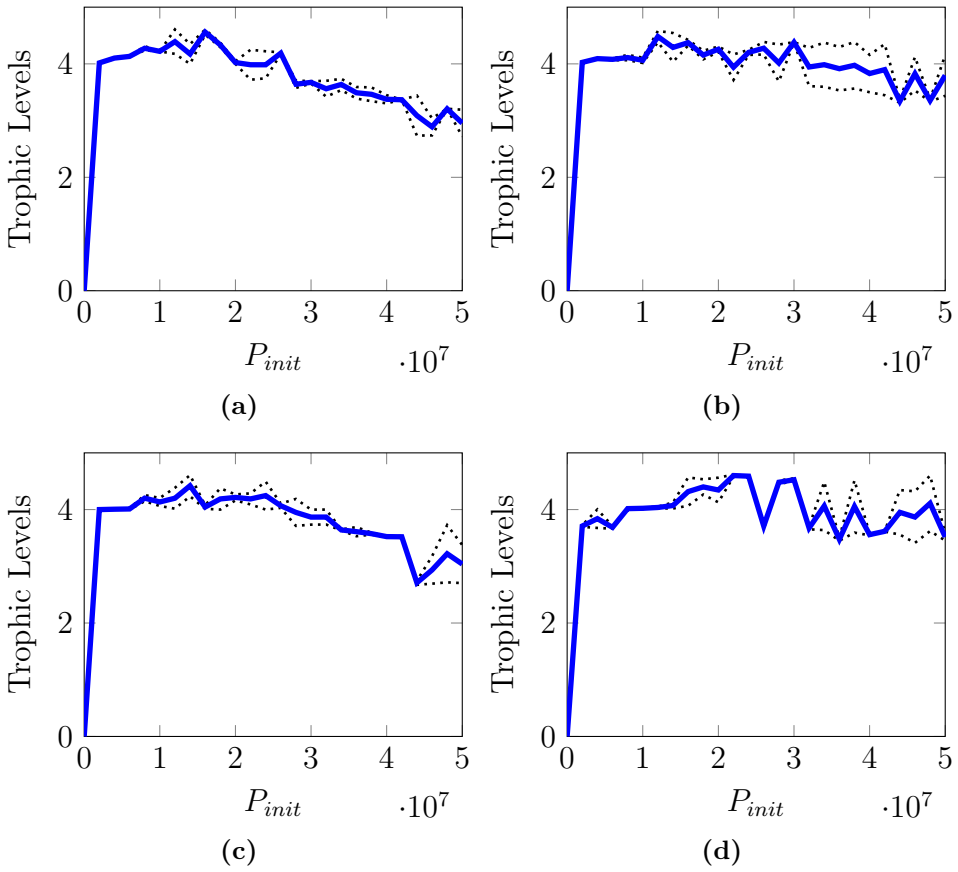

Figure 3.3.13: The minimum, maximum, and mean (blue line) number of trophic levels from an ensemble of three runs, varying the initial/maximum phytoplankton volume (P_{init}). The top two plots use a log-normal preference function with **(a)** a type 1 and **(b)** a type 2 functional response. The bottom two plots use an inverse parabolic preference function with **(c)** a type 1 and **(d)** type 2 functional response.

All the results above show a counter-intuitive drop in the number of trophic levels as the phytoplankton is increased. This reflects the fact that higher volumes provide more material to build new individuals. Since the phytoplankon is immediately accessible, it is rapidly assimilated by the herbivores. This produces many new individuals. When combined with the log-normal preference function and type 2 functional response, the number of heterotrophs exceeds 6e+06. Computation runs extremely slowly with populations that large, even

with the approximated calculation of effective prey volume. The system is not able to compute enough time steps to show the stable emergence of higher trophic levels, even though they do begin to appear. For this reason, the trophic level count is constrained by the amount of real time the model was run for.

This set of experiments varies the value of H_{init}.

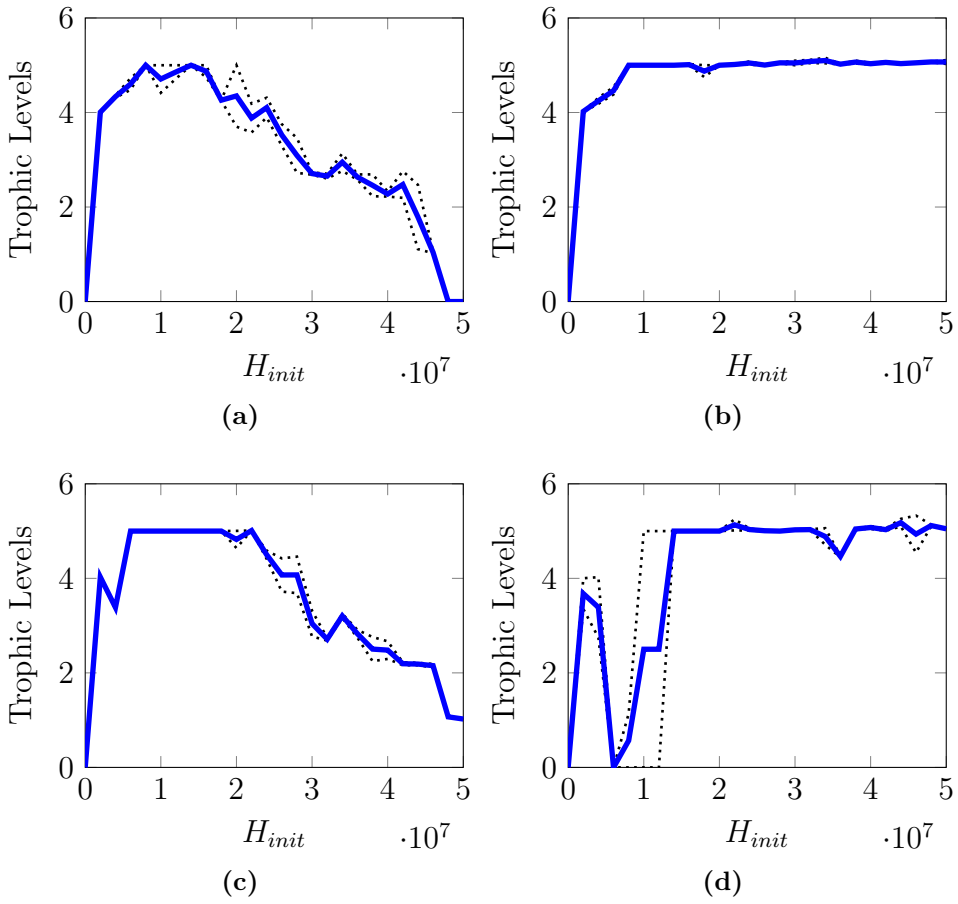

Figure 3.3.14: The minimum, maximum, and mean (blue line) number of trophic levels from an ensemble of three runs, varying the initial heterotrophic volume (H_{init}). The top two plots use a log-normal preference function with **(a)** a type 1 and **(b)** a type 2 functional response. The bottom two plots use an inverse parabolic preference function with **(c)** a type 1 and **(d)** type 2 functional response.

The results here show that higher initial heterotroph volumes seed the size classes with a higher number of individuals occupying a greater range of viable trophic positions. This causes an initially high probability of consuming for H_{init} values above zero. The aggressive rates of predation cause a desta-

bilisation of the trophic levels. A sudden drop in heterotroph volume causes a sharp rise in the nutrient volume. This produces reduced probabilities of feeding. The rate of material flow through the trophic levels is reduced. For some configurations one or more trophic levels disappear completely. Some continue to function with a reduced number of trophic levels, others collapse.

The specific pattern of the results shown in figure 3.3.14 are again seen to be a reflection on the combinations of preference function and functional response, and the rates of feeding. The type 1 functional response appears to produce a decreasing probability of feeding for higher H_{init} values. Use of the inverse parabolic function and type 2 functional response with increasing H_{init} values (figure 3.3.14d) appears to cause aggressive rates of predation that destabilise the system. However, there are H_{init} values beyond which the system is prevented from driving itself into extinction. The combination of log-normal preference function, and type 2 functional response appears to be the most stable across the tested H_{init} values.

In the set of experiments below the initial heterotrophic volume (H_{init}) was reduced from its default value in increments, and the difference added to the nutrient pool. This kept total volume in the system fixed at 2e+06.

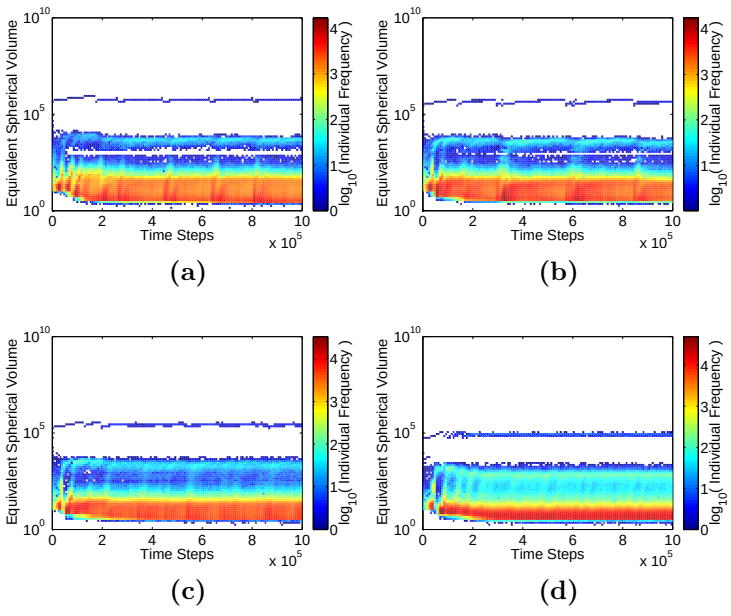

Figure 3.3.15: The number of individuals from each size class over time from models configured with initial heterotrophic volumes of **(a)** 1e+06, **(b)** 7e+05, **(c)** 4e+05, and **(d)** 1e+05. All used a log-normal preference function and a type 2 functional response.

The results in figure 3.3.15 show that the trophic systems function in a similar way, but with a different dynamic. Each configuration shows variation in structure where those that use less initial heterotrophic volume occupy a narrower region of volume trait space. The volume of the largest individuals appears to determine a ceiling for the rest of the system. It is considered that the model itself restricts the trophic system from evolving to occupy a greater width of volume trait space.

This limitation was noticed during development of the model and is the reason for the initialisation method described in section 2.5. This spread the initial volume across trait space, seeding the first size classes with sufficient trait variation to produce a system that worked. This was at the cost of determining the nature of the trophic system. Despite this, the four model configurations that produced the results in figure 3.3.14 all had a trophic level count of about 4. This demonstrates the adaptive potential of the individuals, and how that contributes to an adaptive whole. It also highlights that in this version of the model, the emergent trophic structure is strongly determined by the initial conditions.

The cause behind this is considered to be the current abstract method of using constant thresholds for reproduction (see section 2.6.4) and starvation (see section 2.6.3). These introduce an element of rigidity to the system that have repercussions in terms of its evolvability. The materially closed and conserved nature of the model means that the volume of the parent has to be shared with a child. The imposed, mechanistic point of starvation implied a basic method for reproduction. One in which parents grow to twice their heritable volume in order that a clonal child start life with zero probability of starvation. This means that parent and child would be unlikely to have more than twice the heritable volume of the parent to share.

Mutations that increase the heritable volume trait a significant distance from the parent would also increase the chance of the child starving. The only way such a mutant may survive is if it manages to assimilate enough to sufficiently reduce its chances of starving on the next time step. There is little likelihood of this happening. However, children can mutate lower in volume trait space. Doing so would increase their reproductive fitness. It would provide a child with an excess of volume that would bring them instantly nearer to their reproduction threshold. However, the preference matrix (figure 2.4.3) shows

that small individuals would have a very low probability of feeding. For certain parameter combinations EATSM would undoubtedly expose small individuals to a trade-off between the rate of assimilation and metabolism.

There may also be additional predatory controls that prevent mutations higher in volume trait space. For individuals not in the highest trophic level, growth within an active trophic system would likely increase the chance of being consumed by larger individuals. Growth of individuals in the highest trophic level would reduce the probability of consuming as the available prey would be relatively more distant from the middle of their preference function. In this way mutations of the heritable volume carries trade-offs.

3.3.6 Size Spectra

Sheldon et al. (1972) collected data on the concentration of particles in the surface and deep waters of the Atlantic and Pacific Oceans within size classes approximately in the range 1–100 μm. They found variation between geographic locations and depths, but that there was similar amounts of material in logarithmic size classes. The consistency in the data led to the hypothesis that roughly equal concentrations of material occurs at all particle sizes in the range 1–$10^6\mu$m. They extended this hypothesis to the pelagic ecosystem and reinforced Elton's (1927) ecological pyramid by proposing that there were more smaller organisms than large ones, and the volumes of each would be approximately the same. Sheldon et al. (1972) acknowledged that organisms generally feed on smaller prey, and that for a species to maintain a constant volume the rate of production must vary inversely with somatic size.

Platt and Denman (1977) challenged the conjecture of Sheldon et al. (1972) and asserted that at steady-state the total biomass in each size class decreases with body size. They defined the "normalised size spectrum" ($\beta(w)$) as the total biomass ($b(w)$) in the size class characterised by weight (w), divided by the width of that size class (Δw):

$$\beta(w) = \frac{b(w)}{\Delta w}$$

Since volume is used interchangably with mass (and weight) here, Platt and Denman's (1977) equation can be redefined in terms of volume. If we say that

the total volume of size class i is given by $v(i)$, and use the discrete size class vectors defined in section 2.4.2, the normalised size spectrum of EATSM can be redefined as:

$$\beta(i) = \frac{v(i)}{v_b(i+1) - v_b(i)} \tag{3.3.1}$$

Equation 3.3.1 has been used with the data shown in figure 3.1.3c at the end of the model run (at 1e+06 time steps), and the result is shown in figure 3.3.16 below.

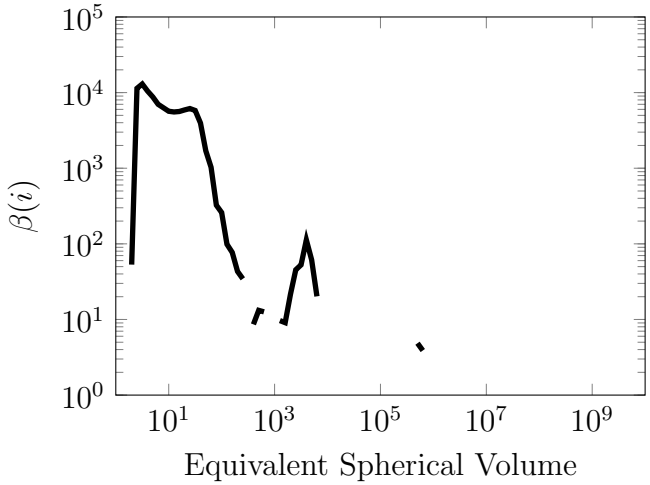

Figure 3.3.16: The normalised size spectra of EATSM based on Platt and Denman's (1977) method. Data were taken for the volume in each size class at 1e+06 time steps from those plotted in figure 3.1.3c.

The data in figure 3.3.16 certainly exhibits a negative gradient, as Platt and Denman (1977) suggested. However, it should be noted that their method for viewing the size spectra is not the only one. Sheldon et al.'s (1972) hypothesis established an approach for viewing data on the size distribution of individuals in an ecosystem that has been adapted by many authors over the years (Dickie et al., 1987; Gaedke, 1993; Quinones et al., 2003; Benoît and Rochet, 2004; Rossberg, 2012).

Dickie et al. (1987) found two size-dependent processes that determined the size-spectra. They acknowledged the well established body-size-metabolism relationship, but also presented analysis that showed the spatio-temporal distribution of species is critical to the state of the whole system. This led to the conclusion that populations cannot be described as sums of individual

attributes. Gaedke (1993) used seasonal changes in the size spectra of a phytoplankton community and a metabolic scaling law to estimate the efficiency of energy transfer between trophic levels. The slope of the 'size distribution of metabolic activity' indicated transfer efficiency, and was therefore a measure of how productive the system was. This approach has been extended for use in ecosystem management to assess the state of commercially exploited systems (Rossberg, 2012).

Jennings and Blanchard (2004) constructed size spectra of a North Sea fish community. The data were collected at 74 locations during a period from August to September 2001. The size spectra was plotted as the logarithm of the body mass, against the logarithm of the average biomass of that size class. This approach has been appropriated here and the results are plotted in figure 3.3.17 below.

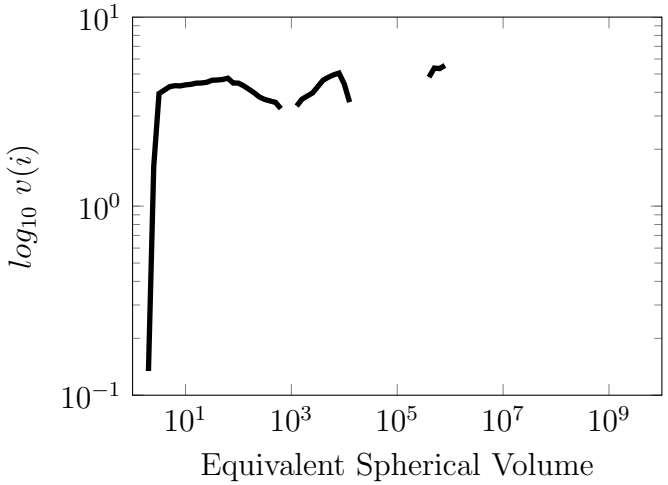

Figure 3.3.17: The size spectra of EATSM based on Jennings and Blanchard's (2004) method. Data were taken for the volume in each size class and averaged from 5e+05 to 1e+06 time steps from those plotted in figure 3.1.3c.

As before the volume data are taken from figure 3.1.3c. However, Jennings and Blanchard (2004) used a more rigorous data sampling progress. To approximate this and instead of plotting the data from a particular time step, the average volume from each size class within a range of time steps is plotted in figure 3.3.17 above. The gradient of this size spectra is closer to zero. This is in contrast to the results of Jennings and Blanchard (2004) who showed a negative gradient for their data.

Rossberg (2012) established a slightly different method for plotting a size spec-

tra. Reviewing several sets of published data from natural systems, the size spectra ($\beta(i)$) calculation for each size class i was described as the product of the biomass in size class i ($b(i)$) and the mid-point of that size class (m_i) divided by the linear width of the mass interval (Δm_i).

$$\beta(i) = \frac{b(i) \cdot m_i}{\Delta m_i}$$

As before, this method has been redefined for use with volume data from EATSM.

$$\beta(i) = \frac{v(i) \cdot v_m(i)}{v_b(i+1) - v_b(i)} \tag{3.3.2}$$

Much like the approach of Jennings and Blanchard (2004), Rossberg (2012) used averages of data taken over a period of time. For that reason data from each size class were again taken from those plotted in figure 3.1.3c and were averaged from 5e+05 to 1e+06 time steps. The result of this is shown in figure 3.3.18 below.

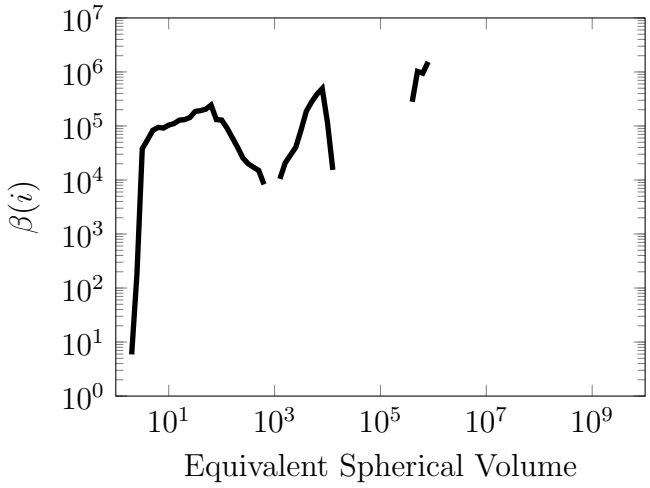

Figure 3.3.18: The size spectra of EATSM based on Rossberg's (2012) method. Data were taken for the volume in each size class and averaged from 5e+05 to 1e+06 time steps from those plotted in figure 3.1.3c.

Some size spectra plots in Rossberg (2012) showed peaks and trophs, and some showed gaps in the data. These patterns superficially appeared to mark the positions and boundaries between trophic levels. However, all the plots showed a general gradient of zero. The size spectra plot in figure 3.3.18 also gestures

to the positions and boundaries between trophic levels, but with a positive gradient.

The differences between the size spectra plots from the literature and those presented here may be due to the method by which the size classes are initialised (see section 2.5). However, it is considered more likely that the assumption that all material has a constant density is the cause. This assumption was made in order that volume can be directly comparable with mass. In pelagic ecosystems phenotypic density appears to evolve in order to balance feeding strategy (see chapter 5) and metabolic rate (Kiørboe, 2011). In addition, Gaedke (1993) pointed out that allometric scaling and the often assumed rules of a size-structured trophic system break down at bacterial scales. While it may be convenient to use simplistic descriptions of life, it seems that there is always something in the missing detail. Despite this, the plots in this section at least provide a way to qualitatively compare the results from EATSM with data from the natural world.

3.3.7 Conclusions

There were several key observations in two major categories from the results in this section. The science conclusions are summarised below:

1. Dynamic trophic levels.
2. Lotka-Volterrra population cycling between the trophic levels.
3. 'Cannibalism' appears when populations experience reduced food.
4. The metabolic rate significantly affects the number of trophic levels.
5. The assimilation efficiency more weakly affects the number of trophic levels.
6. There is a wide range of viable metabolic scaling exponent values.
7. There is a limit to the number of trophic levels that cannot be exceeded with altering the metabolic rate or the assimilation efficiency.
8. The preferred prey volume ratio strongly determines the number of trophic levels.

9. The height of the preference function has very little effect on the number of trophic levels, but does influence the rate of turnover.
10. The rate of mutation has a negligible effect on the system.
11. High initial nutrient volumes increase the time that is needed to reach a stable/repeatedly oscillation trophic structure.
12. High initial/maximum phytoplankton volumes slightly reduce the number of trophic levels.
13. High inital heterotrophic volumes cause more aggressive predation that destabilises the system.
14. A combination of log-normal preference function, and type 2 functional response was the most stable across the ranges of parameters tested.

The conclusions of the model are listed below:

1. The approximate calculation of effective prey volume is sufficiently like the unapproximated calculation to justify its use.
2. Outputs from configurations that push the system to the boundary of survival can produce stochastic variation.
3. The heterotroph initialisation method sets the variety of heritable volume trait values in the system.

4 The Evolution of Reproductive Invesment in Offspring

4.1 Introduction

Interspecies comparisons can reveal enormous phenotypic variation (Roff, 1992; Stearns, 1992). These differences are in some cases matched by intraspecies comparison of individuals at different ages and points of development. The ways in which organisms change over time refer to their specific life history. Life history theory has been developed alongside work on trade-offs (Stearns, 1989). A trade-off refers to the costs paid in the currency of fitness when a beneficial change in one attribute is causally linked to a detrimental change in another (Reznick, 1985; Stearns, 1989; Roff, 1992). Life history analysis reveals that the schedule of development is intimately related to the timing of reproduction and mortality. For example, theory predicts that *reduced juvenile survival will select for delayed maturation and decreased reproductive effort, and reduced adult survival will select for the opposite* (Reznick et al., 1990). For most organisms, reproduction represents the exchange of a set of capable adult individuals for a different set of resource deplete and vulnerable individuals (Roff, 1992). It is therefore no surprise that the evolved reproductive strategy requires some form of obligate compromise. In addition to the age and size at maturity, organims can vary significantly in their brood size and relative size at birth (Stearns, 1977, 1992).

David Lack (1947) published a thorough review of the literature and data on bird clutch-sizes in an attempt to find the ecological drivers of the parental investment in offspring. Latitudinal patterns in species' reproductive strategies prompted the suggestion of a causal link between the evolution of life history traits and the environmental conditions. General correlations between disparate species experiencing similar ecological conditions prompted Lack to propose his 'food-limited' hypothesis. This treats food availability, or the rate at which it can be gathered as the force that determines clutch size. More than 20 years later, Ricklefs (1970) challenged this idea and offered an alternative model that placed predator-prey interactions at the centre of the evolution of clutch size. He pointed out that organisms evolve to maximise their resource gathering and reproductive success, whilst minimising that of their predators.

This process gives rise to an 'arms race', where a change in predator strategy selects for an evolutionary response in the prey. The balance between the two would ultimately be determined by potential rates of evolutionary change, which may be constrained by the adaptability of predator and prey. This led to the 'counteradaptation' hypothesis, that asserts that clutch size represents a single facet of a coevolutionary dynamic.

There is evidence that for a number of species, the genotype can express a range of phenotypes depending on the environmental conditions (Stearns and Koella, 1986; Stergiou, 1999). This concept is referred to as a reaction norm. There is also evidence that the schedule of development is tied to interactions with predators (Beckerman et al., 2010). Collectively, this work implies that an organism's size can be due to epigenetic changes. Stearns and Koella (1986) acknowledged this phenotypic plasticity and produced a model that attempted to predict an organism's schedule of development as a function of a dynamic environment. This work necessarily included assumptions about fitness, age distribution, and the conditions for juvenile mortality. The predictions it generated were found to correlate with data for fish. However, Day and Rowe (2002) questioned this work. They asserted that current life history theory failed to satisfactorily explain why for example, many species mature earlier when experiencing high-growth. They emphasised the fact that many species need to make certain ontogenetic tranisitions before being able to reproduce. This work led Day and Rowe (2002) to propose an alternative model that predicted that individuals may mature sooner or later when exposed to poor growth conditions, depending on how close they are to any such threshold. However, it was found that the model did not apply generally. This was attributed to a lack of data regarding the physiological mechanisms underlying ontogeny.

Despite the literature that acknowledges the plasticity in the life history of an organism, there is a parallel thread of research that considers life history evolution to have genetic, rather than an epigenetic basis. One experimental study on life history evolution was carried out on *Daphnia magna* (Edley and Law, 1988). Two cloned populations were exposed to two culling regimes. One targetted small individuals, and the other targetted large individuals. After 150 days of applying the culling regimes it was found that individuals from each population expressed differing life histories. The population exposed to selection of small individuals grew rapidly to adulthood. Constrasting this,

the population exposed to increased adult mortality exhibited slow growth. In both cases it was found that the evolved life history resulted in minimal time spent in the life stage when individuals were most at risk of selection. Edley and Law (1988) acknowledged that culling at least temporarily reduced the population densities, but they saw no reason to consider that significant to their results. They were certain that their subject species had undergone a genetic change as a result of size selective mortality. Edley and Law (1988) considered their experiment analogous to commercially exploited systems and stressed the importance of effective ecosystem management.

Reznick et al., (1990) published details of a long-term study that confirmed how the general age of mortality affects reproductive investment. The experiment was performed on guppies (*Poecilia reticulata*) as earlier research had illustrated a relationship between the specific life history and the type of predator with which the guppies live (Reznick et al., 1990). At one location the main predator was *Crenicichla alta*. This particular species consumes large, sexually mature guppies. At another site the main predator was *Rivulus hartii*; a species that consumes smaller, sexually immature guppies. In 1976, a population of guppies that had previously experienced predation from *Crenicichla alta* were introduced to a site that previously contained *Rivulus hartii* and no guppies (Reznick et al., 1990).

Data collected over the subsequent years revealed persistent changes in the life history attributes of the guppies at the introduction site (Reznick and Endler, 1982; Reznick, 1982a). Females initiated reproduction at a larger size and produced larger offspring. In dry seasons there was a trend toward lower reproductive effort and smaller brood sizes, but not in wet seasons. Subsequent generations from both populations were later reared in a common laboratory environment (Reznick, 1982a,b). The phenotypic differences were found to persist, but the brood size increased after two generations. Reznick et al. (1990) considered this enough evidence to conclude that the guppies experienced genetic evolution of their reproductive strategy.

Martinez-Garmendia (1998) constructed an individual-based, evolutionary model that was parameterised for cod (*Gadus morhua*). The purpose was to test for genetic changes in response to, and set bounds on selective fishing mortality. With the benefit of data the model was parameterised to describe different fishing scenarios. The results showed that evolution of fish populations could

be brought about by fishing, but that it might be too slight to be noticed by empirical study. Dunlop et al. (2007) produced a model that attempted to ascertain the impact of fishing on smallmouth bass (*Micropterus dolomieu*) at two separate lakes. It was parameterised with empirical data collected since the 1900s. The model predicted that populations exposed to high size-dependent mortality will evolve toward smaller sizes and younger ages of maturation. Despite this, the data showed that the lakes experienced different rates of fishing yet produced no detectable evolutionary divergence in the subject species.

Both of these model studies attempted to answer questions about the potential evolutionary response of specific species experiencing significant rates of size-specific mortality. With the benefit of data with which to parameterise the models they were able to produce quantiative, measureable predictions. However, both studies took a very reductionist view of evolution. The prey were not represented, and neither were the effects of non-human predators. The species were thereby decoupled from the environment on which their evolution intrinsically relies. While predator-prey interactions may still be viewed as central to the trade-offs surrounding a reproductive strategy, it is considered that modelling only one species and one source of predation undermines any attempt to deliver robust predictions. The reproductive strategy adopted by a species may very well be a function of its relationship to its predators and prey. This suggests there may still be value in Lack's (1947) food limited hypothesis.

Abrams and Rowe (1996) acknowledged that previous experimental work had revealed evolutionary change that could be attributed to both genetic change and phenotypic plasticity. They set out to describe the effects of non-selective predation on a population. A number of mechanisms were identified by which it was suggested that life history evolution could be brought about, without imposing a size-dependent mortality regime. To explore and test these ideas a theoretical model was constructed. The results highlighted that life history evolution could be brought about through indirect effects, and that often this would oppose and be larger in magnitude than the direct effect. Contradicting the assertion made by Edley and Law (1988), they found that a reduction in prey population density brought about by predation has density dependent consequences that can significantly influence life history evolution. Their findings reflect the work of Dickie et al. (1987) who pointed out the "homeostatic" mechanisms in a community structure that are emergent properties of

the spatial interactions between individuals.

Life history theory predicts: *reduced juvenile survival will select for delayed maturation and decreased reproductive effort, and reduced adult survival will select for the opposite*. It is considered that the relative size of offspring will change depending on the trophic position of both parent and child. Top-level predators will likely harm their reproductive success by producing many small children, as doing this would place offspring among individuals experiencing higher levels of predation. Conversely, heavily predated individuals would likely lower the cost of child mortality by spreading the risk over a larger number of smaller offspring. To investigate this hypothesis EATSM will be modified to permit the evolution of parental investment in offspring in a trophic context. It is hoped that this may yield insights into the ways in which the reproductive strategy employed by an organism is balanced by the effects of predation, and the availability of prey. We are effectively asking *do the predictions of life history theory completely explain the evolution of reproductive effort?* In asking this question, we are also evaluating the validity of Lack's and Ricklefs' hypotheses.

4.2 Method

EATSM is founded on the principle that individuals are materially coupled to their environment. The use of a functional response makes the rate of consumption, and subsequent growth a function of prey population density. Similarly, individuals are at risk of predation by others. Thereby making their reproductive success a function of prey and predator population densities, as well as their own. However the current representation of reproduction and starvation described in chapter 2 is too rigid to permit the evolution of life histories. This section therefore describes a number of changes that refine some of the earlier methods. All other methods are unchanged.

4.2.1 Individuals

In the previous version of the model, individuals were generally initialised with a volume that was the same or near their heritable volume. Reproduction occured when they reached twice their heritable volume, at which time their volume was divided between parent and child (see section 2.6.4). In this ver-

sion individuals can start life much smaller than their heritable volume, and reproduction occurs when they grow to exceed a specific fraction of it. To model this individuals carry an additional heritable trait. It controls the fraction of volume that is subtracted from a parent and given to a new child, when and if that individual should reproduce. This trait is referred to as the child volume fraction and is given the symbol Ω. There is a constraint on the value a child volume fraction can take.

Allowing the trait to take any value between 0 and 1 introduces a mathematical inconsistency that would allow the smallest individuals to continue producing smaller and smaller children, potentially to the maximum extent allowable by the numerical precision of the model. In addition, there must be a minimum size, below which an organism can not include all the necessary machinery for feeding, metabolism and reproduction. In the model this minimum size is represented by v_{small}.

To keep the model from producing children that are smaller than v_{small}, Ω has a minimum value (Ω_{min}) that is the multiplicative inverse of the heritable volume (v_h).

$$\Omega_{min}(v_h) = \frac{v_{small}}{v_h} \tag{4.2.1}$$

The range of possible Ω values is therefore limited by the heritable volume (v_h).

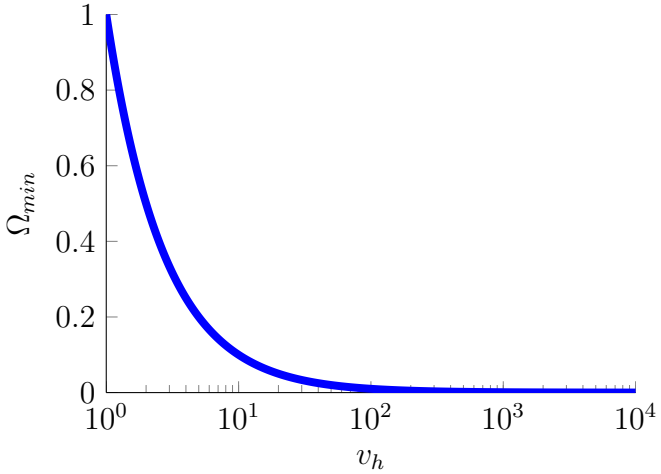

Figure 4.2.1: Minimum child volume fraction trait (Ω_{min}) values as a function heritable volume (v_h).

Using an unprocessed heritable trait (g - a value between 0 and 1), Ω is defined by:

$$\Omega = g \cdot (1 - \Omega_{min}) + \Omega_{min} \tag{4.2.2}$$

4.2.2 Starvation

Empirical evidence shows that many marine organisms continue to grow toward an asymptotic size after reaching sexual maturity (Andersen and Beyer, 2006). Some population-level models have included representations of this pattern of growth (Andersen and Beyer, 2006; Hartvig et al., 2011). However, as explained in section 2.6.2, somatic growth of individuals in EATSM is a mechanistic function of volume consumed. A solution that would reconcile the mechanistic representation of growth and reproduction, with growth toward an asymptotic volume is considered to be unnecessarily complex. For this reason the heritable volume (v_h) will continue to serve as a fixed threshold for reproduction in the context of individuals potentially starting life well below it. The change in perspective of this trait means that it is now referred to as the volume at maturation.

The potentially large change in somatic volume over time means that the probability of starvation can no longer be calculated against a constant value, else children would likely starve immediately after being born (see section 2.6.3). A growth function is used to calculate a dynamic threshold for starvation that follows an expected growth trajectory. Classical models consider somatic growth to be a function of time (Essington et al., 2001). An example such as the von Bertalanffy growth function can be fitted to size-at-age data and incorporated into predictive models. However, these functions are based on empirical observation of natural organisms. The simplistic representation of individuals in EATSM ignores details of complex internal dynamics, such as absorption rates (e.g. Atkinson et al. 2012). It is believed that these are at the centre of why biological organisms can exhibit smooth and consistent growth under variable conditions. The mechanistic representation of growth in EATSM means that surviving individuals often exhibit stochastic growth, or they enter a consistent pattern of growth and reproduction in which changes to volume over time take the form of a sawtooth wave. To avoid these complexities, a linear growth trajectory is used as the simplest starting point.

In the absence of a mechanistic model of growth *and* starvation, the approach here is to assume that for any age there is an ideal volume that an individual should be at. The ideal volume (v_t) necessitates that individuals' volumes at birth (v_r) and ages in abstract time steps (t_a) are recorded. An additional parameter (λ) is introduced to control the rate of expected growth over time. The expected age at maturation (t_e) is therefore defined by:

$$t_e = \frac{v_h - v_r}{\lambda} \tag{4.2.3}$$

Following a linear form, the expected volume of an individual (v_t), born with a volume v_r and age t_a is defined by:

$$v_t = \begin{cases} v_t = v_r + \lambda \cdot t_a & \text{if } t_a < t_e \\ v_h & \text{else} \end{cases} \tag{4.2.4}$$

In equation 4.2.4 the value of λ represents the gradient of the expected change in an individual's volume over time when $t_a < t_e$. The expected volume is truncated at the heritable volume, as it produces unrealistic values of v_t for individuals with age (t_a) in excess of t_e.

A dynamic minimum volume (v_{min}) is calculated with reference to the expected volume (v_t). This is controlled by the minimum volume fraction parameter (δ) on the condition that:

$$0 < \delta < 1$$

The starvation threshold is therefore defined by:

$$v_{min}(v_t) = \delta \cdot v_t \tag{4.2.5}$$

A graphical representation of the growth trajectory can be seen in figure 4.2.2.

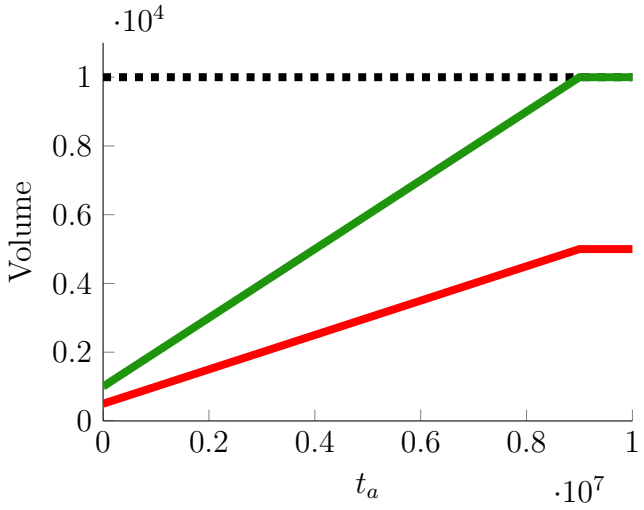

Figure 4.2.2: The expected volume (v_t - green line) and minimum volume (v_{min} - red line) as a function of age (t_a) for an individual with v_r of 1,000, and v_h of 10,000 (black dotted line) when using a growth coefficient (λ) value of 0.001 and a minimum volume fraction (δ) value of 0.5.

Equation 4.2.4 makes the assumption that the rate of growth to v_h is constant through volume space. A smaller individual is therefore assumed to take longer to reach its size at maturation than one with the same volume at maturation born with a higher volume (v_r).

The dynamic expected and minimum volumes imply a change to equation 2.6.8. In an effort to introduce an increased phenotypic plasticity in terms of resistance to starvation, a beta function in form published by Yin et al. (2003) was utilised to produce a new definition for the probability of an individual starving. Individuals with a volume (v) greater than or equal to their expected volume (v_t) have P_s set to 0. Individuals that reach or fall below their minimum volume v_{min} have P_s set to 1. The beta function is used for individuals with v between these thresholds.

$$P_s(v, v_t) = \begin{cases} 0 & \text{if } v \geq v_t \\ 1 & \text{if } v \leq v_{min}(v_t) \\ 1 - \left(1 + \frac{(v_t - v_{min}(v_t)) - (v - v_{min}(v_t))}{v_t - v_{min}(v_t)}\right) \cdot \left(\frac{v - v_{min}(v_t)}{v_t - v_{min}(v_t)}\right) & \text{else} \end{cases} \tag{4.2.6}$$

The calculations for the probability of starvation across a range of volumes (v) that intersect minimum volume (v_{min}) and the expected volume (v_t) can be

seen below.

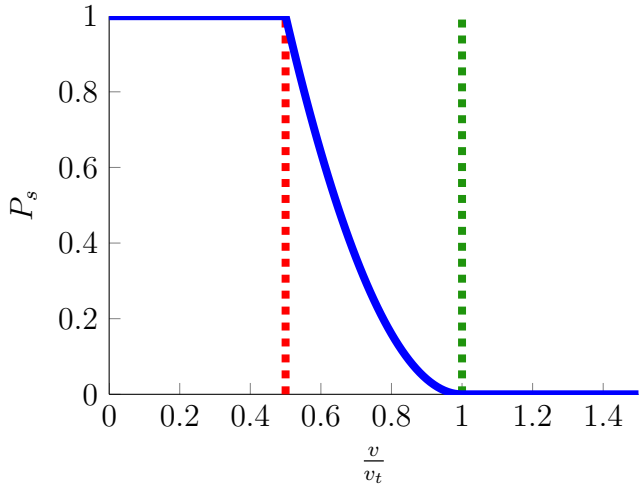

Figure 4.2.3: A plot showing the probability of starving (P_s - blue line) with respect to changes in volume (v) relative to their expected volume (v_t). Individuals do not starve if they are at or above their expected volume (v_t - green dotted line). This example uses a δ value of 0.5 used to calculate the minimum volume (v_{min} - red dotted line).

4.2.3 Reproduction

Individuals cannot reproduce while they are below their volume at maturation (v_h). Until they are, assimilated volume is used to cover metabolic expense with any excess contributing toward growth. Once an individual reaches maturity surplus volume can be used to produce a child. Reproduction occurs when an individual (v) reaches its reproduction threshold (v_{max}). Using the child volume fraction trait (Ω) this is redefined as:

$$v_{max}(v_h) = v_h + (\Omega \cdot v_h) \tag{4.2.7}$$

The Ω trait also implies a change that supercedes equations 2.6.10 and 2.6.11. The volume subtracted from the parent and given to a child at birth is a function of the child volume fraction and volume at maturation trait values.

$$v_r = v_h \cdot \Omega \tag{4.2.8}$$

In constrast to section 2.6.4, mutations that go out of bounds in this version of the model are truncated at their minimum or maximum value. This is to

prevent a large mutation of a small child fraction trait from being reflected outside the opposite bound.

The potentially large change in individuals' volume over time means that they may move through some or all of the trophic levels during the course of their life. For this reason offspring no longer inherit their parent's τ attribute. Each new child starts with an uninitialised τ value of 0.

4.2.4 Maturation Factor Attribute

In order to test the predictions of life history theory there needs to be some measure of how mature an individual is when and if it becomes prey. For this, individuals carry an additional attribute referred to as the maturation factor. It is represented with the symbol ρ and defined by:

$$\rho(v, v_r, v_h) = \begin{cases} 0 & \text{if } v \leq v_r \\ 1 & \text{if } v \geq v_{max}(v_h) \\ \frac{v - v_r}{v_{max}(v_h) - v_r} & \text{else} \end{cases} \tag{4.2.9}$$

An individual's maturation factor changes according to the volume of and relative position to v_{max}. When an individual is at its birth volume ρ takes the value 0, when at v_{max} it takes the value 1. Because of the way growth and reproduction are modelled here, the maturation factor can decrease if an individual loses volume. However, once an individual has reproduced it is assumed to have reached maturity and so ρ will take the value 1 thereafter.

4.2.5 Initialisation

As explained in section 2.5, individuals are given a volume that matches their heritable volume. This means that in this version of the model, the size classes are initialised with mature individuals. The child fraction traits are assigned a random value in the range Ω_{min} to 1.

4.3 Results

The results presented in this section used the parameter values defined table 4.3.1.

Table 4.3.1: The default parameter values for this version of EATSM.

Symbol	Value	Description
d	100	Number of heterotrophic size classes.
N_{init}	0	Initial nutrient volume.
P_{init}	1e+06	Initial phytoplankton volume.
H_{init}	1e+06	Initial heterotrophic population volume.
v_{small}	1	Smallest individual volume.
v_{large}	1e+10	Largest individual volume.
β	10	Preferred prey volume ratio.
c	0.85	Feeding kernel width.
a	1	Feeding kernel height.
α	0.01	Size class subset fraction.
K_{frac}	0.15	Half-saturation constant fraction.
γ	0.5	Assimilation efficiency coefficient.
ϵ	1e–05	Fractional metabolic expense per time step.
k_m	0.67	Metabolic scaling exponent.
λ	1e–05	Growth coefficient.
δ	0.2	Individuals' minimum fraction of expected volume.
P_μ	0.001	Probability of mutation.
σ	0.01	Standard deviation of mutation distribution.

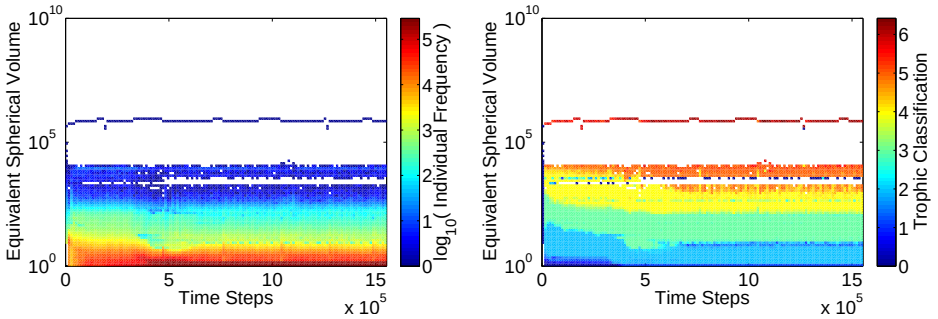

Figure 4.3.1: The evolution of the d size classes on the y-axis, over time on the x-axis. Plots show: **(a)** the number of all individuals, and **(b)** the mean trophic classification of each size class.

The creation of individuals in many viable positions in volume trait space provides a foundation on which to reorganise and establish a stable system. Using the method described in section 2.7.2, this configuration produced a trophic level count of 5. There are dynamics of damped and periodic oscillations that are similar to those described in sections 3.1.1 and 3.1.2. From around 750,000

in model time the trophic structure is largely realised, and the system enters a periodic oscillation.

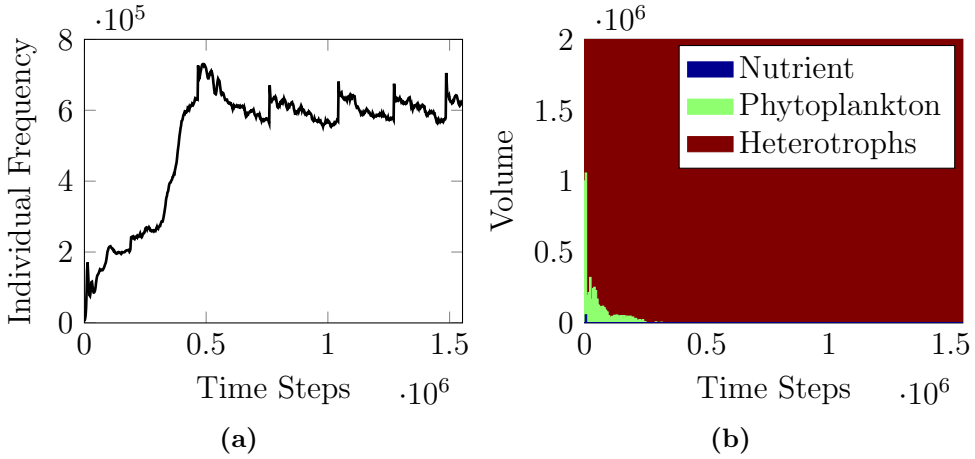

Figure 4.3.2: Plots show: **(a)** the total number of heterotrophic individuals, and **(b)** the volumes of each of the pools of matter over time.

Figure 4.3.2a illustrates the periodic oscillation in the total number of heterotrophs in the system. Figure 4.3.2b shows that the volume in the system is almost entirely comprised of heterotrophic individuals. The transiently occuring volumes of nutrient and phytoplankton are too small to be seen in this plot. This suggests that a greater number of smaller individuals are in competition with each other.

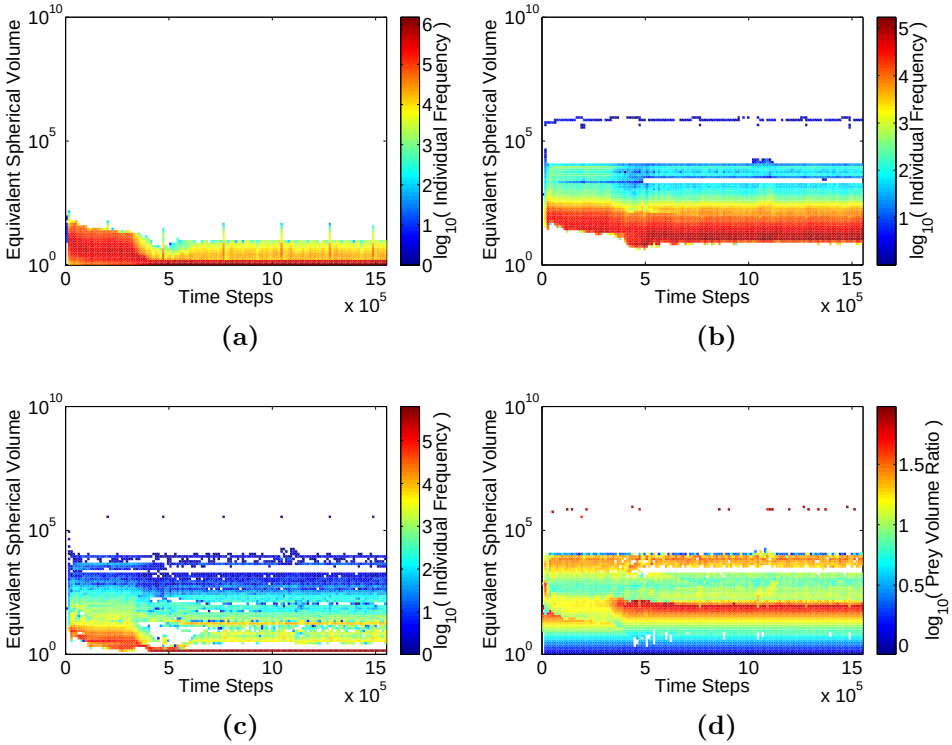

Figure 4.3.3: The evolution of the d size classes on the y-axis, over time on the x-axis. Plots show the numbers of: **(a)** herbivores, **(b)** carnivores, **(c)** corresponding prey, and **(d)** the actual predator-prey volume ratios from each size class.

Figure 4.3.3a shows the numbers of herbivores. It also illustrates that the phytoplankton is accessed by larger herbivores at times that correlate with the periodicity observed in the system. Figure 4.3.3b shows the number of carnivores. From looking at the number of prey individuals (figure 4.3.3c) it can be seen that the periodicity of the system correlates with times when a very large individual is consumed. Figure 4.3.3d shows the average actual predator-prey volume ratio. This is defined as the predator volume divided by the prey volume. It illustrates that individuals in most of the occupied size classes consume individuals that consistently deviate in either direction from the constant predator-prey volume ratio of $log_{10}(\beta) = 1$ because smaller or larger prey are more numerous and therefore preferred.

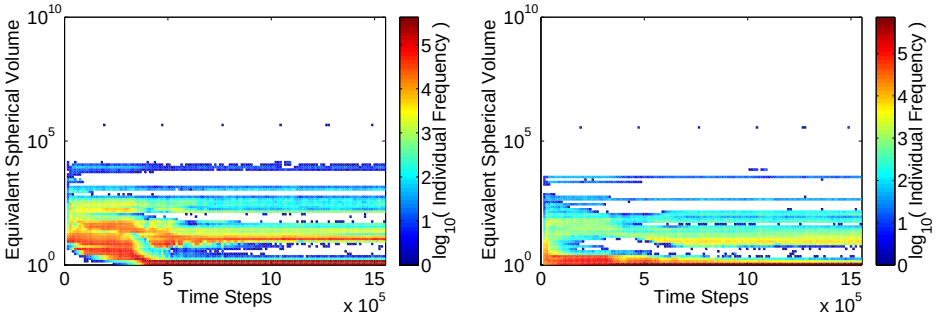

Figure 4.3.4: The evolution of the d size classes on the y-axis, over time on the x-axis. Plots show the numbers of: **(a)** parent, and **(b)** child individuals from each size class.

Figure 4.3.4a shows the numbers and position in volume trait space of parents, and figure 4.3.4b provides the same information of children. These plots illustrate that evolution of the Ω trait generally produces children that are smaller than their parents. Comparing these plots with those for carnivore (figure 4.3.3b) and prey individuals (figure 4.3.3c) shows the overall periodicity of the system is the result of a trophic cascade and correlates with times when the top-level carnivores produce a child and soon after consume it, or the parent as a result of its reduced volume. This is the same mechanism for the periodicity discussed in section 3.1.2.

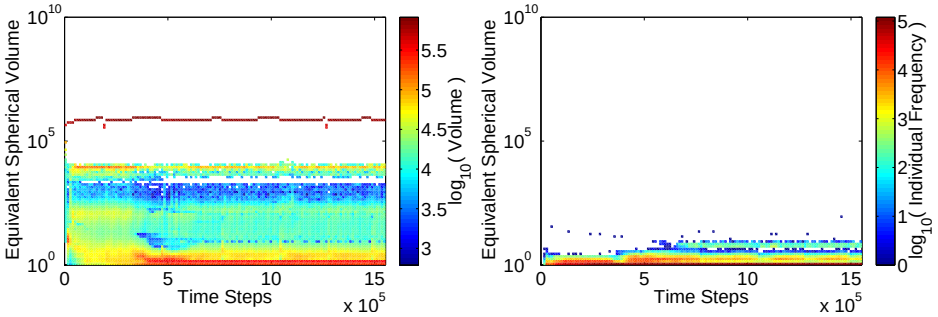

Figure 4.3.5: The evolution of the d size classes on the y-axis, over time on the x-axis. Plots show the **(a)** volume of, and **(b)** numbers of starved individuals from each size class.

Figure 4.3.1a illustrates that the frequencies of individuals illustrate an Eltonian trophic pyramid, whereas figure 4.3.5a shows that the majority of the volume is concentrated in the largest and smallest individuals.

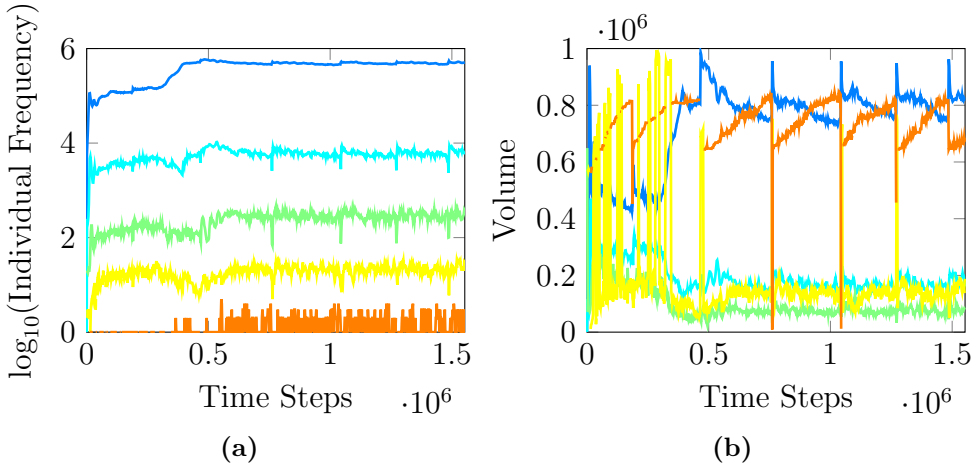

Figure 4.3.6: Plots show: **(a)** the numbers of, and (b) total volume of the secondary (blue), tertiary (cyan), quaternary (green), quinary (yellow), and senary (orange) producers over time.

This observation is confirmed in plots of the data contributing to each trophic level. Figure 4.3.6a shows that the number of individuals in each trophic level inversely correlates with their position in the ecological hierarchy. This is a similar result to the plot in figure 3.1.4a. However, there are many more small individuals in this configuration. The increased number of secondary producers means that at times their volume exceeds that of the quinary producers (figure 4.3.6b). This is the cause of the heavily grazed phytoplankton shown in figure 4.3.2b.

Figure 4.3.5b shows that the majority of the starvation events are confined to individuals in size classes with $v_m < 10$. This is seen to be a product of the way in which growth is assumed to take a linear trajectory through volume space. The results being discussed in this section took place over little more than 15e+05 time steps, with λ set to 1e–05. This configuration implies the assumption that an individual of any size would have added 15 to their volume during that time. This expected growth trajectory therefore has decreasing significance for individuals higher in volume trait space.

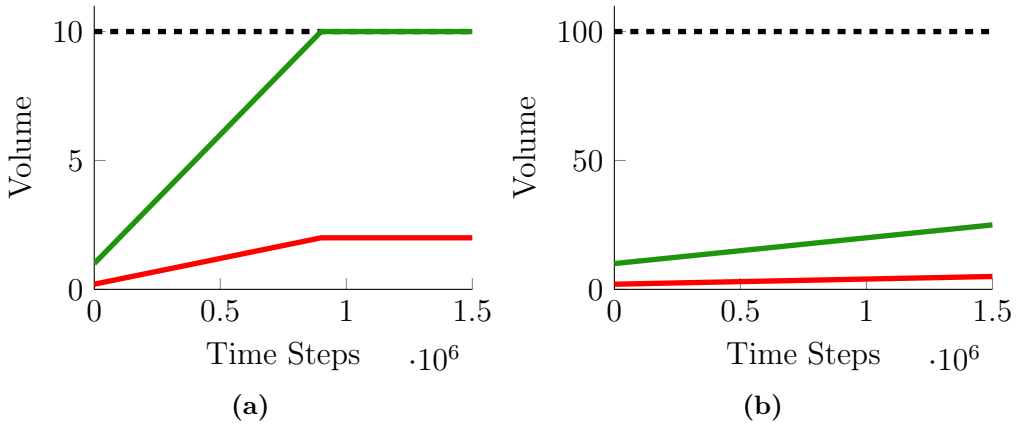

Figure 4.3.7: The expected volume (v_t - green line), and minimum volume (v_{min} - red line) as a function of age (t_a) for individuals with **(a)** $v_r = 1$ and $v_h = 10$ (black dotted line), and **(b)** $v_r = 10$ and $v_h = 100$ (black dotted line) over 15e+05 time steps, with $\lambda =$ 1e–05 and $\delta = 0.2$.

To emphasise this point, figure 4.3.7 shows two example growth trajectories for individuals born and reproducing at different volumes. It is clear that the expected volumetric change as a function of time is comparatively less for a larger individual. In this configuration, the threshold for starvation for individuals with $v_r \geq 10$ was effectively little more than their birth volume.

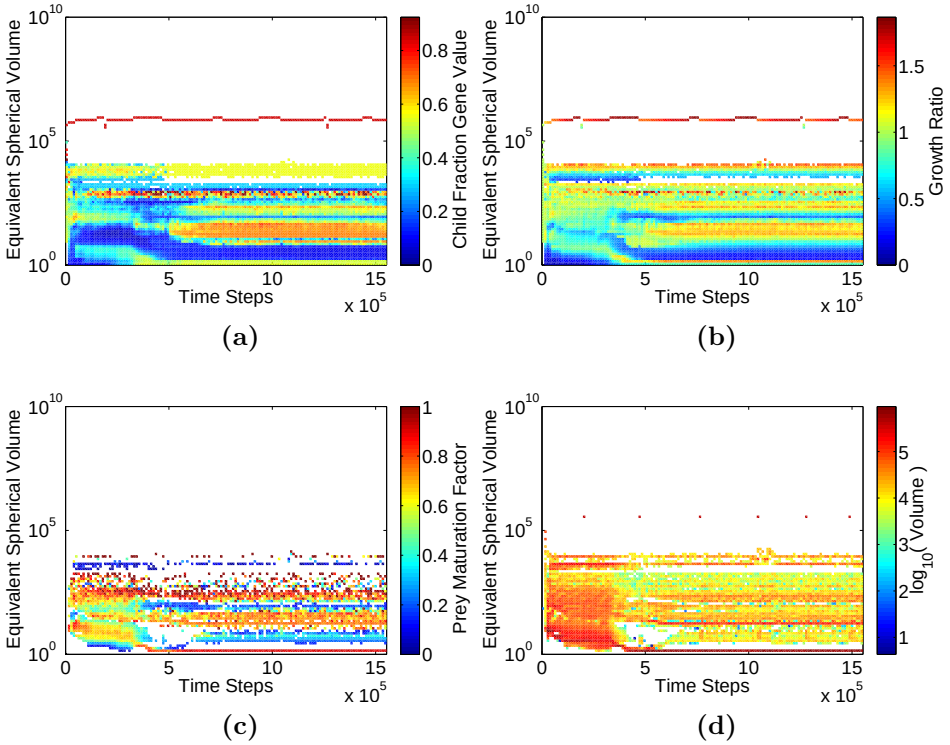

Figure 4.3.8: The evolution of the d size classes on the y-axis, over time on the x-axis. Plots show the mean **(a)** child fraction trait, **(b)** growth ratios, **(c)** prey maturation factors, and **(d)** volume flux of prey individuals from each size class.

Figure 4.3.8a shows the average Ω trait values in each size class. The other three plots in figure 4.3.8 introduce previously unseen views of the system. These will be explained before the outputs are discussed. Figure 4.3.8b shows the mean growth ratio from each size class. The growth ratio is an individual's actual volume relative to its volume at maturation ($\frac{v}{v_h}$). It provides a normalised measure of how much volume individuals have lost or gained, regardless of their Ω trait values. Figure 4.3.8c shows the mean maturation factor (ρ) attribute (equation 4.2.9) of prey individuals. The definition of ρ is in section 4.2.4. Figure 4.3.8d shows the total volume flux of prey from each size class.

The set of heterotrophs occupy almost the full width of Ω trait space, and there is significant structuring of the Ω trait values (figure 4.3.8a). The emergence of, and maintenance of extremes of Ω trait values after the model enters the periodic oscillation phase indicates the presence of strong selective pressures. If the predictions of life history theory completely explain the evolution of reproductive effort, we would expect the Ω trait values to correlate only with

the maturation factor of prey individuals (figure 4.3.8c).

Comparison of figures 4.3.8a and 4.3.8c illustrates some correlation. Size classes that generally lose mature prey have higher Ω trait values, and those that lose immature prey show lower Ω values. However, there are size classes where the general age of prey does not correlate linearly with the mean Ω trait value for that size class. Figure 4.3.8a appears to most closely correlate with the growth ratio (figure 4.3.8b). However, this could be due to fact that there are gaps in figure 4.3.8c as a result of data resampling, and times where no predation too place. Figure 4.3.8d shows a complete record of data from predation, and so is illustrative of the gaps in figure 4.3.8c.

The general observation is that individuals with $v > v_h$ have $\Omega > 0.5$. In addition, both the child fraction trait and growth ratio values correlate with size classes where the highest number of children are being born (figure 4.3.4b). To evaluate the correlation, points in volume trait space where there were data for Ω and the growth ratio, and Ω and the maturation factor were extracted from the end of model time and a linear regression performed on them.

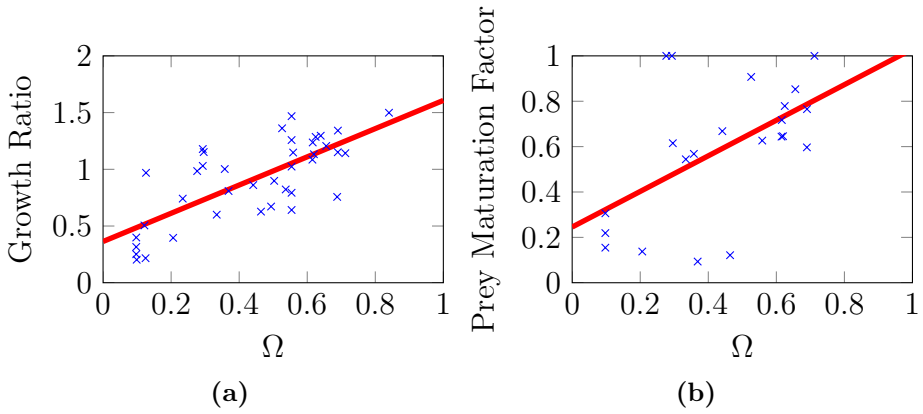

Figure 4.3.9: Linear regressions of **(a)** Ω and the growth ratio, and **(b)** Ω and the maturation factor.

There were 39 common data points for Ω and the growth ratio, and only 22 for Ω and the maturation factor. This is because the growth ratios were recorded each time the data were sampled, and the prey maturation factor was only captured when a predation event occured. Comparison of the linear regressions in figures 4.3.9a and 4.3.9b show that at the end of model time there is indeed a positive relationship between both Ω and the prey maturation factor, and between Ω and the growth ratio. The correlations illustrate the nature of

the selection pressures within the model. A high Ω trait value imposes a larger reproductive effort on an individual. This strategy is only viable in size classes where there is high growth. If an individual finds itself in a size class with high growth, it has an increased chance of meeting the higher cost of reproduction. Individuals with a high Ω trait value in size classes that experience low growth are not able to reproduce. A more stringent starvation function would increase the selection pressure against slow growing individuals. However, the configuration for the starvation threshold in this model has a negligible deductive effect on the individuals. In this way, selection only has an additive influence.

4.4 Discussion

These results show that the predictions of life history theory are generally correct, but they do not completely explain the evolution of reproductive investment. The results presented in section 4.3 indicate that in a materialist view of the natural world, reproduction and food consumption are part of the same overall process. This suggests Lack's (1947) food limited hypothesis, and Ricklefs' (1970) counteradaptation hypothesis are two perspectives of the same system. The food limited hypothesis cannot completely explain the evolution of reproductive strategies because it considers the response of a single species to an environment composed of varying resources. The counteradaptation hypothesis considers the adaptive potential of a predator, but it considers just a single predator and prey in isolation. Neither of these hypotheses can explain the evolution of reproductive strategies in their entireity because they fail to consider the evolution of species in a whole systems context. In a trophic system, predators may also be prey for other species. Individuals may evolve their reproductive strategy to balance the effects of predation risk, but selection would ensure this strategy is also balanced against those of their prey. It is therefore likely that the evolutionary response of a single individual could have a cascading effect throughout the entire system, as appears to occur with the consecutive evolution of higher Ω values in small secondary producers around timestep 3.5e+05, small tertiary procucers around 5e+05 and large tertiary procucers around 6e+05 (figure 4.3.8b).

This study allowed individuals to start life much smaller than their size at maturation. The method described in section 4.2.2 produced a probability of an

individual starving that changed as a linear function of time. An individual's somatic growth was a function of assimilated volume. Growth and starvation were thereby decoupled. Despite the apparent scarcity of literature that links models of growth and starvation, it is considered reasonable to assert that these are not independent processes. The classical perspective considers growth to be a simple function of time. Contemporary literature illustrates promising work that considers growth to be a function of the environmental conditions. However, all of these models necessarily include a point beyond which the description ends and assumptions begin. This unfortunately made them unsuitable for use in EATSM. It is considered that growth and starvation cannot be disentangled from each other. The link between food consumption and reproduction is a topic already discussed in the literature (Ginzburg, 1998). However, the findings from this study suggest the general conclusion that food consumption, growth, starvation, and reproduction are all part of the same process.

Material conservation necessitated that growth be some function of assimilation. The approach described in section 2.6.2 was to simply add assimilated volume to an individuals somatic volume. In reality growth is a function of a nested hierarchy of metabolic processes operating at the interface between physiology and chemistry (Braakman and Smith, 2013). It is therefore considered that a model of growth would require explicit representation of metabolisms, and internal physiological dynamics. However, the only practical way to include such descriptions in EATSM would be to include a more realistic selective pressure from starvation, which it has been argued above might drive evolution of child investment in the same direction as food shortage.

It is considered that the adaptability of species may be constrained by the potential rates of reproduction. Under constant growth conditions in EATSM, a lower parental investment in offspring can increase the rate of reproduction. If it is assumed that there is a proportional probability of mutation at each reproductive event, then evolution of lower parental investment in offspring represents a mechanism by which a less numerous or generally food limited organism can increase its evolvability. Evolvability itself may be an evolvable trait. If it were not, selection would likely favour more rapidly reproducing organisms. There may be cases of this, but the general coevolutionary examples of predator and prey lend themselves to the 'arms race' metaphor. This may

be one of the reasons why many fish species produce offspring that start life in a low trophic position, and have to grow through several orders of magnitude to reach their mature size (Hartvig et al., 2011).

4.5 Conclusions

1. The predictions of life history theory do not completely explain the evolution of reproductive investment. Lack's (1947) food limited hypothesis and Ricklefs' (1970) counteradaptation hypothesis are two perspectives of the same system. The evolution of reproductive investment is a function of prey and predators, and the strategies employed by all species in the system.

2. Evolution of the reproductive strategy represents a mechanism by which evolvability can become an evolvable trait.

3. Parental investment in offspring provides a way in which less numerous individuals can increase their evolvability.

5 On The Coexistence of Planktonic Generalists and Specialists

5.1 Introduction

It is estimated that phytoplankton are responsible for up to 50 percent of global primary production yet account for only 0.2 percent of the global autotroph biomass (Field et al., 1998). Primary production is the natural process to convert carbon dioxide into organic compounds. It therefore serves as the energetic and material bridge to heterotrophic life (Calbet, 2008). Haldane (1926) noted how "the most obvious differences between different animals are differences of size". Terrestrial organisms necessarily invest comparatively more energy in structural biomass to resist gravity in the reduced buoyancy of air. Since phytoplankton do not have to do this, they can remain very small. This permits some similarly small heterotrophs.

The general term "plankton" refers to many phylogenetic groups that span several orders of magnitude in size. Table 5.1.1 has been taken from Omori and Ikeda (1984) and shows the size ranges in equivalent spherical diameter (ESD), and classifications of plankton found globally.

Table 5.1.1: The range of sizes and categories of plankton found globally in aquatic environments (from Omori and Ikeda, 1984)

Category	Size (ESD)	Major Organisms
Ultrananoplankton	< 2 μm	*Viruses and free living bacteria.*
Nanoplankton	2–20 μm	*Fungi, small flagellates, small diatoms.*
Microplankton	20–200 μm	*Most phytoplankton species, foraminiferans, ciliates, rotifers, copepod nauplii.*
Mesoplankton	0.2–2 mm	*Cladocerans, copepods, larvaceans.*
Macroplankton	2–20 mm	*Pteropods, copepods, euphausiids, chaetognaths.*
Micronekton	2–20 cm	*Cephalopods, euphausiids, sergestids, myctophids.*
Megaloplankton	> 2 cm	*Scyphozoans, thaliaceans.*

Pelagic heterotrophs determine the fluxes and flows of organic material in marine food webs as a result of their feeding habits (Hansen et al., 1994). There are several factors that determine what prey a predator selects. A constant

predator-prey size (ESD) ratio of 10:1 has historically been assumed. This facilitated the construction of trophic models (Hansen et al., 1994; Moloney and Field, 1991). Hansen et al. (1994) reviewed this assumption for pelagic predators of 5–1,000μm in length (nano-, micro-, and mesozooplankton). They found a range of predator-prey ESD ratios of 1:1 to ∼100:1. These differences are due to the variety of ways that species have evolved to find and capture their prey. They suggested that more quantitative data on size selectivity would permit the classification of heterotrophic plankton based on feeding mechanism instead of taxonomy. This lead to the definition of zooplankton functional types.

Kiørboe (2011) published a comprehensive review of zooplankton feeding mechanisms and established a contemporary nomenclature for them. Of the observed data there were found to be four major strategies: passive ambush, active ambush, feeding-current, and cruise feeding. Predators that adopt the *passive ambush* feeding strategy cannot detect prey remotely. They remain motionless and wait for the motile prey to collide with them. There are two subdivisions within this strategy, depending on prey motility. Diffusion feeders consume prey that move diffusively, either by Brownian motion or by actively swimming. Ballistic feeders consume prey that move only by the force of gravity. They exist deeper in the water column and have specialised structures to capture falling particles of marine snow. The *active ambush* feeding strategy differs from the passive ambush strategy in that the prey particle is perceived and attacked before physical contact is made.

Grazers that adopt the *feeding-current* strategy actively generate a flow into which prey particles are susceptible to being pulled (Kiørboe, 2011). There are three subdivisions of this strategy, depending on how the generated current serves the predator. Filter feeders have specially developed structures through which the current is directed. These sieve out prey particles for consumption. Direct interception feeders do not have any such filtering structure. They perceive and intercept prey caught in the feeding current once physical contact is made. Scanning current feeders perceive individual prey items caught in their current before contact is made. Feeding in this way can cause the grazer to move through the water as the current is generated. Some plankters have adopted strategies or evolved structures to prevent or limit this. The *cruise feeding* strategy is opportunistic, whereby zooplankton actively swim in search of their prey. There are two specialisations of this strategy depending on the

preferred prey size. There are predators that hunt for motile prey smaller than themselves, and those that actively search for marine snow aggregates that can be much larger.

The viability or efficiency of each feeding strategy changes depending on the size scale it is required to function. At sufficiently small scales water behaves with an increased viscosity (Kiørboe, 2011). This is due to a decrease in the ratio of inertial to viscous forces, and is termed a lower Reynolds number. Kiørboe (2011) points out that the direct interception feeding strategy is less efficient at lower Reynolds numbers. The increased viscous boundary layer will force small prey particles to move with the flow field around an approaching predator. Physical constraints for the active ambush strategy limit modes of detection to vision and changes in hydrodynamic pressure. Chemical or olfactory detection is not possible since leaked substances will form a plume behind a motile prey particle. However, the refractory indices of water restrict true vision to eyes above a certain size. Otherwise visual organs can only detect movement and changes in light.

There are evolutionary trade-offs with all feeding strategies (Kiørboe, 2011). For example, the passive ambush feeding strategy is one of the least efficient in terms of finding food. The reduced metabolic pay-off means that this strategy is only viable for smaller species. However, those that adopt it have been found to have rates of respiration that are around eight times lower than similar sized organisms that take more active feeding strategies (Castellani et al., 2005). Being smaller and less active also makes visual or hydrodynamic detection by predators more difficult. Passive strategies therefore confer a decreased rate of predation mortality (Eiane and Ohman, 2004). There are also trade-offs associated with mate finding. This is likely the reason why males of species that adopt passive feeding strategies tend to be smaller than females.

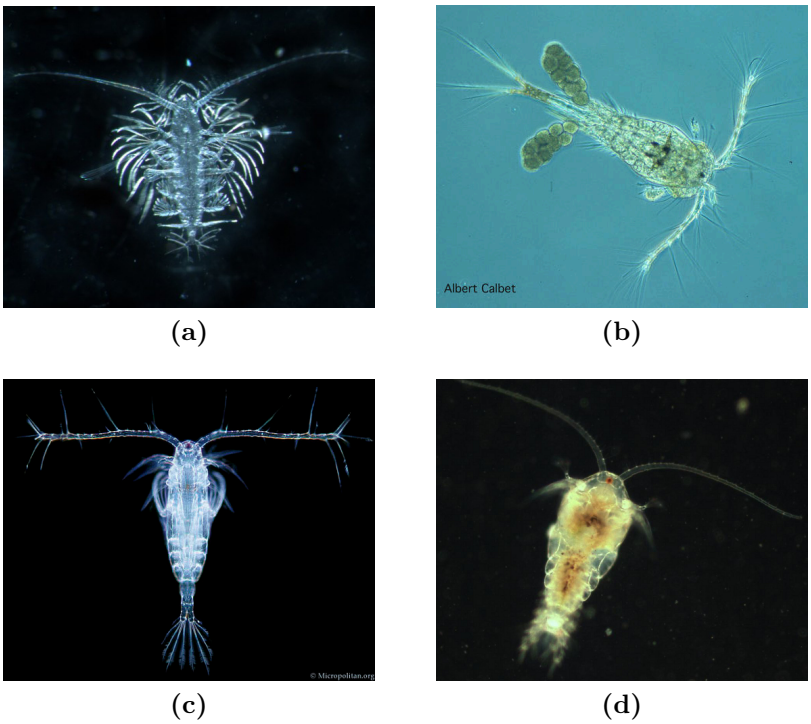

Figure 5.1.1: Photo images of four example species from the phylogenetic subclass *Copepoda* that represent the major zooplankton feeding strategies. **(a)** *Haloptilis plumosa* employs the passive ambush strategy (image: R. Hopcroft). **(b)** *Oithona davisae* uses the active ambush strategy (image: A. Calbet). **(c)** *Acartia tonsa* is a feeding current feeder (image: W. van Egmond). **(d)** *Temora longicornis* employs the cruise feeding strategy (image: K. Embleton). In each case the species has evolved structures that facilitate the particular method of feeding.

Figure 5.1.1 shows four example zooplankton species from the phylogenetic subclass *Copepoda*. Each has adopted different feeding strategies resulting in the evolution of structures to facilitate prey finding and consumption. The morphology of the feeding apparatus places mechanistic limits on the size range of prey that can be ingested (Hansen et al., 1994). For example, a maximum prey size may be set by the opening width of the mouth. Species adopting filter feeding strategies will have a minimum prey size set by the gaps between their filtration structures. In addition to the mechanistic constraints, species also exhibit size preferences for prey.

The ingestion rate of zooplankton is usually expressed as the biovolume consumed per unit time (e.g. $\mu m^3\ h^{-1}$) as a function of prey density (Fenchel, 1980). This takes the form of a functional response (figure 5.1.2a). Prey size selectivity of zooplankton means that they have different functional responses to varying concentrations of different sized particles. The clearance rate of a

plankter is defined as the ratio of ingestion rate to prey density (Hansen et al., 1994). Figure 5.1.2b illustrates that the maximum clearance rate occurs at low prey densities (Fenchel, 1980; Hansen et al., 1994).

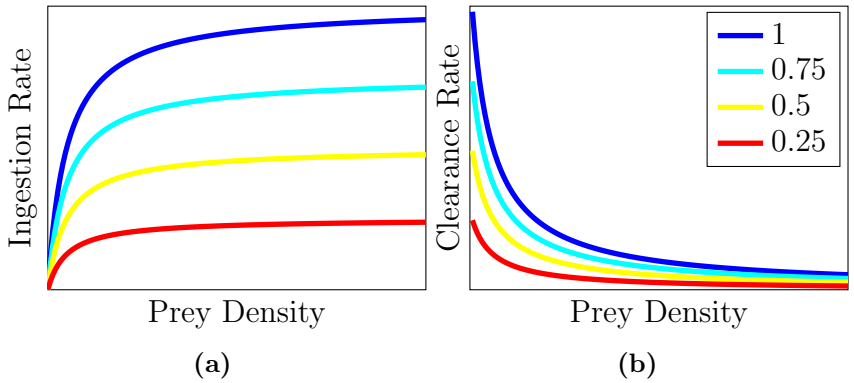

Figure 5.1.2: Plots show: **(a)** example ingestion rates, and **(b)** clearance rates as functions of prey density and prey of maximal (blue), three quarters (cyan), half (yellow), and quarter (red) preference.

Zooplankton particle size discrimination can be expressed as the maximum clearance rate as a function of prey size (Fenchel, 1980; Hansen et al., 1994). Morphological variations within species mean that data on the maximum clearance rate for a wide range of prey sizes will begin to take on a "bell-shaped distribution" (Hansen et al., 1994). This reveals the origin of functions frequently used to determine the size selectivity of marine organisms (see figure 2.4.1). Unpublished work by Sailley et al. (2009) illustrated curves fitted to data for the maximum grazing rate of pelagic ciliates and heterotrophic dinoflagellates. A copy of this plot shown in figure 5.1.3.

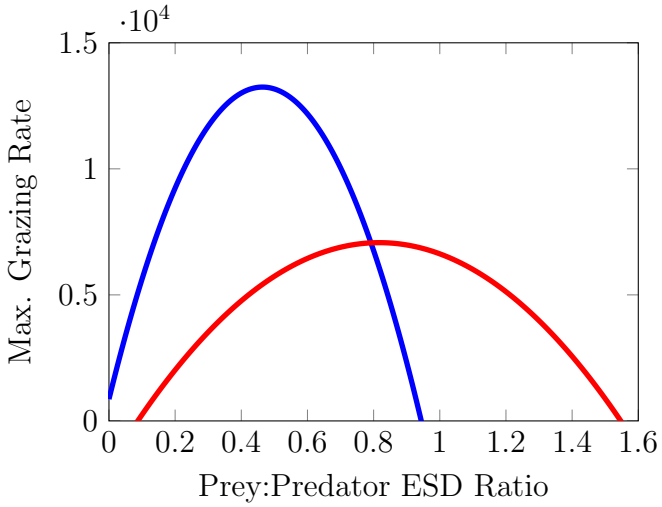

Figure 5.1.3: The maximum grazing rate (in units of μm^{-3} predator^{-1} hour) as a function of predator-prey ESD ratio for pelagic ciliates (blue line) and heterotrophic dinoflagellates (red line).

At between 20 and 200 μm in size, ciliates and dinoflagellates are two major groups of microplankton species (Sherr and Sherr, 2007; Kiørboe, 2008). Both contain heterotrophic species that share a similar biogeography (Levinsen and Nielsen, 2002; Sherr and Sherr, 2007; Buitenhuis et al., 2010). Empirical observations show that at certain locations and points in the year the biomass of species belogining to each group is approximately the same. This contradicts a suggestion made by Hansen (1994) that the plankton functional groups rarely coexist. Despite the contemporary knowledge that these two species do coexist, the mechanisms behind their coexistence remain largely unexplored.

The observation that plankton species often compete for the same resources has raised questions of coexistence (Hutchinson, 1961). Hutchinson (1961) addressed the problem of plankton coexistence in an apparently homogeneous environment. He said that two prey species competing for the same resource can coexist if each experiences different pressures from predators. This concept is referred to as "predator-mediated coexistence" (Caswell, 1978). While there are several empirical studies that show evidence of predator-mediated coexistence, there is also evidence to show that predation can decrease the number of competing prey species (Caswell, 1978).

Ciliates and dinoflagellates have evolved different methods of feeding. This results in very different mechanical constraints on the types of prey they can exploit (Kiørboe, 2008). For example, heterotrophic dinoflagellates can either

suck out the contents of their prey through a proboscis, or digest them externally by means of a pallium. This negates the need to engulf the prey individual and so enables species with such adaptations to consume prey that may be larger than themselves. Ciliates do not have such feeding adaptations and so generally consume smaller prey (Kiørboe, 2008, 2011). This suggets that species belonging to each group are not necessarily in direct competition. Since both are prey for the same predators, the situation becomes the opposite of predator mediated coexistence (Sherr and Sherr, 2007).

It is considered that the data summarised in figure 5.1.3 shows that the feeding strategies adopted by pelagic ciliates and heterotrophic dinoflagellates are the result of a trade-off. The ciliates appear to specialise in consuming smaller prey, and the dinoflagellates generalise by consuming a wider range of prey sizes less efficiently. Generalists and specialists may coexist as a result of the relative ease with which they can exploit different prey. In order to explore this further EATSM will be modified to capture a similar trade-off.

5.2 Method

The method outlined here is an extension of that outlined in chapter 2.

5.2.1 Individuals

The preference function defined in chapter 2 is set by parameters that remain constant for the duration of the model run. In this version of the model the distance in volume trait space between the predator and prey is still defined by a constant parameter, but the height and width of the preference function can now differ between individuals. The value is set by an additional, independent heritable trait. The width of preference trait space is set by minimum (c_{min}) and maximum (c_{max}) function width values. As with other heritable traits the heritable preference trait is passed to offspring subject to potential mutation.

Using an unprocessed heritable trait value (g), the heritable preference function width (c_h) is defined as:

$$c_h = g \cdot (c_{max} - c_{min}) + c_{min} \tag{5.2.1}$$

To capture the empirical trade-off described in section 5.1 there is an inverse relationship between the width of the preference function, and its height. Individuals benefitted by having the widest preference function, are disadvantaged by it also being the least tall. An individual's heritable preference function height (a_h) is a function of the same unprocessed trait value (g) as used in equation 5.2.1.

$$a_h = 1 - g \tag{5.2.2}$$

The trade-off between c_h and a_h can be seen in figure 5.2.1 below.

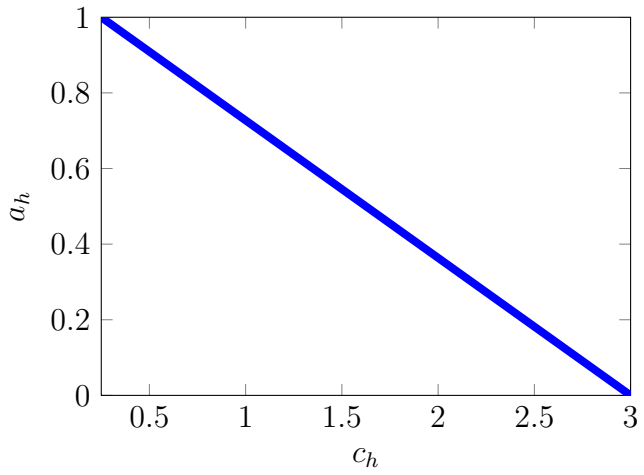

Figure 5.2.1: A plot of the trade-off between heritable preference function width (c_h) and height (a_h). In this example the minimum (c_{min}) and maximum (c_{max}) preference function widths are set to 0.25 and 3 respectively.

The inclusion of a heritable trade-off implies a modification to the preference functions. One of the conclusions from the sensitivity analysis (chapter 3) was that the combination of log-normal preference function and non-linear (type 2) functional response was the most stable. The empirical observations in the zooplankton literature reviewed here suggest that these are more realistic. This model will make exclusive use of the type 2 functional response, but since it addresses evolution of the predator preferences both the log-normal and inverse parabolic preference functions will be used. The log-normal preference function is redefined as:

$$\phi(v, a_h, c_h, v_p) = a_h \cdot exp\left[\frac{-\left(ln\left(\frac{\beta v_p}{v}\right)\right)^2}{2c_h^2}\right] \tag{5.2.3}$$

The inverse parabolic preference function is redefined as:

$$\phi(v, a_h, c_h, v_p) = max\left[0, a_h \cdot 1 - \left(\frac{log_{10}\left(\frac{v/\beta}{v_p}\right)}{c_h}\right)^2\right] \tag{5.2.4}$$

The result of the trade-off on the height and width of the preference function can be seen in figure 5.2.2 below.

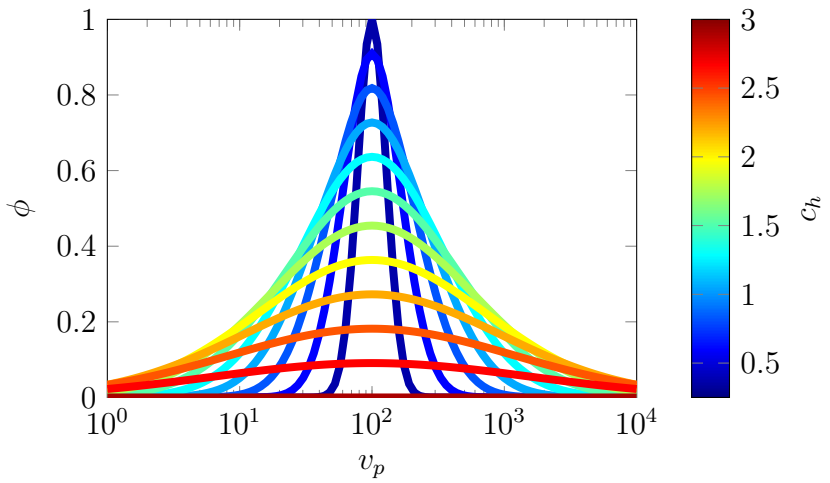

(a)

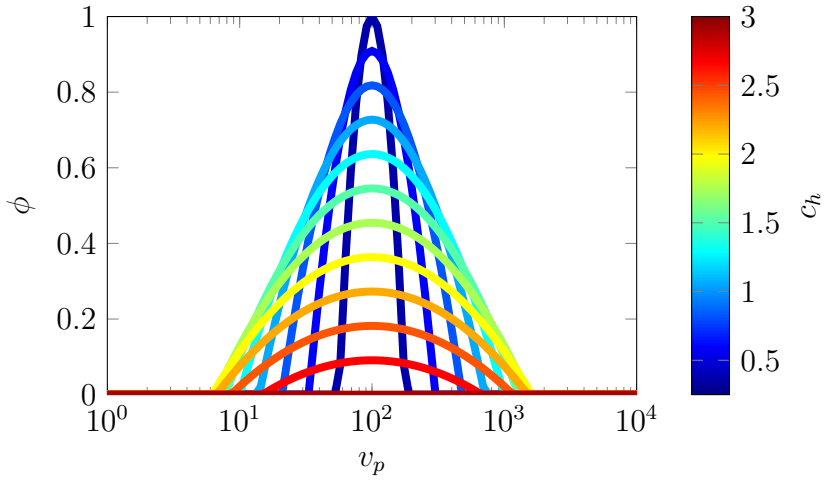

(b)

Figure 5.2.2: Plots show: **(a)** the log-normal, and **(b)** inverse parabolic predator preference (ϕ) as a function prey volume (v_p) for a range of preference function widths (c_h) and corresponding heights (a_h). In both the predator/grazer volume (v) is 10,000, the preferred prey volume ratio (β) is 100, c_{min} is 0.25, and c_{max} is 3.

The preference functions in figure 5.2.2 are centred above a v_p value of 10^2; the volume of the maximally preferred prey. Individuals that have a preference function width (c_h) that reaches the maximum (c_{max}) also have an a_h value of 0. It is also apparent that both functions carry caveats. For high c_h values, the log-normal function offers a significant probability of an individual consuming another the same size or larger than itself. If the value of β is decreased, the distance between the predator and the centre of the plots in figure 5.2.2 is also decreased. This will confer an increased probability of a predator consuming prey that could be larger than itself. In addition, the inverse parabolic func-

tion can only reproduce the trade-off for the lower two thirds of trait space. Individuals with $g > 0.67$ experience a reduction in their chances of consuming anything.

5.2.2 Preference Trait Discretisation

Reflecting the approach of section 2.4.2, preference space for an unprocessed trait g was divided into d discrete locations. This again necessitated vectors for the preference function heights (a_m) and widths (c_m). They are used to give each individual a preference index (i) such that the ith position of each preference vector approximately equals their heritable traits. This applies to the preference function height:

$$a_h \approx a_m(i)$$

And width:

$$c_h \approx c_m(i)$$

The preference index is set by a heritable trait. Therefore it does not change during the life of the individual. In addition, individuals remain grouped by volume. Their preference traits have no effect on whether they are selected as prey. The purpose of discretising preference trait space is to facilitate the calculation of effective prey volume.

5.2.3 Effective Prey Volume

The approximated method of calculating effective prey volume (see equation 2.4.14) has been tested and shown to differ only slightly from an explicit calculation (see section 3.2). For that reason this version of EATSM will make use of a modified version of the approximation. This was facilitated by the preference matrix. Using a constant preference function, the preference each size class had for every other was pre-calculated based on the predator and prey size class mid-point values. The result was a two-dimensional matrix (see figure 2.4.3). In this version of the model, individuals remain grouped by volume, but now carry a preference index that can potentially specify one

of d slightly different preference functions. The preference matrix therefore becomes three-dimensional (d-by-d-by-d). It contains the preference each size class has for every other as a function of their mid-point values, for each of the d preference functions.

$$\hat{\phi}(i,j,k) = \phi(v_m(i), a_m(j), c_m(j), v_m(k)) \tag{5.2.5}$$

In much the same way, the equations from section 2.4.3 are given an extra dimension to account for the effective prey volume being a function of an additional variable. However, in that section the term "coupling strength" was used to describe the effecive prey volume experienced by one size class of another. This was because size classes were coupled to feed from the one that produced the highest effective prey volume. Since coupling is performed differently here the use of the term has been dropped, but the equations are functionally equivalent. The approximate effective prey volume experienced by size class i with preference function j of size class k is therefore approximated by the product of the preference (j) it has for, by the mid-point value (v_m) and the number of individuals in size class k ($M(k)$).

$$\hat{s_h}(i,j,k) = \hat{\phi}(i,j,k) \cdot v_m(k) \cdot M(k) \tag{5.2.6}$$

Phytoplankton cells are assumed take the smallest volume in trait space (v_{small}). The calculation of effective prey volume of the first size class for size class i with preference j also includes the effect of the phytoplankton population:

$$\hat{s_p}(i,j,P) = \hat{\phi}(i,j,1) \cdot P \tag{5.2.7}$$

These are added together to produce the approximate effective prey volume experienced by size class i with preference j.

$$\hat{v_e}(i,j,P) = \hat{s_p}(i,j,P) + \sum_{k=1}^{d} \hat{s_h}(i,j,k) \tag{5.2.8}$$

The calculated value of $\hat{v_e}$ is plugged into a type 2 functional response to produce the probability that an individual from size class i with preference index j will feed.

$$P_f(i,j,P) = \frac{\hat{v_e}(i,j,P)}{V \cdot K_{frac} + \hat{v_e}(i,j,P)} \tag{5.2.9}$$

The approximate effective prey volume is calculated every time step. To reduce computation further these calculations are only applied to size classes that are occupied and preference indices that are owned by individuals that size class.

5.2.4 Prey Selection

The purpose of the trade-off (figure 5.2.1) is to model generalists and specialists. In the previous versions of EATSM, the calculation of effective prey volume resulted in each predator size class being coupled to feed from the prey size class that produced the highest value. This is certainly possible here, but coupling size classes in this way would mean that individuals from the same size class would be coupled to feed from the same prey size class regardless of their preference trait. This outcome would negate the purpose of including evolvable preference functions. To include the effect of a wide or tall preference function, the coupled size class is now selected probabilistically. This is made possible by calculating the probability of an individual consuming prey from each size class (P_c).

Each predator size class i with preference index j has a total effective prey volume ($\hat{v_e}$) and an effective prey volume for each size class ($\hat{s_p}$ and $\hat{s_h}$). The effective prey volume of each size class (k) is divided by the total for that predator size class. This puts each into a relative context and produces the total prey volume fraction that is from that size class. The fraction is used as the probability of that size class being selected. The probability of an individual from size class i with preference index j being coupled to feed from size class k (where $k \neq 1$) is therefore given by:

$$P_c(i,j,k,P) = \frac{\hat{s_h}(i,j,k)}{\hat{v_e}(i,j,P)} \tag{5.2.10}$$

Because the result of the phytoplankton is included when calculating the effective prey volume for the first size class, equation 5.2.10 is slightly different when calculating the probability of an individual from size class i with preference index j being coupled to feeding from size class where $k = 1$:

$$P_c(i,j,1,P) = \frac{\hat{s_h}(i,j,1) + \hat{s_p}(i,j,P)}{\hat{v_e}(i,j,P)} \tag{5.2.11}$$

The probabilities of each size class (k) being selected for prey by every other size class (i), and for every preference (j) index (where $i \in [1,d]$, $j \in [1,d]$, and $k \in [1,d]$) are calculated. The round of feeding starts in the same way as described in section 2.6.2, but this time the coupled size class index is determined probabilistically. Each time an individual is selected to feed, a unique random number ($\in [0,1]$) is drawn. An algorithm steps through each of the prey indices and compares the random value with a running total of the probabilities. The prey size class that produces a running probability sum that exceeds the random value is the one that is picked. After determining the prey size class, everything else continues as described in section 2.6.2.

5.2.5 Initialisation

The method for initialising the size classes is the same as described in section 2.5. The only change is that the first generation of individuals are given a random trait value (g) to specifiy their preference function height (a_h) and width (c_h).

5.3 Results

Table 5.3.1: The default parameter values for this version of EATSM.

Symbol	Value	Description
d	100	Number of size classes/trait indices.
N_{init}	0	Initial nutrient volume.
P_{init}	1e+06	Initial phytoplankton volume.
H_{init}	1e+06	Initial heterotrophic population volume.
v_{small}	1	Smallest individual volume.
v_{large}	1e+10	Largest individual volume.
β	-	Preferred prey volume ratio.
c_{min}	0.1	Minimum feeding kernel width.
c_{max}	-	Maximum feeding kernel width.
α	0.01	Size class subset fraction.
K_{frac}	0.15	Half-saturation constant fraction.
γ	0.5	Assimilation efficiency.
ϵ	1e-05	Fractional metabolic expense per time step.
k_m	0.67	Metabolic scaling exponent.
P_μ	0.001	Probability of mutation.
σ	0.01	Standard deviation of mutation distribution.

5.3.1 Sensitivity

The method described in chapter 3 for testing the model sensitivity was utilised here. The model was run for range of β and c_{max} values four times. The mean and the standard deviation of the number of trophic levels produced for each combination is shown in figure 5.3.1.

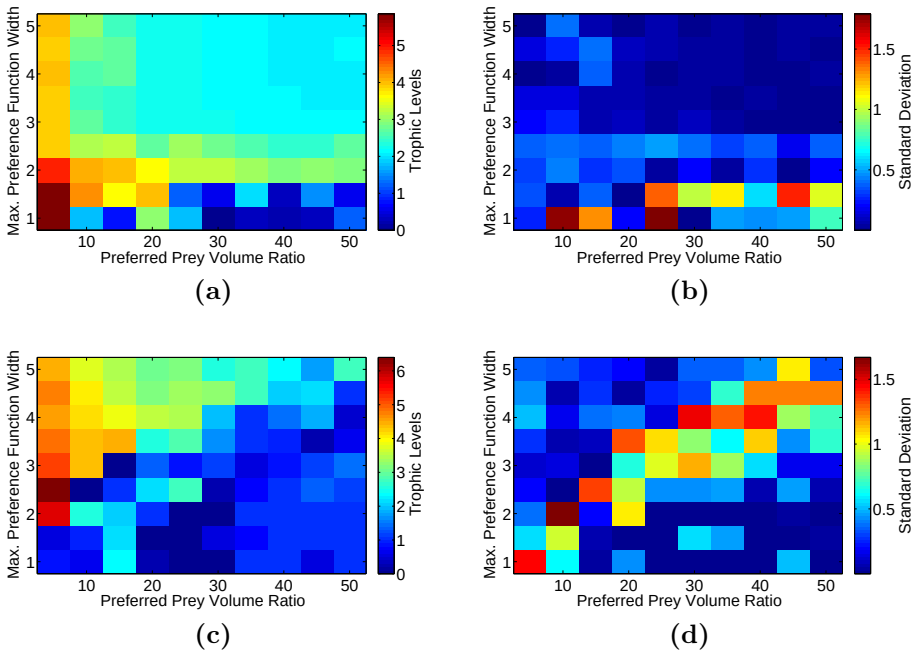

Figure 5.3.1: The mean number of trophic levels and the standard deviation from an ensemble of four runs **(top)** using the log-normal preference function, and **(bottom)** the inverse parabolic preference functions. The preferred prey volume ratio (β) is varied against the maximum preference function width (c_{max}) across a range of values. All other parameters took the values specified in table 5.3.1.

The model configurations on which figure 5.3.1 is based were run for 2 days. Some produced reasonable results in a much shorter time than that, whereas others ran slowly due to large populations. The different combinations β and c_{max} produced some dynamic behaviours. The sensitivity analysis reveals that some parameter combinations produced a wider range in the number of trophic levels. These are considered to be the result of stochastic fluctuation rather than a robust property of the model. Understandably, it is not possible to explore all the results. Those that are presented produced a low standard deviation.

5.3.2 Exponential Population Growth

Many of the tested β and c_{max} parameter values produced population numbers that reach in excess of one million. It was found that for higher c_{max} values there was a tendency for the smallest individuals to evolve toward even smaller volumes. Once there, their size classes grew exponentially until the

phytoplankton was exhausted. This result was common for both preference functions although there were differences. Using the log-normal preference function with values of c_{max} above 1.5 produced populations that were too large to compute sufficient data, despite running the model for two days. Some of these configurations demonstrated that the rate of growth of the smallest individuals was so great that it resulted in the collapse of the higher trophic levels. This provided more volume for the smaller individuals to grow even further. Use of the inverse parabolic function also illustrated this dynamic, but the growth was not so aggressive. The higher trophic levels did not collapse and the model remained stable with comparatively higher values of c_{max}.

This section presents two sets of results side-by-side for comparison. Each configuration uses different values for the predator-prey volume ratio (β) and the maximum preference function width (c_{max}), and preference functions. In the figures that follow those on the left use the log-normal preference function, a β value of 25, and a c_{max} value of 2. The figures on the right use the inverse parabolic preference function, a β value of 10, and a c_{max} value of 3. All other parameter values are defined table 5.3.1.

The first thing to note is that both sets illustrate a rapid increase in the number of individuals.

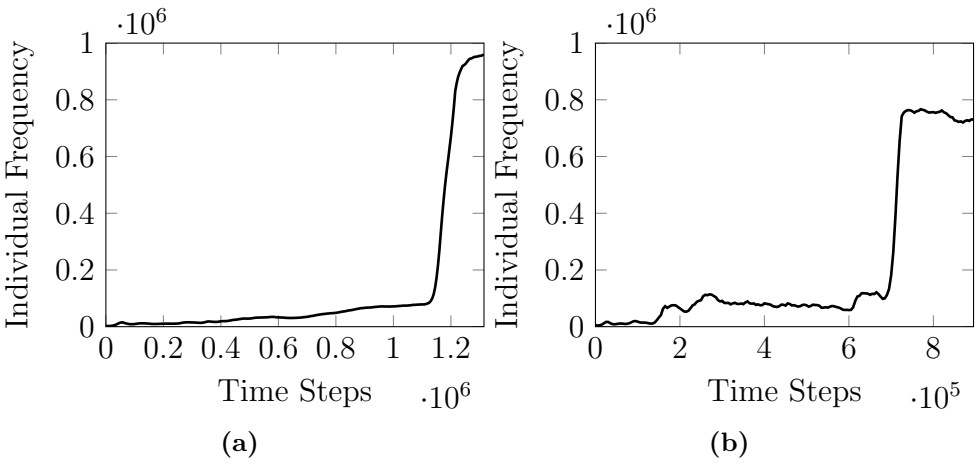

Figure 5.3.2: The total number of heterotrophic individuals with use of the **(a)** log-normal, and **(b)** inverse parabolic preference function over time.

The population growth is coupled to a rise of the inward flux of material and the coversion of all the phytoplankton into heterotrophic volume (figure 5.3.3).

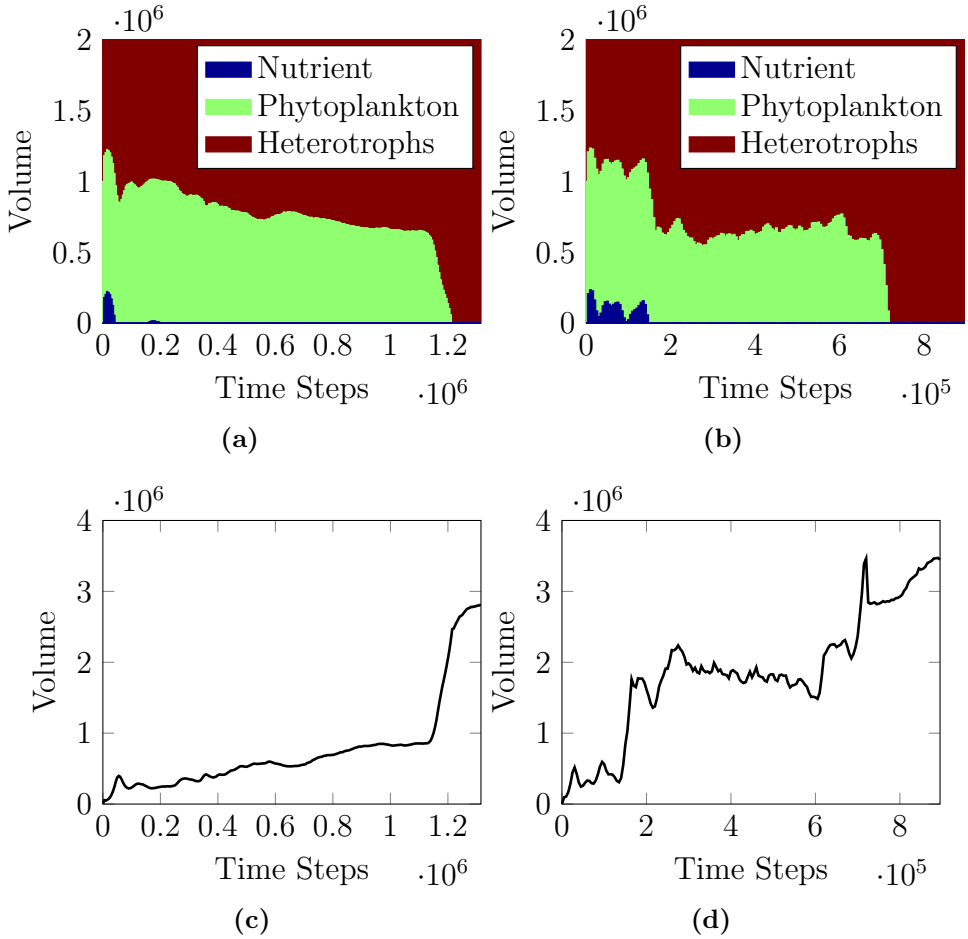

Figure 5.3.3: The top row shows the volumes of each of the pools of matter, and the bottom row shows the flux from consumption of phytoplankton over time, with use of the **(left)** log-normal, and **(right)** inverse parabolic preference functions.

Viewing the system in terms of contributions to each size class illustrates that the increase in the number and volume of heterotrophs is due almost entirely to the smallest individuals in the system (top two rows, figure 5.3.4). The rate of consumption of both phytoplankton and other individuals goes up for the smallest individuals, and down for the larger individuals (bottom row, figure 5.3.4). This is also visible as a drop in the number and volume of larger individuals (top two rows, figure 5.3.4).

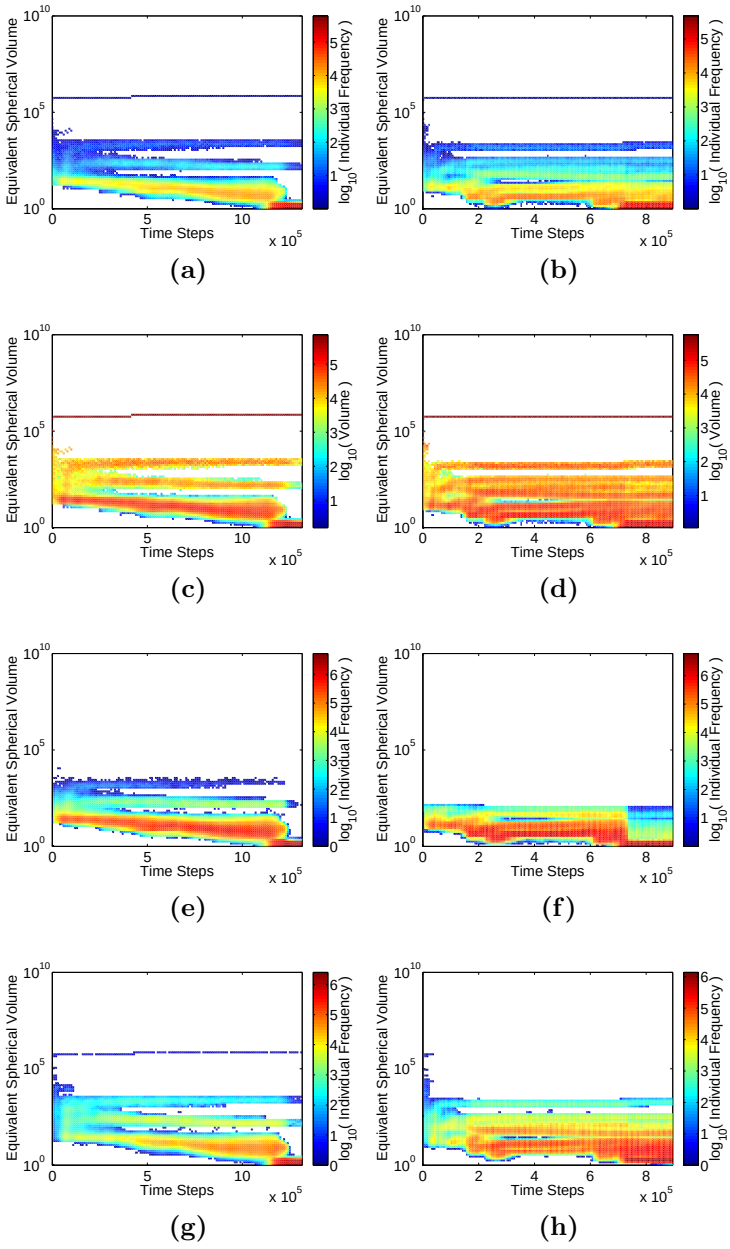

Figure 5.3.4: The evolution of the d size classes on the y-axis, over time on the x-axis. Plots show: **(top)** the number of all individuals, **(second row)** the volume of each size class, and **(third row)** the numbers of herbivores and **(bottom)** carnivores, with use of the **(left)** log-normal, and **(right)** inverse parabolic preference functions.

This large change to the feeding dynamics alters other attributes of the system. The top row in figure 5.3.5 shows that the average trophic classification of the smaller individuals goes up, thereby increasing the number of trophic levels in the system. This happens because the smallest individuals are taking a

mixed feeding strategy by consuming the phytoplankton (if available) and other individuals. A plot of the average preference trait values (bottom row, figure 5.3.5) illustrates that there are sustained periods where there is a range of feeding strategies in each trophic level.

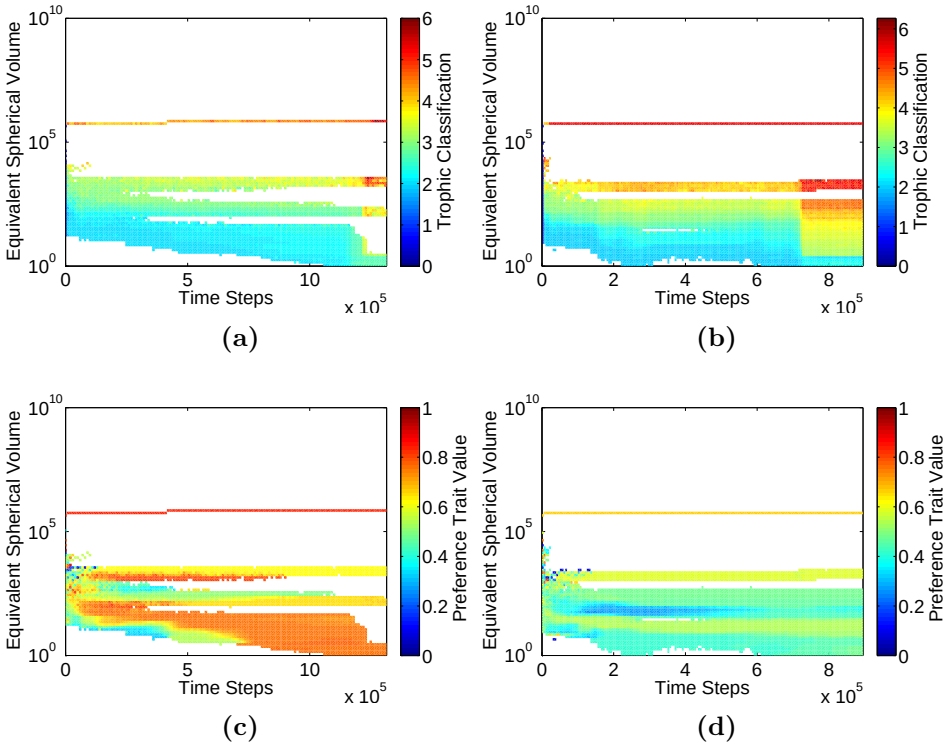

Figure 5.3.5: The evolution of the d size classes on the y-axis, over time on the x-axis. Plots show: **(top)** the mean trophic classification and **(bottom)** preference trait value of each size class, with use of the **(left)** log-normal and **(right)** inverse parabolic preference functions.

Coexistence is both more pronounced, and apparently more fragile with use of the log-normal over the inverse parabolic preference function, as figure 5.3.5c shows that coexistence disappears when the exponential increase of small individuals occurs. Figure 5.3.5d shows that the largest individuals have a preference trait value of around 0.67. Figure 5.3.4h shows that these individuals do not consume anything for most of the model run. This confirms the observation made in section 5.2.1; that trait values in the top third of trait space are not viable. The reduction in viable trait space with the inverse parabolic function may be the reason why coexistence of individuals of the same trophic level and different feeding strategies is not apparent in these plots. However, it is less affected by the exponential increase of small individuals.

The exponential growth of the small individuals is not so pronounced when using the inverse parabolic preference function. This is evident by comparing the plots of the number of heterotrophs. Figure 5.3.2a shows that the population reaches almost 1e+6, whereas figure 5.3.2b shows that it reaches around 8e+5. The lower total number of individuals is the reason that use of the inverse parabolic function permits the computation of a greater number of abstract time steps when running the model for the same amount of real time. In additon, the system remained stable and avoided exponential growth of the smallest individuals for higher values values of c_{max} when using the inverse parabolic function. However, figure 5.3.3d shows that the material flux into the heterotrophs is greater with the use of the inverse parabolic preference function. The fact that the number of heterotrophs is lower must mean the volume is spread over a smaller number of larger herbivores than in the configuration that makes use of the the log-normal preference function.

5.3.3 Coexistence

Fortunately not all of the combinations of β and c_{max} values tested produced the exponential population growth illustrated in section 5.3.2. Many parameter combinations produced trophic systems that remained stable. The results in this section were selected as they exhibited sustained periods where a range of preference functions coexisted in the same trophic level.

The first set of results use the log-normal preference function, a β value of 10, and a c_{max} value of 1.5. All other parameter values are defined table 5.3.1.

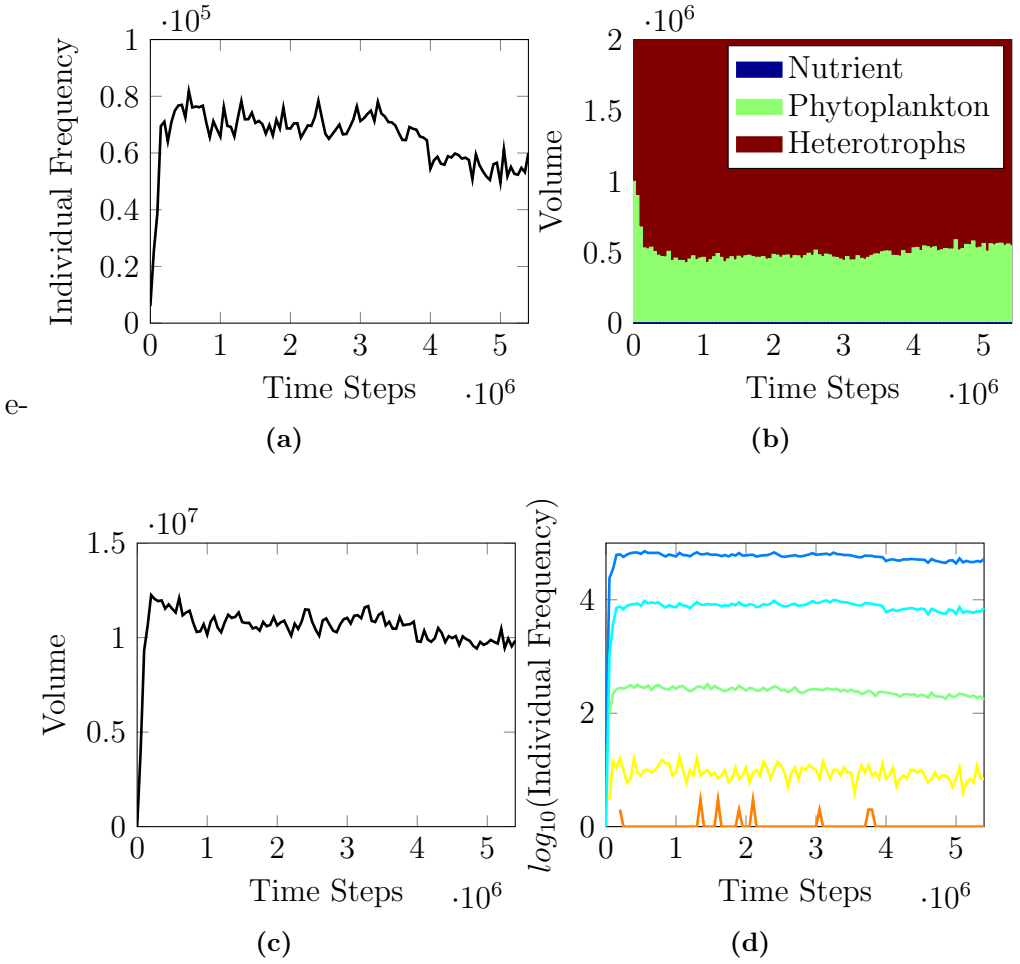

Figure 5.3.6: Plots show: **(a)** the total number of heterotrophic individuals, **(b)** the volumes of each of the pools of matter, **(c)** the flux from consumption of phytoplankton, and **(d)** the frequencies of secondary (blue), tertiary (cyan), quaternary (green), quinary (yellow), and senary (orange) producers over time.

The first obvious result from figure 5.3.6a is that the total number of heterotrophs is much more stable, and actually decreases slightly. This is reflected in the plot of the volume in the system (figure 5.3.6b) and the flux from consumption by herbivores (figure 5.3.6c). However, figure 5.3.6d illustrates that the decrease in heterotroph frequency is consistent, and therefore divided across the trophic levels.

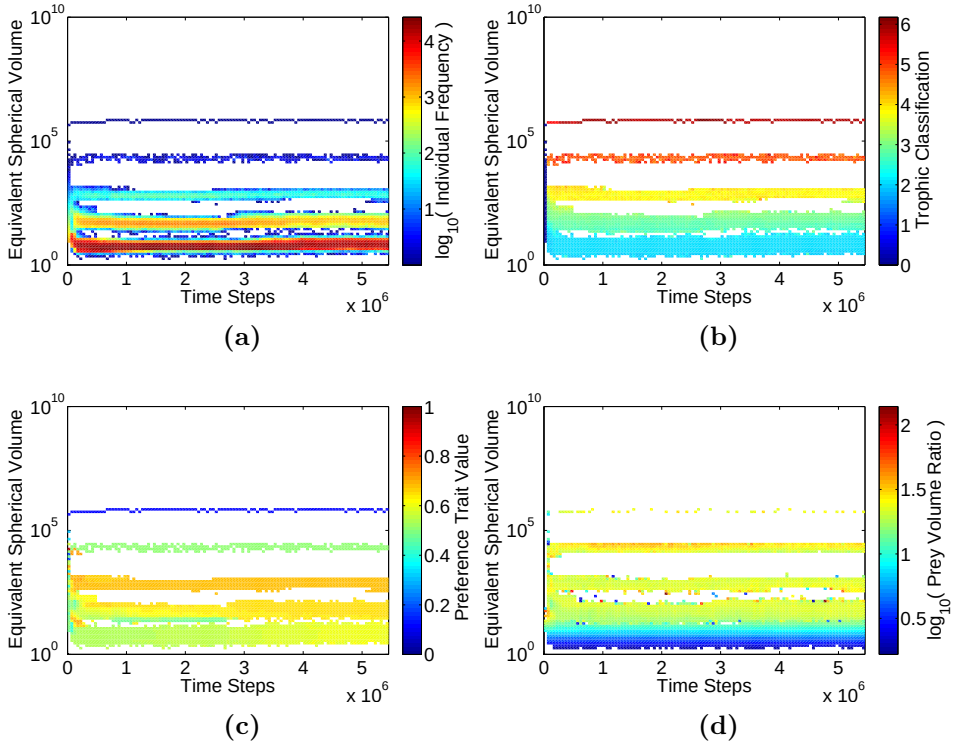

Figure 5.3.7: The evolution of the d size classes on the y-axis, over time on the x-axis. Plots show: **(a)** the number of all individuals, and the mean **(b)** trophic classification, **(c)** preference trait values, and **(d)** actual predator-prey volume ratio of each size class over time in a configuration that uses the log-normal preference function, a β value of 10, and a c_{max} value of 1.5.

The size class view of the system (figure 5.3.7a) confirms the stability of the system. Figure 5.3.7b shows there are a comparatively large number of trophic levels that are near to each other in volume trait space. This is a function of the relatively low β value of 10. Figure 5.3.7c shows that from around 8e+05 time steps the tertiary producers have been selected to use two distinct feeding strategies. The larger tertiary producers have a preference trait value of around 0.65 (generalist), and the smaller individuals' trait value is around 0.5 (specialist). From 2.7e+06 time steps onwards, the generalists slowly replace the specialists.

The apparent disappearance of this coexistence and the decrease in the number of heterotrophs (figure 5.3.6a) is believed to be the result of a trophic cascade. At around 2.5e+06 time steps the quaternary producers move slightly higher in trait space. In doing this they exert a reduced grazing pressure on the tertiary producers. This is apparent at around 2.7e+06 time steps when they move

higher in volume trait space. At the same point in time the coexistence of feeding strategies in the tertiary producers apparently disappears. From that point until the end of the model time the secondary producers move towards larger volumes and evolve toward a more generalist feeding strategy. This is illustrated in figure 5.3.7c by the gradual change from an average preference trait of around 0.5 to 0.6. However, it should be emphasised that the plot in figure 5.3.7c shows the mean preference trait value for the size class. The presence or absence of coexistence within a single size class cannot be determined from that plot alone. An individual-level view of the system should illustrate the detail of what happens in the model during this time.

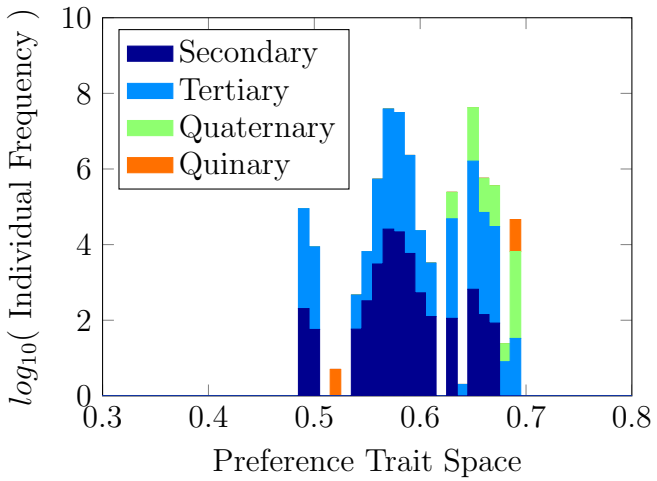

Figure 5.3.8: A stacked bar chart showing the frequencies of preference trait values in the range 0.3–0.8 within each trophic level at 2.5e+06 time steps.

The first thing to note from figure 5.3.8 is that it does not show the largest individual that drifts between the quinary and senary trophic level because the plot shows log_{10} of the numbers of individuals. Figure 5.3.8 illustrates that there is much more variation in trait values within each trophic level than is shown in figure 5.3.7c. The tertiary specialists are comprised of more than two hundred individuals that have a preference trait value of 0.47–0.5. The rest of the tertiary producers make up the group previously referred to as the "tertiary generalists". It is clear in figure 5.3.8 that they occupy a much wider range of preference trait space than is apparent from figure 5.3.7c.

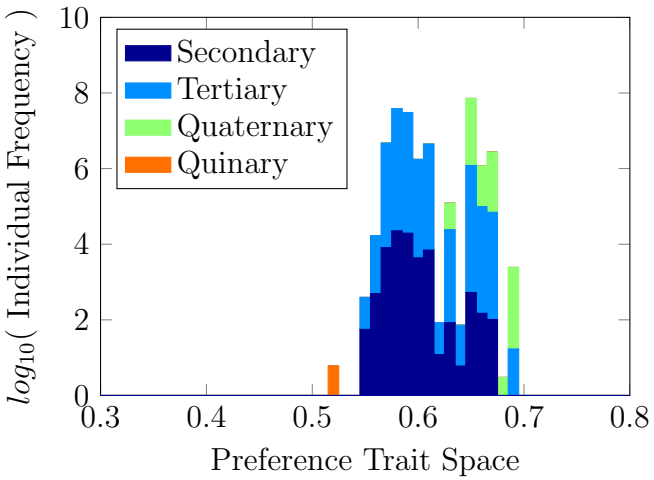

Figure 5.3.9: A stacked bar chart showing the frequencies of trait values in the range 0.3–0.8 within each trophic level at 3.05e+06 time steps.

Figure 5.3.9 confirms that by 3.05e+06 time steps the tertiary specialists are no longer present. It also shows that a group of secondary specialists have disappeared. There is a general shift of the secondary, tertiary and quaternary producers toward a more generalist feeding strategy. This can only have happened because a generalist feeding strategy was selectively beneficial. This is seen to be due to the spread of the trophic levels over a wider region of volume trait space. Having a wider preference function in that situation enables easier access to more distant prey.

The results suggest that the period of coexistence in the tertiary producers between 0.8e+06 and 2.7e+06 time steps was brought about by the strategy adopted by the secondary producers. Figure 5.3.7c shows that during that time the secondary producers are very near in volume to the tertiary specialists. Figure 5.3.7a shows that the specialists are less numerous than the generalists. It appears that the secondary producers had been selected to exploit the lower evolvability of the less frequently reproducing tertiary producers. The larger secondary producers were easy prey for the tertiary specialists. However, the lower numbers of tertiary specialists permitted greater reproductive success for the secondary producers. Coexistence in this situation was an anti-predator adaptation to avoid the more numerous tertiary generalists.

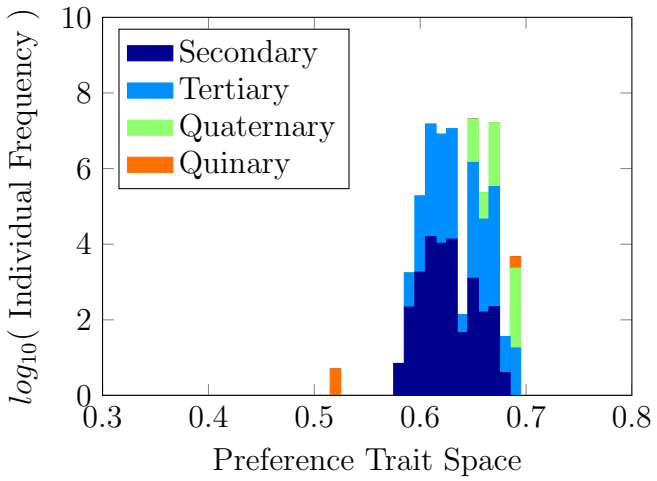

Figure 5.3.10: A stacked bar chart showing the frequencies of trait values in the range 0.3–0.8 within each trophic level at 5e+06 time steps.

By 5e+06 time steps, figure 5.3.10 illustrates that nearly all the heterotrophs have converged in a preference that reflects a generalist strategy.

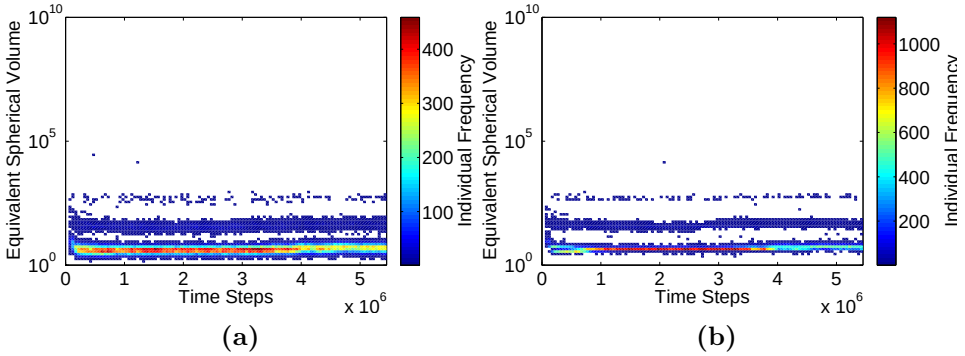

Figure 5.3.11: The evolution of the d size classes on the y-axis, over time on the x-axis. Plots show: the number of mutations of the **(a)** volume, and **(b)** preference heritable traits in each size class over time in a configuration that uses the log-normal preference function, a β value of 10, and a c_{max} value of 1.5.

The anti-predator adaptation explained above is only possible due to the reduced rate at which larger individuals reproduce, and therefore the reduced rate at which they mutate. Any strategy that is successful for a prey individual, is likely to be undermined by a mutant predator at some point. Figure 5.3.11 shows the number of mutations of each trait occuring in each size class over time. It is apparent that this configuration has a high turnover and so the tertiary, quaternary, and even quinary producers show mutations during

the time it was run for.

The second set of results use the inverse parabolic preference function, a β value of 25, and a c_{max} value of 2.5. All other parameter values are defined table 5.3.1.

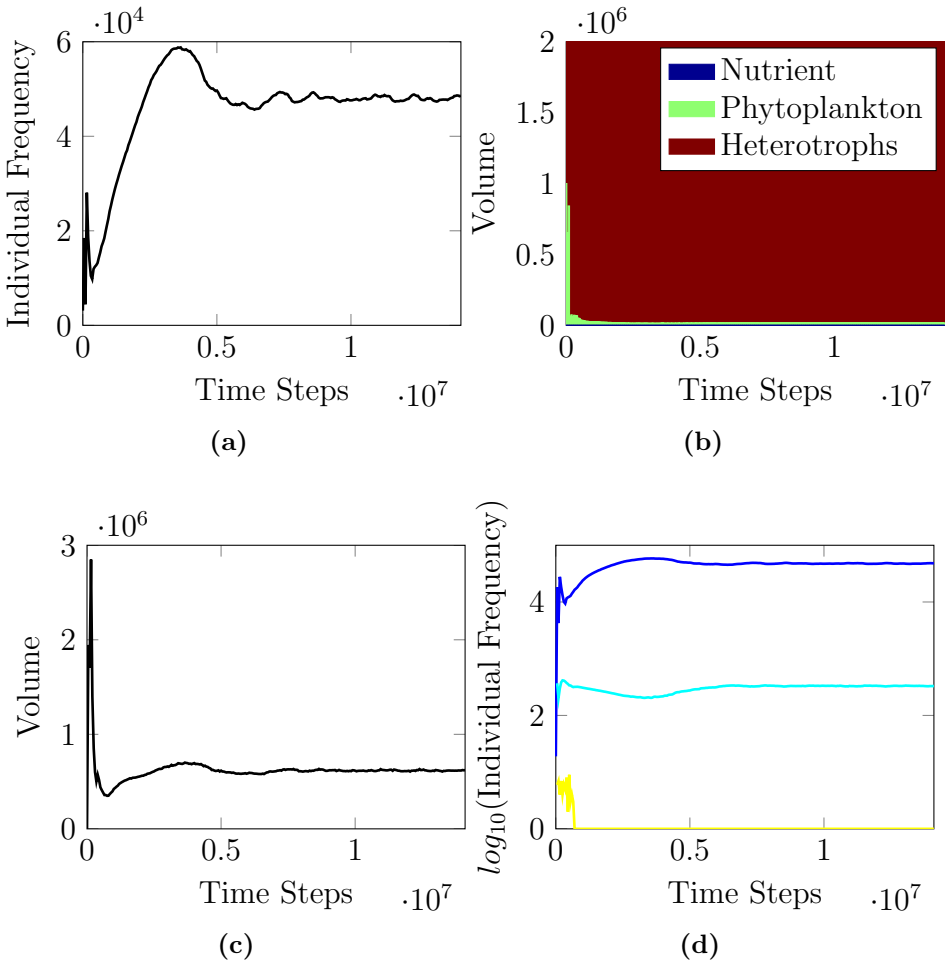

Figure 5.3.12: Plots show: **(a)** the total number of heterotrophic individuals, **(b)** the volumes of each of the pools of matter, **(c)** the flux from consumption of phytoplankton, and **(d)** the frequencies of secondary (blue), tertiary (cyan), quaternary (yellow) producers over time.

The first thing to note from from figure 5.3.12a is that the number of heterotrophs in the system is lower, but after 5e+06 time steps it is generally more stable than in the previous configuration. Figure 5.3.12c shows relatively constant grazing on the phytoplankton. This is reflected in figure 5.3.12b that illustrates almost all of the volume in the system exists in the heterotrophs for most of the model run. Figure 5.3.12d shows that the high β value provides

only enough niche space for three trophic levels. The change in the numbers of heterotrophs suggests there are changes in trophic structure, despite the consistent net effect of the individuals.

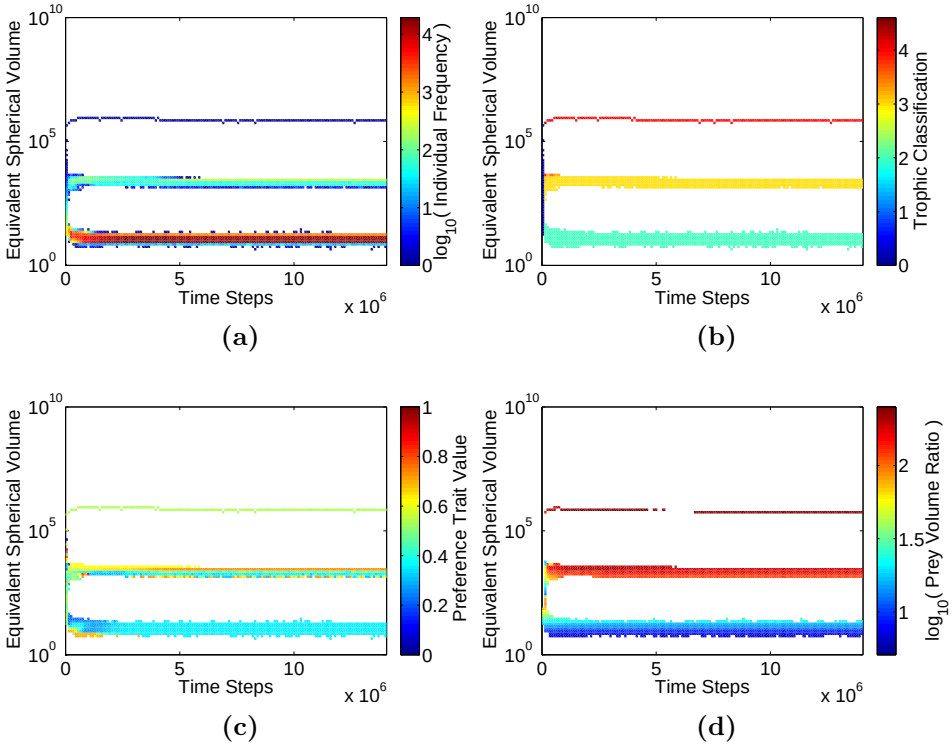

Figure 5.3.13: The evolution of the d size classes on the y-axis, over time on the x-axis. Plots show: **(a)** the number of all individuals, and the mean **(b)** trophic classification, **(c)** preference trait values, and **(d)** actual predator-prey volume ratio of each size class over time in a configuration that uses the inverse parabolic preference function, a β value of 25, and a c_{max} value of 2.5.

The size class view of the system confirms three well spaced trophic levels (figure 5.3.13b). This is seen to be a function of the comparatively high values of c_{max} and β. Figure 5.3.13c shows sustained coexistence of feeding strategies in the tertiary producers over a narrow range of volumes. The tertiary producers are comprised of generalists that are larger and smaller in volume than a group of individuals that take a more specialist feeding strategy. Reflecting the observation of figure 5.3.12a, after 5e+06 time steps figure 5.3.13a shows that the larger generalists are the most numerous, the specialists are less so, and the number of smaller generalists is dwindling.

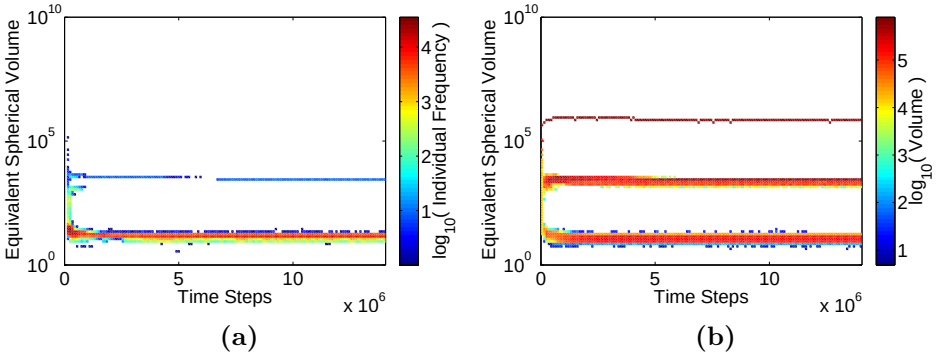

Figure 5.3.14: The evolution of the d size classes on the y-axis, over time on the x-axis. Plots show: the number of **(a)** prey, and the **(b)** volume of each size class over time, in a configuration that uses the inverse parabolic preference function, a β value of 25, and a c_{max} value of 2.5.

Figure 5.3.14a illustrates that the quaternary producers are only just able to reach the tertiary producers. Before 5e+06 time steps they feed exclusively on the largest tertiary producers. The reason why these individuals disappear from the system is because the grazing pressure exerted on them was not matched by their ability to assimilate. Once they have disappeared from the system the competition amongst the tertiary producers is reduced. It is shown in figure 5.3.14b that the larger generalists become the most volumous when that occurs. The quaternary producers are not able to feed until they shrink slightly as a result of their metabolism. This is shown in figure 5.3.14a as the break in feeding on the tertiary producers, and figure 5.3.14b that shows the quaternary producers move to a size class with a lower v_m value.

This new trophic structure is more sustainable. Despite being grazed consistently, the larger tertiary generalists are able to assimilate at a rate that balances all material losses. This is shown in figure 5.3.14b as the near constant volume of these individuals. The tertiary specialists are not being predated upon, but their volume also remains consistently in the same order of magnitude as their larger generalist counterparts. This suggests that the tertiary specialists' feeding strategy was selected as a result of its lower efficiency. When contrasted against the more successful, larger generalists, the tertiary producers avoid being predated upon.

To investigate this configuration further an individual-level view of the system is taken.

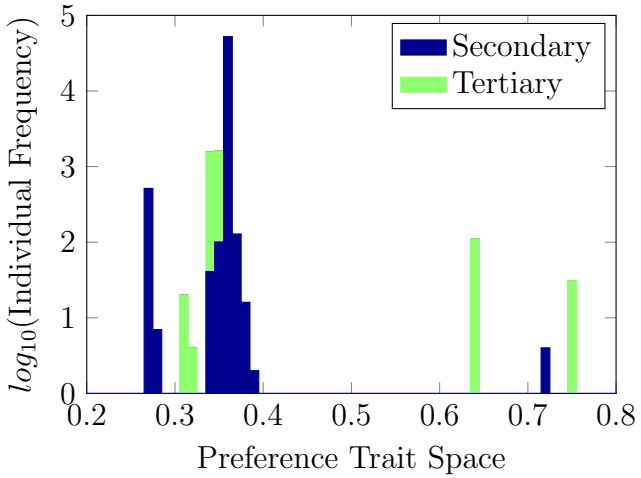

Figure 5.3.15: A stacked bar chart showing the frequencies of trait values in the range 0.2–0.8 within each trophic level at 2.7e+06 time steps.

There is only a single tertiary producer, and so it does not show in figure 5.3.15. However, the plot confirms that at 2.7e+06 time steps both the secondary and tertiary producers take a range of feeding strategies. This is most significant in the tertiary producers because figure 5.3.15 shows that the individuals occupying the distinct points in preference trait space are approximately equally abundant.

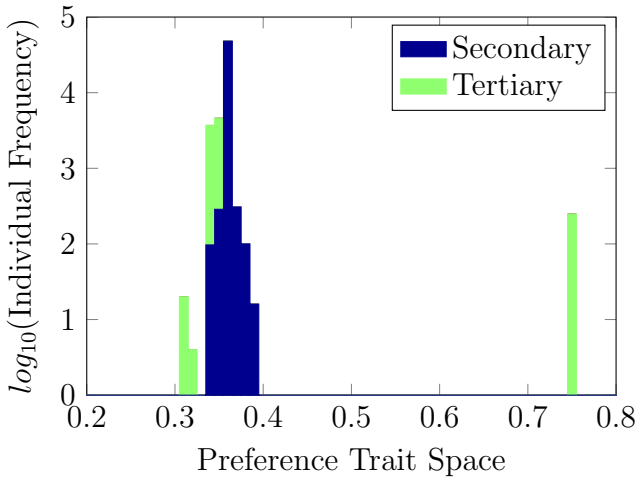

Figure 5.3.16: A stacked bar chart showing the frequencies of trait values in the range 0.2–0.8 within each trophic level at 7.5e+06 time steps.

Figure 5.3.16 shows that by 7.5e+06 time steps the secondary producers have converged on a narrower range of trait values that reflect a specialist strategy. Conversely, the tertiary producers have maintained their diversity. It also

appears the tertiary generalists with preference trait $g = 0.75$ have increased in number. This is despite the observation that the trade-off is only captured with $g < 0.67$ (figure 5.2.2b). This suggests these individuals were selected, but are now unable to evolve to a more efficient feeding strategy due to their low numbers. The trait frequencies stay this way until the end of the model run.

The mechanism behind these results are more intuitive. The tertiary generalists are larger than the specialists in this configuration. Being higher in volume trait space they are more distant from their prey, so a wider preference function gives them a greater ability to feed. Conversely, the tertiary specialists are nearer to their prey and so are benefitted by their feeding strategy. Figure 5.3.13c shows that there are also some smaller generalists. However, this strategy is not very effective as figure 5.3.13a illustrates their numbers to be very low. They are hanging on to a tenuous existence by feeding on smaller secondary producers.

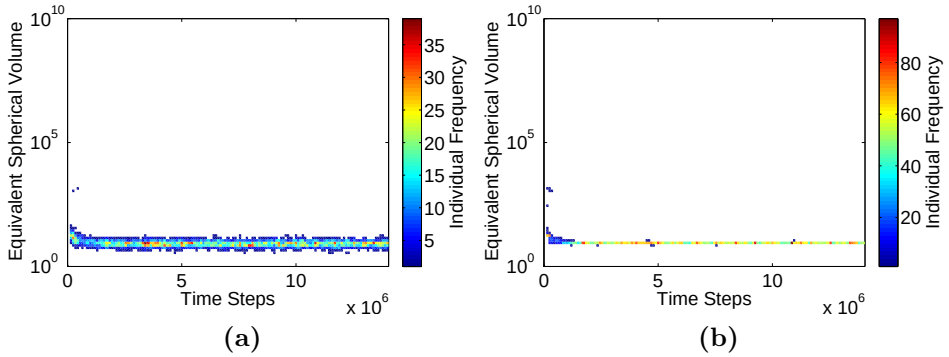

Figure 5.3.17: The evolution of the d size classes on the y-axis, over time on the x-axis. Plots show: the number of mutations of **(a)** the volume, and **(b)** preference heritable traits in each size class over time in a configuration that uses the inverse parabolic preference function, a β value of 25, and a c_{max} value of 2.5.

Figure 5.3.17 shows the number of mutations of the volume and preference traits over time. Reflecting the conclusion of chapter 4, the rate of reproduction of the tertiary and quaternary producers is too low to produce mutants. This means that the trait values of the tertiary and quaternary producers in this configuration entered the population during initialisation, and were reinforced only through reproduction and starvation.

The two sets of results presented used different parameter combinations and

preference functions. However, the results produced with the log-normal preference function show a tendency of the system to converge on a preference trait value of ∼0.64 (figure 5.3.10). Aside from the individuals stuck with a less efficient feeding strategy, use of the inverse parabolic function shows a tendency of the system to converge on a preference trait of ∼0.36 (figure 5.3.16). To investigate this contrast between the tendency towards generalism in the first case, and specialism in the second case, the convergent trait values are used to visualise their resultant feeding strategy.

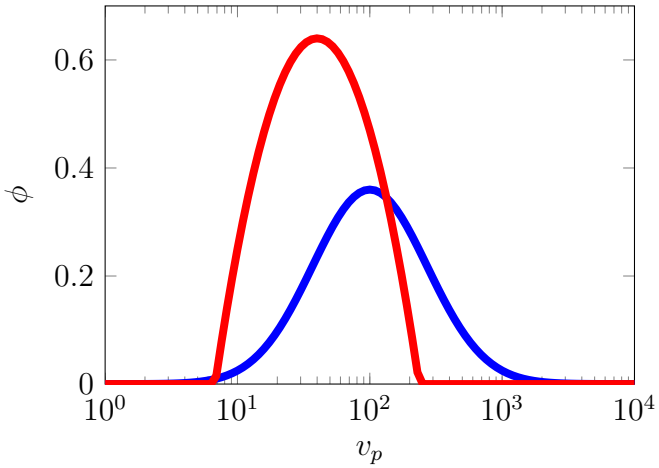

Figure 5.3.18: A comparison of the convergent log-normal (blue - $g = 0.64$, $\beta = 10$ and $c_{max} = 1.5$), and inverse parabolic (red - $g = 0.36$, $\beta = 25$ and $c_{max} = 2.5$) preference functions using their respective parameter configurations and a constant predator volume of 1000.

Figure 5.3.18 shows the convergent log-normal and inverse parabolic preference functions from the model configurations that produced the results in this section. In both cases, the convergence of trait values was most apparent in the secondary producers. Their high numbers and comparative rapidity of reproduction and mutation suggest that the preference functions in figure 5.3.18 may represent an optimal solution for each system. However, contrary to what might have been expected, the log-normal preference function, which is widest and could be classified as more generalist to begin with, converged towards even more generalist gene values, and vice versa for the inverse parabolic function. The mechanism behind the convergence of trait values is not obvious and would require further investigation.

5.4 Discussion

5.4.1 Exponential Population Growth

The exponential growth of the smallest individuals that was exhibited for many combinations of c_{max} and β can be explained as a feature of both preference functions for individuals at the smallest end of volume trait space. Figure 5.4.1 below shows plots of both preference functions for a range of c_h values with c_{max} set to 1.5.

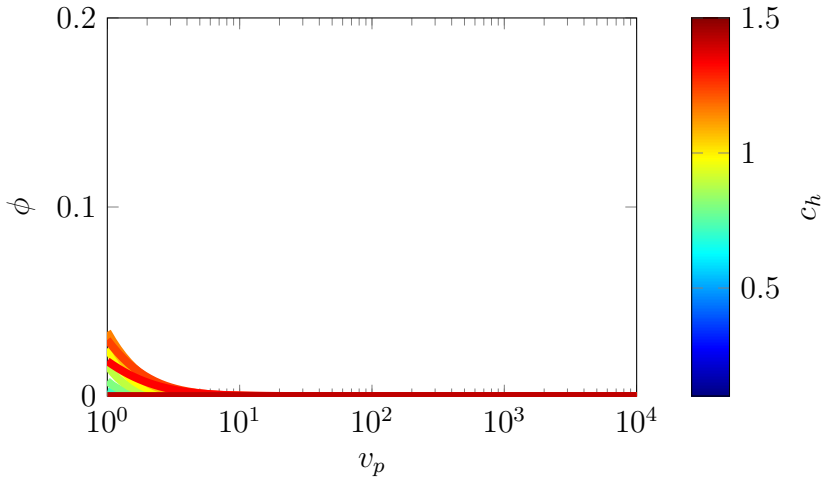

(a)

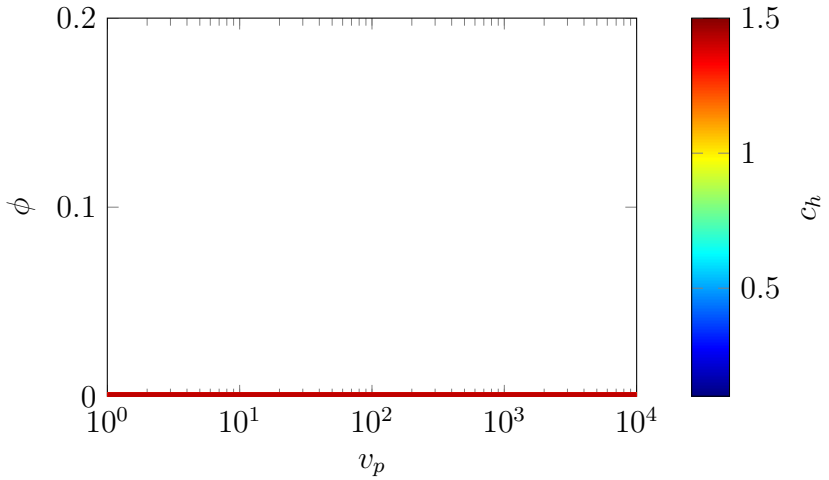

(b)

Figure 5.4.1: The **(left)** log-normal and **(right)** inverse parabolic predator preference (ϕ) as a function prey volume (v_p) for a range of preference function widths (c_h) and corresponding heights (a_h) for c_{max} set to 1.5. In both the predator/grazer volume (v) is v_{small}, the preferred prey volume ratio (β) is 10, and c_{min} is 0.1.

Figure 5.4.2 below shows plots of both preference functions for a range of c_h values with c_{max} set to 3.

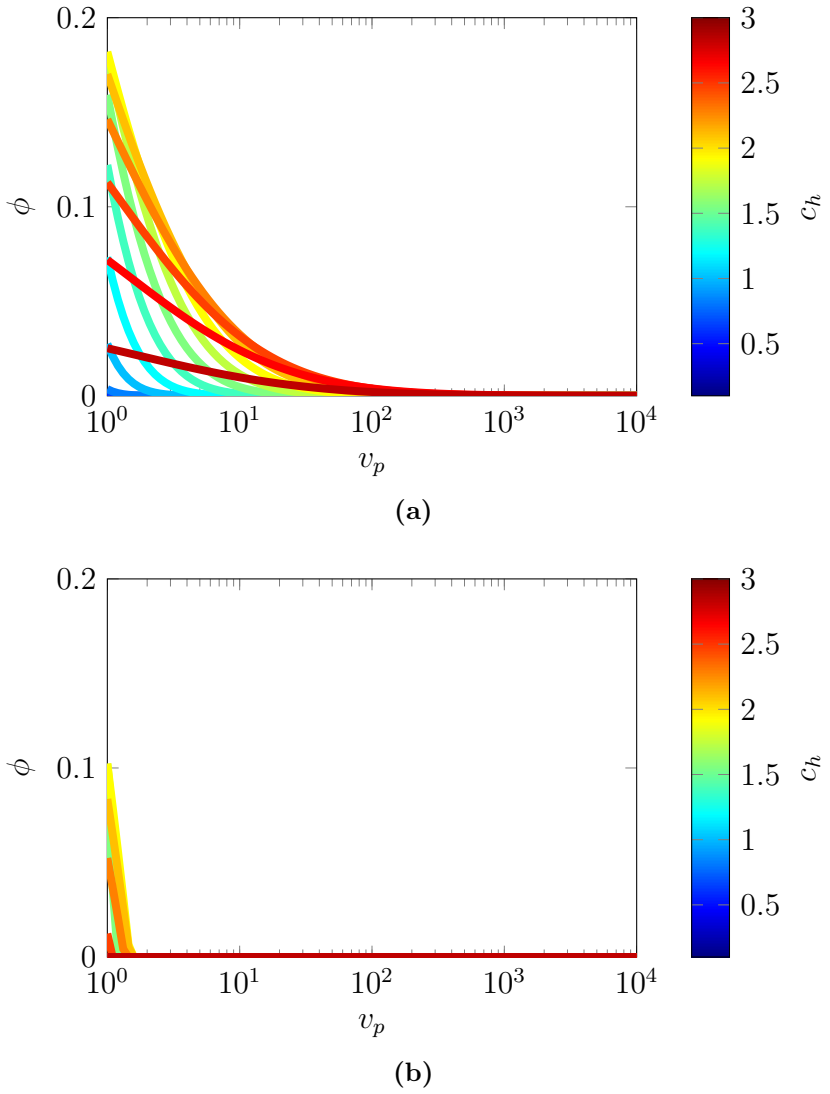

Figure 5.4.2: The **(left)** log-normal and **(right)** inverse parabolic predator preference (ϕ) as a function prey volume (v_p) for a range of preference function widths (c_h) and corresponding heights (a_h) for c_{max} set to 3. In both the predator/grazer volume (v) is v_{small}, the preferred prey volume ratio (β) is 10, and c_{min} is 0.1.

As shown in figures 5.4.1 and 5.4.2, sufficiently high c_{max} and low β values provide individuals at the smallest end of volume trait space with some possibility of consuming from their own size class. This probability is higher for the log-normal function than with the inverse parabolic function. As explained in section 2.6.2, despite phytoplankton being represented with a single value for its volume, it is treated as though it were comprised of discrete particles. Her-

bivores consume the volume of a single phytoplankton cell, set at v_{small}. For individuals at the smallest end of volume trait space, this single event would put them much closer to their reproduction threshold.

Combining these observations of the preference function with the results, it seems apparent that certain combinations of c_{max} and β provide an evolutionary attractor that can get size classes with low v_m values caught in runaway growth. Their chances of consuming increase as their numbers grow. The reason for the comparatively low β value is due to issues of computation and Elton's "pyramid of numbers" (Elton, 1927). High β values would require a vast number of small individuals just to sustain a low number of trophic levels. Since the purpose of EATSM is to explore evolution in a trophic context, the choice of parameter values is a greater reflection on pragmatism than realism.

Exponential growth of the smallest individuals also occurred during the development of the model in chapter 4. Since this was due to the relative size of children it happened immediately, and consistently for all parameter configurations. This was the reason for constraining the size of the Ω trait based on the size of the individual. Because the exponential growth of the smaller size classes in this model did not always appear, understanding how and why it happened became a large part of the work. The plots in figure 5.1.3 summarised size selectivity data of heterotrophic dinoflagellates and pelagic ciliates. The literature revealed that the wider (generalist) preference curve of the dinoflagellate was a function of complex feeding structures that are smaller than the body of organism. The model uses v_{small} to set the size below which an organism would be unable to contain the machinery required to maintain its substance. Allowing the smallest individuals to take any preference trait value effectively violates this assumption. It is therefore concluded that the preference traits should be constrained for the smaller individuals, in a similar way to the previous chapter.

This conclusion illustrates that trade-offs are not universal. A biological trade-off carries rules that may seem to apply generally, but in reality there are likely to exist scales at which some of them can be bent, others can be broken. Or as in this case, scales at which the trade-off does not apply. This implies that an identified trade-off may require careful consideration of its general applicability.

5.4.2 Coexistence

This study aimed to determine the mechanisms behind the coexistence of generalists and specialists in planktonic ecosystems. The results showed that coexistence of different feeding strategies in the same trophic level was possible, and that it fell into two regimes. The less stable form of coexistence (shown in figure 5.3.7) was reinforced by the prey of the coexisting individuals. It was selectively advantageous for them to be an easier target for their less numerous specialist predators and avoid predation from their more numerous generalists. This outcome is only possible due to the reduced evolvability of the tertiary producers. This was not a sustainable form of coexistence because with enough time a mutant predator would appear and exploit the strategy adopted by the prey.

Figure 5.3.7 illustrated a stable form of coexistence where a generalist strategy benefitted larger individuals who were more distant from their prey. The mechanism of coexistence in this case was the result of predators who were only just able to reach coexisting individuals. In this scenario the group was comprised of larger, more successful generalists and smaller, less efficient specialists. The less efficient specialists were selected because of their slightly smaller size, and their lower efficiency. When constrasted against their more successful counterparts they experienced a reduced rate of predation. This suggests that coexistence can occur even if similar individuals are exploiting the same sources of prey. It also shows that predator mediated coexistence does not have to include two predators, as long as the efficiency of the prey's feeding strategy results in some change in the rates of predation.

5.4.3 Unexplored Detail

As highlighted in the literature, a plankter's size selectivity is a mechanistic function of evolved phenotypes. The approach of this model was to approximate those structures by allowing evolution of the width of the preference function. The reviewed literature suggests that one of the most measured features of a plankter's feeding strategy is the preferred prey volume ratio, characterised in this model by the parameter β. This study chose to keep the value of β fixed, and evolve only the width of the preference function in isolation. This work has paved the way for the introduction of β as an additional

evolutionary trait. However, it is worth noting from the plots of the actual predator-prey volume ratios (figures 5.3.13d and 5.3.7d) that the changes to this model permitted predators to consume prey that were significantly different from the constant β value.

As suggested in section 5.1, a plankter's feeding strategy introduces many trade-offs that are not exclusively related to prey finding. Gerritsen and Strickler (1977) produced some early mathematical models of predator-prey encounters between zooplankton. They discussed the concept of a "detection sphere" that provides both predator and prey with a early indication of approaching targets or threats. Later work by Costello et al. (1999) analysed high-speed footage of encounters between copepods and a common predator. Combining their findings with those of other researchers they found that encounters between planktonic predators and prey fell into a general pattern they referred to as the "predation cycle":

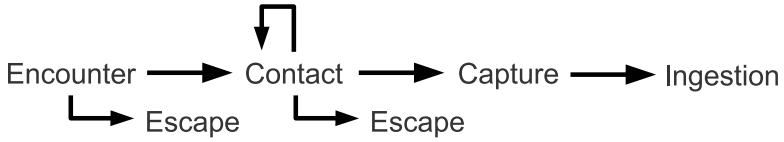

Figure 5.4.3: Costello et al.'s (1999) "predation cycle".

Individuals in this version of EATSM have no evasive or defensive capability. Benefit comes only from an individual's ability to capture prey. However, the literature suggests that detection and detectability are intimately related to the strategy a plankter has adopted to feed. In addition, the literature revealed evidence of metabolic trade-offs associated with predator avoidance. The model presented here made no link between the feeding strategy and the metabolic rate. However, such a link could realistically be established as part of some future work.

5.5 Conclusions

The conclusions of the model:

1. The preference needs to be constrained for small individuals.

The science conclusions:

1. Not all trade-offs are universal.
2. Prey mediated coexistence is possible, although transient by nature.
3. Stable coexistence can occur even if similar individuals are exploiting the same sources of prey.
4. Individuals can be selected to take a less efficient feeding strategy, if it makes their more successful competitors the target for predators.
5. Preference function width viability is a function of prey availability.

The future work suggestions:

1. Individuals could carry β as an evolvable trait.
2. Individuals could be adapted to include some form of evasive or defensive capability.
3. The feeding strategy could be associated with a metabolic cost.

6 Discussion

Chapters 4 and 5 are summarised in this chapter. Each summary contains some higher-level discussion not previously seen. A wider context section looks at broader considerations that came out of this study, as well as evaluates some of the problems faced with the modelling approach. Some suggestions for future work are made. The chapter finishes with the main conclusions of the thesis.

6.1 Chapter Summaries

6.1.1 Chapter 4

Life history theory predicts that a reduced juvenile survival will select for delayed maturation and decreased reproductive effort, and reduced adult survival will select for accelerated maturation and increased reproductive effort. This prediction was considered to reflect Ricklefs' counteradaptation hypothesis (1970) from the perspective of prey. The counteradaptation hypothesis was written to describe the mechanism behind the variation in frequency and size of bird clutches observed. Individuals in EATSM did not lay clutches, and so there was no immediate connection with clutch size. However, it was found that clutch production is tied to lifecycles of other organisms in the community and is therefore a phenological process (Phillimore et al., 2013). EATSM does not represent physical conditions, and so ignores seasonality. It was therefore assumed that the size and number of clutches laid by a bird could be seen simply as a material investment over time. The approach of including the Ω trait was to model the fraction of the adult volume invested in offspring. Under constant growth conditions and over a fixed period of time, individuals with a low Ω trait value would produce a greater number of small children than one with a high Ω trait, yet the material investment would be the same. This was considered analgous to clutch size, and was therefore seen as a method for describing a reproductive strategy.

Despite the literatue on reaction norms and plasticity in growth exhibited by many species, time to maturation was also viewed in a materialist way. A large and a small child experiencing the same conditions in EATSM, with the same v_h and Ω trait values would exhibit different growth trajectories. The small child would be disadvantaged because it would take longer to reach its size

at maturity, but also because $k_m < 1$ it would have a proportionally higher metabolic cost. This was seen to represent delayed maturation. Conversely, a large child would require less time to reach its adult size, and may also benefit from a relatively lower metabolic rate. This was considered analogous to accelerated maturation.

Classical models of growth were found to be a function of time. However the contemporary literature on the subject illustrated a move towards considering growth to be a more dynamic process that is ultimately a function of environmental conditions. Individuals in EATSM are linked to their environment through their interactions with predators and prey. In addition to a measure of growth, an individual's actual volume was also seen as an adequate metric to determine how mature it is. The trajectory from birth volume to volume at maturation was mapped onto a linear scale from 0 to 1, on the assumptions that this value could not become negative and that it would never become less than 1 once the individual had reproduced. Although abstract, this provided a way of testing the results against the predictions of life history theory. The incorporation of a single trait to represent the fraction of adult volume above v_h given to a child enabled investigation of "clutch size".

The results presented in chapter 4 showed that individuals' Ω trait values correlated positively with the general age at which they became prey. This represented confirmation of the predictions of life history theory and by extension, Ricklefs' (1970) counteradaptation hypothesis. However, the results also revealed there was strong positive correlation between the Ω trait values and the growth conditions. This was seen to confirm Lack's (1947) food limited hypothesis. This conclusion implied these hypotheses do not contradict each other, despite the fact that Ricklefs set out specifically to offer an alternative explanation for clutch size.

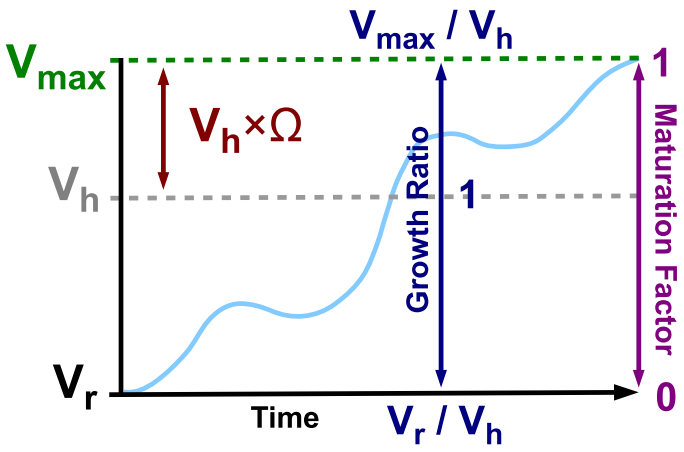

Figure 6.1.1: A visualisation of an individual's growth trajectory (v - light blue) from its volume at birth (v_r) to its reproduction threshold (v_{max} - green) relative to its volume at maturation (v_h - grey) over time. Representations for the scales of the maturation factor (ρ - purple) and growth ratio (dark blue) relative to volume space are also marked.

Figure 6.1.1 is a visualisation that illustrates the relationship between Ω and ρ, and Ω and the growth ratio. It highlights that the correlation between them was due to the fact that they were mapped into the same numerical space. The only exception to this that ρ was fixed at 1 when an individual reproduced, and could not go lower than 0. As discussed following figure 4.3.7, even the very relaxed starvation function used in this model would be unlikely to allow individuals to fall below their birth volume. This suggests the method of determining an indvidual's maturity is invalid. However, ρ was introduced simply to test the predictions of life history theory. Edley and Law (1988), and Reznick et al. (1990) have proven these predictions experimentally. Subsequent modelling approaches have produced similar results (Martínez-Garmendia, 1998; Dunlop et al., 2007). The predictions of life history theory are robust. The primary conclusion from chapter 4 is to reconcile Lack's (1947) and Ricklefs' (1970) hypotheses as two descriptions of the same system. It is believed that this conclusion holds, inspite of the problems with ρ.

It is suggested that the work from chapter 4 could be better integrated into life history theory if an improved method for measuring the maturity of an individual was established. As explained in section 4.2.4, mapping the measure of an individuals maturity onto volume permits an individual to become less 'mature' if it were to lose volume. This approach could be improved by

changing the calculation of ρ so that it only increases. However, even this approach would permit an individual to apparently stay young if it were only able to cover metabolic cost. We would expect an individual in such a situation to starve with the passing of time. There may be a way of calculating the maturity of an individual as a function of age and volume. Although this remains unexplored.

6.1.2 Chapter 5

Ciliates and dinoflagellates are two groups of microzooplankton that both contain heterotrophic species that share a similar biogeography, and are known to exhibit proportional biomasses. Despite the contemporary knowledge that species from each group do coexist, the mechanisms behind their coexistence remain largely unexplored. Data collected by Sailley et al. (2009) showed that pelagic ciliates generally consumed smaller prey, and heterotrophic dinoflagellates less efficiently consumed a wider range of prey sizes (see figure 5.1.3). The data were seen to reflect a feeding strategy trade-off illustrating that ciliates specialise, and dinoflagellates generalise. The hypothesis examined was the possibility that generalists and specialists may coexist as a result of the relative ease with which they can exploit different prey. EATSM was modified to capture the observed trade-off in the individuals' preference function.

The results presented in chapter 5 showed evidence that stable coexistence of feeding strategies could occur, despite individuals consuming the same prey. This outcome may be a product of the individual-based modelling approach. The classical approach to modelling ecological systems is to ignore space and assume that each individual has equal access to a universal or "mean-field" environment (Levin and Pacala, 1997). The results from models of this type suggested that two or more competing species were not able to coexist on the same resource (Lotka, 1925; Lehman and Tilman, 1997). This prompted Hardin (1960) to introduce the competitive exclusion principle; a concept that was generalised with the statement that "n species could not coexist on fewer than n resources or limiting factors" (Lehman and Tilman, 1997). Despite model predictions, Hutchinson (1961) found diverse communities of coexisting phytoplankton competing for the same resources in an apparently homogeneous environment. He observed that the cause was spatial heterogeneity on scales previously overlooked. Individuals are situated in, and compete for dis-

parate resources in space. EATSM does not explicitly represent space, but as an individual-based model it does incorporate some of the rules that apply to interactions in space. This includes the principle that not all individuals interact with the model environment in the same way. Discretisation of encounters alone may provide a mechanism for coexistence.

Some of the results (see discussion following figure 5.3.9) show evidence of a more rapidly producing group of individuals exploiting the comparatively low evolvability of another group. In this particular case it was concluded that the secondary producers had been selected to become an easier target for a group of tertiary specialists. Since the tertiary specialists were less numerous, the secondary producers' rate of assimilation was more easily balanced against the rate of predation. This promoted the coexistence of feeding strategies in the tertiary producers. However, instabilities arose and the coexistence ended before the model did. The tertiary predators in this example were reproducing at a comparatively a high rate. The change in the system may have been due to the emergence of a new tertiary mutant that could exploit the strategy adopted by the secondary producers (see figure 5.3.11). It was therefore concluded that this form of *prey mediated coexistence* is inherently unstable.

Hutchinson (1961) said that two prey species competing for the same resource can coexist if each experiences different pressures from predators. This concept became known as *predator mediated coexistence* (Caswell, 1978). Some results (see discussion following figure 5.3.14) were suggestive of this mechanism, the difference being that one group of individuals were experiencing predation and the others were not. Analysis of the data suggested that the group avoiding predation had been selected to take a less efficient feeding strategy, leaving the more successful competitors as the sole target for predators. This was stable, and continued throughout the the long model run. However, in this example the population levels remained consistently low. This resulted in a low rate of reproduction where few mutants were produced. It is therefore seen as an unfair test of the true stability of this form of coexistence.

The model produced for chapter 5 made use of two different preference functions in order to better understand the exponential population increase presented (see section 5.3.2). Results that were suggestive of coexistence from a high-level perspective were selected from among hundreds (see section 5.3.1 for the parameter combinations tested). This is the reason for the choice of signif-

icantly different parameter configurations in each configuration. Results like those presented in section 5.3.3 were uncommon. This leads to four possible reasons for this rarity. These are presented below with a current evaluation of each.

1. **High-level level views of the system may not be the best way to determine if coexistence occurs.** Data were observed for each size class, trophic level, and preference trait space for hundreds of seperate model runs that took a range of parameter values. Those that did not exhibit the exponential population increase illustrated a convergence that appeared characteristic of selection balancing a sustainable flow of incoming energy (volume) with the spacing between the trophic levels. It has been suggested that there is a tendency of the system to produce generalists with the log-normal preference function, and specialists with the inverse parabolic. The fact that the log-normal preference function is already wide, and the inverse parabolic function is already narrow suggests this is a viable avenue for investigation.

2. **The encounter algorithm or the parameter configuration may not be tuned sufficiently to confer significant cost or benefit to the individuals as a result of a wide or tall preference function.** The fact that coexistence occurs at all suggests that tuning the model parameters or encounter algorithm is not an issue. The selective forces apparent from the results presented were powerful enough to generate dynamics that suggest this is not the cause for the rarity of coexistence.

3. **The unconstrained allocation of preference traits to individuals of any size affects the model outputs even when no exponential population increase occurs.** It was concluded at the end of chapter 5 that both preference functions should be constrained for small individuals. Fixing this would negate the need to use the less efficient inverse parabolic function (see section 3.3.7), particularly as it does not reproduce the trade-off with $g > 0.67$. Constraining the preference functions would be a comparatively short task. Running a full sensitivity analysis with the updated model would serve the evaluation of response 1 and 2.

4. **Capturing the trade-off in the assigned trait values may be incorrect in this case.** The literature revealed that plankters feeding

strategies are tied to metabolic costs (Kiørboe, 2011; Castellani et al., 2005), and to prey detectability and detection by predators (Gerritsen and Strickler, 1977; Eiane and Ohman, 2004). It is therefore considered possible that the data in figure 5.1.3 may be an incidental outcome of a more complex set of metabolic and/or predatory trade-offs.

It is considered that 1, 2, and 3 could be completed in a comparatively short space of time. If no obvious mechanism for coexistence is determined after that, the likelihood of 4 being the explanation would be increased. However, investigating it would represent a significant amount of additional work.

6.2 Wider Context

6.2.1 Evolvability

Kirschner and Gerhart (1998) defined evolvability as "an organism's capacity to generate heritable phenotypic variation." They went on to discuss the criticality of time in the processes of evolution. Selection operates only on what is present at the time, not what was or could be. Gould and Eldredge (1977) noted that on geological timescales life exhibits the capacity for comparatively instantaneous change. Yet there is also evidence for periods where little evolutionary change occurs. They referred to the stepwise nature of evolution on geological timescales as "punctuated equilibria". This suggests a time dependent element in evolution. If we assume that the likelihood of producing novel variation in a reproductive event is approximately constant for all organisms, we could generalise the findings of the results by saying that species that reproduce the most rapidly are likely to be the most 'evolvable', according to Kirschner and Gerhart's (1998) definition.

It should be emphasised that aside from the potential to allometrically scale the metabolic rate, all individuals in EATSM are handled in the same way. What seperates big individuals from smaller ones is the fact that there are more small individuals and fewer large ones. The rate of turnover in the size classes of small individuals is much higher compared to the large individuals. All individuals have the same probability of mutation at reproduction, but there is a decreasing number of reproductive events for individuals higher in the trophic pyramid. This ultimately makes the smaller individuals the most

evolvable. This was the reason for suggesting at the end of chapter 4 that evolution of the Ω trait values represents a mechanism by which evolvability can become an evolvable trait.

The contemporary view is that the relationship between life and the environment is bidirectional (Kirchner, 2002). Understanding the potential rates of change in both is therefore paramount if we wish to mitigate the erosion of biodiversity in the face of climate change. The most generally applicable conclusion we can make from these results is to say that more work needs to be done to bridge the epistemic cut described by Pattee (1995). Many current population-level models are integrated until they reach steady-state. If the natural world is considered a mathematically definiable system and if anthropogenic effects may push the system into a new steady-state, then we will need models that do more to describe the transitional states between stable equilibria.

6.2.2 Trade-Offs

Selection has been operating for long enough to produce many beautifully complex phenotypes. All are constructed out of parts the physical world. They therefore intrinsically conserve mass and obey the laws of thermodynamics. This means they cannot maximise everything. Investment in armour plating, negates the ability to fly; an enhanced power of vision implies that ability be used to find food to cover the elevated metabolic cost. A trade-off is the product of inescapable physical laws. The literature illustrates that capturing a trade-off is integral to the development an adaptive model (Follows et al., 2007; Bruggeman and Kooijman, 2007; Kylafis and Loreau, 2008; Menge et al., 2008, 2009). However, it is considered that implementation of trade-off falls into three known categories.

The term *environmental* is suggested for a trait that captures no trade-off in the value assigned, and only confers cost or benefit when interacting with the model environment. The work of chapter 4 uses this type of trade-off. The term *extrinsic* is recommended for the use of empirical data in capturing trade-offs. This approach takes an observed trade-off and reproduces it in the assignment of trait values. This is illustrated in the work of Follows et al. (2007), and in the approach taken with chapter 5. The third form of trade-off is not represented in this thesis, but appears in the work of Bruggeman

and Kooijman (2007), and Menge et al. (2008). It imposes no restriction on the trait value, but is assumed to represent varying investment in cellular machinery and so carries a corresponding cost. The trade-off is then apparent in the balance of incoming and outgoing energy. We refer to this form of trade-off as *intrinsic*.

There is no reason to consider any one trade-off model better than others. In general trade-offs are universal, but as concluded at the end of chapter 5, a specific trade-off is not. This is seen to be the product of implementations that are functionally independent of their model environment. Current computational constraints mean that this applies to models that have relevance for macro-scale systems. If we wish to produce models that aspire to Maynard Smith's (1992) "comparative biology", we are presently confined to wholly abstract models (e.g. Ray, 1991). The trade-off in modelling trade-offs remains realism versus generality (Levins, 1966).

6.2.3 Epistemic Cuts

This study aspired to the inclusion of the selection pressures and trade-offs brought about by a whole trophic system. This led to the various model incarnations presented in each of the results chapters. By its nature the model attempted to span several scientific domains, including areas where it became apparent that there is a lack knowledge. Abstract descriptions were used to overcome areas where there there are epistemic cuts. Notably were the representations of heritable traits, and starvation in chapter 4 that was decoupled from growth. Pattee (1995) identified an epistemic cut between the genotype and phenotype. He attributed this to the constraints of the tools available to us that prevent experimentation at the scales required in order to understand how living matter can emerge from a non-living substrate. Bridging this knowledge gap will take time, either in the stepwise use of existing approaches, or in the development of a new piece of measurement technology (Rockman, 2008). Until then, trait-based models are confined to idealised numerical representations.

It was identified in chapter 4 that are were two threads of research concerning evolutionary changes as a result of size-specific mortality. The potential for epigenetic changes is acknowledged, but it is assumed this represents a reversable change. In contrast, the observation of heritable changes in size

have led some authors to conclude that such changes are genetic. Dunlop et al. (2007) acknowledged the importance of distinguishing between genetic or plastic changes in fish size for management fisheries and aquaculture. It is considered that a plastic phenotypic change would disappear in the presence of previous conditions (Law, 2000). While the word "plastic" is definitive of this kind of response, it yields no information about the mechanisms that underlie such a change. Work by Ayannathan et al. (2003) shows that the genus of fly *Drosophila* can exhibit stable hertiable epigenetic changes. The literature reveals no attempt to find such mechanisms in fish. It is therefore concluded that fisheries management may be benefitted by efforts to determine if fish can inherit epigenetic changes. This study makes no assumptions about the mechanisms of heredity. This is why what is often referred to as a 'genome' is simply called a "heritable trait" here.

It was discussed at the end of chapter 4 that food consumption, reproduction, growth and starvation can be seen as different facets of the same system. The explicitly simple representation used in EATSM linked food consumption, reproduction and growth, but no method was found to incorporate a dynamic representation of starvation that changed as individuals grew older. The work on reaction norms was suggestive of a solution, but common in these approaches is the consideration of 'fitness' as a possessed attribute, instead of it being simply the quality of existence. When a biological organism's wider context is considered, "fitness" becomes a meaningless word projected onto a complex system as a handle for myriad possible selective events. These boundaries of description made the contemporary work on reaction norms too narrow for use in EATSM. Metabolism is the only process that unites food consumption, reproduction, growth and starvation with each other, and with the physical environment (Braakman and Smith, 2013). Therefore, a more explicit representation of metabolism may be a solution. When and if new models of genetics, growth, and reproduction are made available frameworks like EATSM can unify and test them.

6.3 Future Work

6.3.1 Inclusion in a Physical Model

As a model of heterotrophic life, EATSM has been written to 'eat' the individual-based phytoplankton cells that are part of the EVolutionary Ecosystem (EVE) model eveloped by colleagues at the University of Exeter (Clark et al., 2011, 2013; Lenton, 2012). EVE is a individual-based phytoplankton model that integrates with the MITgcm, where cell-size emerges as a result of strategies for internal resource allocation. The approach of representing individuals with size, and the method of programming in the EATSM model is the same as that used in the EVE model. This approach was taken with the intention of integrating EATSM into the EVE framework in order to produce an end-to-end model that could theoretically provide results for carbon flows through the global marine ecosystem.

6.3.2 Super-Individual

In order to remain consistent with the future goal of including the model in the MITgcm (see section 6.3.1) the model had to be written to run in a single processor core (see appendix 7.2). One of the biggest obstacles towards completion of this model has therefore been the constraints of even today's most powerful computer processors. Many commonly used parameter configurations produced populations of around 1e+06 in size, and take several days to produce some of the results shown in this thesis. The development of the approximated encounter algorithm took place alongside the development of the approach itself (see section 2.4). In fact, the unapproximated encounter algorithm as written was reverse engineered after the final approximated solution was produced.

Rose et al.'s (1993) method for combining individuals with similar trait values into a single "super-individual" (Hellweger and Kianirad, 2007; Hellweger, 2008; Hellweger and Bucci, 2009) was briefly investigated. However, the attempt ran into technical difficulties in the process of combining two different methods for approximation. Time constraints meant the work was dropped, but the technical difficulties are known to be solvable. It is believed that no more two weeks work would be required to successfully combine the two meth-

ods of approximation. However, preliminary tests suggested that the overheads of the super-individual method may confer little computational benefit if it were not implemented elegantly. It may take more time to refine after the completion of a prototype.

6.4 Concluding Remarks

1. Chapter 4 set out to discover whether the predictions of life history theory completely explain the evolution of reproductive effort. It was concluded that the answer is no, and that Lack's (1947) food limited hypothesis and Ricklefs' (1970) counteradaptation hypothesis are different perspectives of the same system.

2. Chapter 5 set out to explain mechanisms behind the coexistence of pelagic ciliates and heterotrophic dinoflagellates. Unfortunately the results were inconclusive. Section 6.1.2 above offers four reasons why that could be. The favourite of the four was the suggestion that the coexistence of generalist and specialist feeding strategies in microzooplankton ecosystems may be the result of more complex metabolic and predatory trade-offs that the model presented failed to capture. However, more work needs to be done to determine if that is the case.

7 Appendices

7.1 Appendix 1 - Table of Symbols

Table 7.1.1: Table of Symbols

Symbol	Description
a	Height of the preference function.
$\mathbf{a}_b$	Preference function height boundary vector.
a_b	Preference function height boundary value.
a_h	Heritable preference function height.
$\mathbf{a}_m$	Preference function height mid-point vector.
a_m	Preference function height mid-point value.
α	Size class subset fraction.
$b(i)$	Biomass in size class i.
$b(w)$	Biomass in size class characterised by weight w.
β	Preferred prey volume ratio.
$\beta(i)$	Size spectra calculation for size class i.
$\beta(w)$	Size spectra calculation for size class characterised by weight w.
c	Width of the preference function.
$\mathbf{c}_b$	Preference function width boundary vector.
c_b	Preference function width boundary value.
c_h	Heritable preference function width.
$\mathbf{c}_m$	Preference function width mid-point vector.
c_m	Preference function width mid-point value.
c_{min}	Minimum width of the preference function.
c_{max}	Maximum width of the preference function.
d	Number of discrete locations in trait space.
d_{init}	Number of initialised heterotrophic size classes.
δ	Minimum fraction of expected volume.
ϵ	Fractional metabolic expense per time step.
g	An unprocessed heritable trait value (between 0 and 1).
γ	Assimilation efficiency coefficient.
H_{class}	The volume budget for a single size class.
H_{init}	Initial volume of the heterotrophic population.
i	Index of a size class, vector position, or an individual.
i_{first}	Index of the smallest initialised heterotrophic size class.
i_h	Hertibale trait index.

Continued on Next Page...

Table 7.1.1 – Continued

Symbol	Description
j	Index of a size class, vector position, or an individual.
k	Index of a size class, vector position, or an individual.
k_m	Metabolic scaling exponent.
K_{frac}	Half-saturation constant fraction.
λ	Growth rate/coefficient.
$M(i)$	Number of individuals in the ith size class.
m_i	Mid-point of body mass interval.
$m(i)$	Number of individuals the subset from size class i.
$\hat{m}(i)$	The initial subset size from size class i.
$\mathbf{M}$	Matrix containing d size classes.
Δm_i	Linear width of body mass interval.
N	Volume of the nutrient pool.
N_{init}	Initial volume of the nutrient pool.
n	The population size.
P	Volume of the phytoplankton pool.
P_c	Probability of a prey size class being coupled to a predator size class.
P_f	Probability of an individual or size class feeding.
P_{grow}	Phytoplankton growth volume.
P_{init}	Initial and maximum phytoplankton volume.
P_μ	Probability of mutation.
P_s	Starvation probability.
ϕ	Predator preference for prey item.
$\hat{\phi}$	Size class i preference for size class j.
ρ	The maturation factor of an individual.
s	General coupling strength between predator and prey item.
s_h	The coupling strength for/effective prey volume of size class i.
$\hat{s_h}$	Approximate coupling strength for size class i.
s_p	The coupling strength for the phytoplankton pool.
$\hat{s_p}$	Approximate coupling strength for/effective prey volume of the phytoplankton.
σ	Standard-deviation of mutation.
t	Model time.
t_a	The age of an individual.
t_e	Age of an individual at maturation.
t_m	The age of an individual when half grown.
t_{max}	End of model time.

Continued on Next Page...

Table 7.1.1 – Continued

Symbol	Description
t_τ	The point in time when uninitialised τ values disappear.
t_0	Beginning of model time.
τ	Trophic level value.
τ_d	Discrete trophic level value.
τ_p	Prey trophic level value.
V	Total volume in the model.
v	The actual volume of an individual.
$v(i)$	The total volume in size class i.
v_a	Volume assimilated following food consumption.
$\mathbf{v}_b$	Vector of size class boundary values.
$v_b(i)$	The ith size class boundary value.
v_c	Volume consumed.
v_e	Effective prey volume.
$\hat{v_e}(i)$	Approximate effective prey volume.
v_h	The heritable volume/volume at maturation of an individual.
v_l	Metabolic loss volume.
v_{large}	Largest volume in trait space.
$\mathbf{v}_m$	Vector of size class mid-point values.
$v_m(i)$	The ith size class mid-point value.
v_{max}	Reproduction volume threshold.
v_{min}	Starvation volume threshold.
v_o	The heritable volume of a child.
v_p	Volume of a prey item.
v_r	Volume at birth, or that passed to child.
v_{small}	Smallest volume in trait space.
v_t	Expected volume.
v_w	Unassimilated waste volume.
w	Weight.
Δw	Width of weight size class.
Ω	Child volume fraction heritable trait.
Ω_{min}	Minimum child volume fraction value.

7.2 Appendix 2 - Computing Resources

7.2.1 Program Code

EATSM is written in ANSI/ISO C++ and does not use any external libraries. The code can be downloaded from `https://github.com/phlndrwd/eatsm`. It was developed using the NetBeans IDE with the C++ add-on feature

(`http://netbeans.org`). It is recommended that the project directories are opened with NetBeans as the makefile has been generated by this software for execution with it.

7.2.2 Compilation and Execution

EATSM was compiled with the GNU Compiler Collection (GCC) on 64-bit (x86-64) platforms running Linux, and Mac OS X. Compilation on Windows should not be a problem, but it has not been tested. It is anticipated that there may be problems with the function that creates directories for data output. Results were obtained by running the executable on the University of East Anglia's High Performance Computing Cluster "Grace". A summary of Grace's system architecture can be seen here `http://rscs.uea.ac.uk/high-performance-computing/`. Due to the nature of the job queuing system, the precise details of the execution nodes cannot easily be determined. However, processor cores are known to run at around 2.6GHz with access to 2GB of dedicated system memory.

Some chapters make use of a slightly different versions of EATSM that take varying amounts of real time to produce the results shown. Although the model was set running for a precise amount of real time, some result sets were truncated and resampled for the sake of presentation. Execution times are therefore best estimates only. The results in section 3.1 took around 2 hours 30 minutes to run. A run using a single parameter combination in the sensitivity analysis in section 3.3 was completed in just under 2 hours 47 minutes.

Execution takes place on a single processor core.

7.2.3 Random Number Generation

EATSM is a stochastic model. There are several things that occur probabilistically, and others that are stated to occur 'randomly'. These are achieved with use of a pseudo-random number generator (PRNG). For simplicity and speed, EATSM makes use of C++'s standard PRNG (`rand`) that generates numbers with a uniform probability in the range 0 to 2,147,483,647 (or the value specified by the constant `RAND_MAX` - see `http://www.cplusplus.com/reference/cstdlib/rand/`). The code implements a series of transformations that enables numbers to be generated with a uniform probability in different ranges,

including real numbers in the range 0 to 1. A Box-Muller transform was used to convert uniformly distributed random numbers into those drawn from a normal distribution (Box and Muller, 1958). The code to do this was based on a C implementation by Carter (see `ftp://ftp.taygeta.com/pub/c/boxmuller.c`).

EATSM was tested with a PRNG based on the Mersenne twister algorithm originally developed by Makoto Matsumoto and Takuji Nishimura (1998). The "SIMD-oriented Fast Mersenne Twister" implementation used was by Agner Fog and was so called because it utilised the Streaming SIMD Extensions 2 (SSE2) instruction set common in most modern processors (see `http://www.agner.org/random/`). This made execution faster relative to a standard implementation. Although statisically speaking the Mersenne Twister algorithm has better randomness than the C++ standard PRNG, it was found to increase computational expense whilst producing results that were indistinguishable from those generated with the standard PRNG. For this reason its use was abandoned.

The PRNG generates a sequence of numbers that approximate the statistical properties of random numbers. Initialising the PRNG with a unique seed starts the sequence from a different position. EATSM can seed the PNRG with a user configured value, it can produce a random one from the system time when the model begins, or it can avoid seeding all together (by effectively seeding with 0). Different seed values can produce slightly different results for constant parameter values. For example, the results in section 3.1 are only periodic when the PRNG is seeded with 0. This is the reason that the phase plots in section 3.3 are based on three seperate results generated with the same parameter values; to reinforce the output as a product of the parameter values and not a stochastic event.

References

Abrams, P. A. and Rowe, L. (1996). The effects of predation on the age and size of maturity of prey. *Evolution*, 50(3):1052–1061.

Andersen, K. H. and Beyer, J. E. (2006). Asymptotic size determines species abundance in the marine size spectrum. *The American Naturalist*, 168(1):54–61.

Anderson, T. R. (2005). Plankton functional type modelling: running before we can walk? *Journal of Plankton Research*, 27(11):1073–1081.

Atkinson, A., Schmidt, K., Fielding, S., Kawaguchi, S., and Geissler, P. (2012). Variable food absorption by Antarctic krill: relationships between diet, egestion rate and the composition and sinking rates of their fecal pellets. *Deep Sea Research Part II: Topical Studies in Oceanography*, 59-60:147–158.

Aumont, O., Maier-Reimer, E., Blain, S., and Monfray, P. (2003). An ecosystem model of the global ocean including Fe, Si, P colimitations. *Global Biogeochemical Cycles*, 17(2).

Ayyanathan, K., Lechner, M. S., Bell, P., Maul, G. G., Schultz, D. C., Yamada, Y., Tanaka, K., Torigoe, K., and Rauscher, F. J. (2003). Regulated recruitment of HP1 to a euchromatic gene induces mitotically heritable, epigenetic gene silencing: a mammalian cell culture model of gene variegation. *Genes & Development*, 17(15):1855–1869.

Baretta, J., Ebenhh, W., and Ruardij, P. (1995). The european regional seas ecosystem model, a complex marine ecosystem model. *Netherlands Journal of Sea Research*, 33(3-4):233–246.

Beckerman, A. P., Rodgers, G. M., and Dennis, S. R. (2010). The reaction norm of size and age at maturity under multiple predator risk. *Journal of Animal Ecology*, 79(5):1069–1076.

Behrenfeld, M. J. (2010). Abandoning sverdrup's critical depth hypothesis on phytoplankton blooms. *Ecology*, 91(4):977–989.

Benoît, E. and Rochet, M.-J. (2004). A continuous model of biomass size spectra governed by predation and the effects of fishing on them. *Journal of Theoretical Biology*, 226(1):9–21.

Bopp, L., Kohfeld, K. E., Le Quéré, C., and Aumont, O. (2003). Dust impact on marine biota and atmospheric CO_2 during glacial periods. *Paleoceanography*, 18(2).

Box, G. E. P. and Muller, M. E. (1958). A note on the generation of random normal deviates. *The Annals of Mathematic Statistics*, 29(2):610 – 611.

Braakman, R. and Smith, E. (2013). The compositional and evolutionary logic of metabolism. *Physical Biology*, 10(1):1–62.

Brooks, J. L. and Dodson, S. I. (1965). Predation, body size, and composition of plankton. *Science*, 150(3692):28–35.

Bruggeman, J. (2009). *Succession in plankton communities: a trait-based perspective*. PhD thesis, Vrije Universiteit Amsterdam.

Bruggeman, J. and Kooijman, S. A. L. M. (2007). A biodiversity-inspired approach to aquatic ecosystem modeling. *Limnology and Oceanography*, 52(4):1533–1544.

Buitenhuis, E. T., Rivkin, R. B., Sailley, S., and Le Quéré, C. (2010). Biogeochemical fluxes through microzooplankton. *Global Biogeochem. Cycles*, 24(4).

Burmaster, D. E. (1979). The unsteady continuous culture of phosphate-limited *Monochrysis lutheri* Droop: experimental and theoretical analysis. *Journal of Experimental Marine Biology and Ecology*, 39(2):167–186.

Burmaster, D. E. and Chisholm, S. W. (1979). A comparison of two methods for measuring phosphate uptake by *Monochrysis lutheri* Droop grown in continuous culture. *Journal of Experimental Marine Biology and Ecology*, 39(2):187–202.

Calbet, A. (2008). The trophic roles of microzooplankton in marine systems. *ICES Journal of Marine Science: Journal du Conseil*, 65(3):325–331.

Castellani, C., Robinson, C., Smith, T., and Lampitt, R. S. (2005). Temperature affects respiration rate of *Oithona similis*. *Marine Ecology Progress Series*, 285:129–135.

Caswell, H. (1978). Predator-mediated coexistence: a nonequilibrium model. *The American Naturalist*, 112(983):127–154.

Clark, J. R., Daines, S. J., Lenton, T. M., Watson, A. J., and Williams, H. T. P. (2011). Individual-based modelling of adaptation in marine microbial populations using genetically defined physiological parameters. *Ecological Modelling*, 222(23-24):3823–3837.

Clark, J. R., Lenton, T. M., Williams, H. T. P., and Daines, S. J. (2013). Environmental selection and resource allocation determine global patterns in picophytoplankton cell size. *Limnology and Oceanography*, 58(3):1008–1022.

Costello, J. H., Loftus, R., and Waggett, R. (1999). Influence of prey detection on capture success for the ctenophore *Mnemiopsis leidyi* feeding upon adult *Acartia tonsa* and *Oithona colcarva* copepods. *Marine Ecology Progress Series*, 191:207–216.

Day, T. and Rowe, L. (2002). Developmental thresholds and the evolution of reaction norms for age and size at life-history transitions. *The American Naturalist*, 159(4):338–350.

Dickie, L. M., Kerr, S. R., and Boudreau, P. R. (1987). Size-dependent processes underlying regularities in ecosystem structure. *Ecological Monographs*, 57(3):233–250.

Doney, S. C. (1999). Major challenges confronting marine biogeochemical modeling. *Global Biogeochem. Cycles*, 13(3):705–714.

Dowd, J. E. and Riggs, D. S. (1965). A comparison of estimates of Michaelis-Menten kinetic constants from various linear transformations. *The Journal of Biological Chemistry*, 240(2):863–869.

Droop, M. R. (1968). Vitamin B12 and marine ecology. IV. The kinetics of uptake, growth and inhibition in *Monochrysis lutheri*. *Journal of Marine Biological Association, U.K.*, 48:689–733.

Dunlop, E. S., Shuter, B. J., and Dieckmann, U. (2007). Demographic and evolutionary consequences of selective mortality: predictions from an eco-genetic model for smallmouth bass. *Transactions of the American Fisheries Society*, 136(3):749–765.

Edley, M. T. and Law, R. (1988). Evolution of life histories and yields in experimental populations of *Daphnia magna*. *Biological Journal of the Linnean Society*, 34(4):309–326.

Eiane, K. and Ohman, M. D. (2004). Stage-specific mortality of *Calanus finmarchicus*, *Pseudocalanus elongatus* and *Oithona similis* on Fladen Ground, North Sea, during a spring bloom. *Marine Ecology Progress Series*, 268:183–193.

Elton, C. S. (1927). *Animal Ecology*. The Macmillan Company.

Eppley, R. W. and Peterson, B. J. (1979). Particulate organic matter flux and planktonic new production in the deep ocean. *Nature*, 282(5740):677–680.

Essington, T. E., Kitchell, J. F., and Walters, C. J. (2001). The von Bertalanffy growth function, bioenergetics, and the consumption rates of fish. *Canadian Journal of Fisheries and Aquatic Sciences*, 58(11):2129–2138.

Fasham, M. J. R., Ducklow, H. W., and McKelvie, S. M. (1990). A nitrogen-based model of plankton dynamics in the oceanic mixed layer. *Journal of Marine Research*, 48(3):591–639.

Fasham, M. J. R., Sarmiento, J. L., Slater, R. D., Ducklow, H. W., and Williams, R. (1993). Ecosystem behavior at Bermuda Station "S" and ocean weather station "India": a general circulation model and observational analysis. *Global Biogeochemical Cycles*, 7(2):379–415.

Fenchel, T. (1980). Suspension feeding in ciliated protozoa: functional response and particle size selection. *Microbial Ecology*, 6(1):1–11.

Field, C. B., Behrenfeld, M. J., Randerson, J. T., and Falkowski, P. G. (1998). Primary production of the biosphere: integrating terrestrial and oceanic components. *Science*, 281(5374):237–240.

Follows, M. J., Dutkiewicz, S., Grant, S., and Chisholm, S. W. (2007). Emergent biogeography of microbial communities in a model ocean. *Science*, 315(5820):1843–1846.

Gaedke, U. (1993). Ecosystem analysis based on biomass size distributions: a case study of a plankton community in a large lake. *Limnology and Oceanography*, 38(1):112–127.

Gerritsen, J. and Strickler, J. R. (1977). Encounter probabilities and community structure in zooplankton: a mathematical model. *Journal of the Fisheries Research Board of Canada*, 34:73–82.

Ginzburg, L. R. (1998). Assuming reproduction to be a function of consumption raises doubts about some popular predator-prey models. *Journal of Animal Ecology*, 67(2):325–327.

Glazier, D. S. (2005). Beyond the '3/4-power law': variation in the intra- and interspecific scaling of metabolic rate in animals. *Biological Reviews*, 80(4):611–662.

Glazier, D. S. (2006). The 3/4-power law is not universal: evolution of isometric, ontogenetic metabolic scaling in pelagic animals. *BioScience*, 56(4):325–332.

Gould, S. J. and Eldredge, N. (1977). Punctuated equilibria: the tempo and mode of evolution reconsidered. *Paleobiology*, 3(2):115–151.

Grover, J. P. (1991). Resource competition in a variable environment: phytoplankton growing according to the variable-internal-stores model. *The American Naturalist*, 138(4):811–835.

Haldane, J. B. S. (1926). On being the right size. *Harper's Magazine*, pages 424–427.

Hansen, B. W., Bjornsen, P. K., and Hansen, P. J. (1994). The size ratio between planktonic predators and their prey. *Limnology and Oceanography*, 39(2):395–402.

Hardin, G. E. (1960). The competitive exclusion principle. *Science*, 131:1292–1298.

Hartvig, M., Andersen, K. H., and Beyer, J. E. (2011). Food web framework for size-structured populations. *Journal of Theoretical Biology*, 272(1):113–122.

Hellweger, F. L. (2008). Spatially explicit individual-based modeling using a fixed super-individual density. *Computers & Geosciences*, 34(2):144–152.

Hellweger, F. L. and Bucci, V. (2009). A bunch of tiny individuals–individual-based modeling for microbes. *Ecological Modelling*, 220(1):8–22.

Hellweger, F. L. and Kianirad, E. (2007). Individual-based modeling of phytoplankton: evaluating approaches for applying the cell quota model. *Journal of Theoretical Biology*, 249(3):554–565.

Holling, C. S. (1959). Some characteristics of simple types of predation and parasitism. *The Canadian Entomologist*, 91(7):385–398.

Holling, C. S. (1965). The functional response of predators to prey density and its role in mimicry and population regulation. *Memoirs of the Entomological Society of Canada*, 97(Supplement S45):5–60.

Huse, G. and Ellingsen, I. (2008). Capelin migrations and climate change - a modelling analysis. *Climatic Change*, 87(1-2):177–197.

Huse, G. and Giske, J. (1998). Ecology in Mare Pentium: an individual-based spatio-temporal model for fish with adapted behaviour. *Fisheries Research*, 37(1-3):163–178.

Huse, G., Johansen, G. O., Bogstad, B., and Gjster, H. (2004). Studying spatial and trophic interactions between capelin and cod using individual-based modelling. *ICES Journal of Marine Science: Journal du Conseil*, 61(7):1201–1213.

Hutchinson, G. E. (1961). The paradox of the plankton. *The American Naturalist*, 95(882):137–145.

Israel, G. (1988). On the contribution of Volterra and Lotka to the development of modern biomathematics. *History and Philosophy of the Life Sciences*, 10:37–49.

Jennings, B. R. and Parslow, K. (1988). Particle size measurement: the equivalent spherical diameter. *Proceedings of the Royal Society of London. A. Mathematical and Physical Sciences*, 419(1856):137–149.

Jennings, S. and Blanchard, J. L. (2004). Fish abundance with no fishing: predictions based on macroecological theory. *Journal of Animal Ecology*, 73(4):632–642.

Jennings, S. and Warr, K. J. (2003). Smaller predator-prey body size ratios in longer food chains. *Proceedings of the Royal Society of London. Series B: Biological Sciences*, 270(1522):1413–1417.

Kiørboe, T. (2008). *A Mechanistic Approach to Plankton Ecology*. Princeton University Press.

Kiørboe, T. (2011). How zooplankton feed: mechanisms, traits and trade-offs. *Biological Reviews*, 86(2):311–339.

Kirchner, J. W. (2002). The Gaia hypothesis: fact, theory, and wishful thinking. *Climatic Change*, 52:391–408.

Kirschner, M. and Gerhart, J. (1998). Evolvability. *Proceedings of the National Academy of Sciences*, 95(15):8420–8427.

Kleiber, M. (1947). Body size and metabolic rate. *Physiological Reviews*, 27(4):511–541.

Kylafis, G. and Loreau, M. (2008). Ecological and evolutionary consequences of niche construction for its agent. *Ecology Letters*, 11(10):1072–1081.

Lack, D. (1947). The significance of clutch-size. *Ibis*, 89(2):302–352.

Law, R. (2000). Fishing, selection, and phenotypic evolution. *ICES Journal of Marine Science: Journal du Conseil*, 57(3):659–668.

Lehman, C. L. and Tilman, D. (1997). Competition in spatial habitats. In Tilman, D. and Kareiva, P., editors, *Spatial Ecology: The Role of Space in Population Dynamics and Interspecific Interactions*, pages 185–203. Princeton University Press, New Jersey.

Lenton, T. M. (2012). The EVolutionary Ecosystem (EVE) model. https://lifesciences.exeter.ac.uk/research/essg/projects/eve/.

Levin, S. A. and Pacala, S. W. (1997). Theories of simplification and scaling of spatially distributed processes. In Tilman, D. and Kareiva, P., editors, *Spatial Ecology: The Role of Space in Population Dynamics and Interspecific Interactions*, pages 271–295. Princeton University Press, New Jersey.

Levins, R. (1966). The strategy of model building in population biology. *American Scientist*, 54(4):421–431.

Levinsen, H. and Nielsen, T. G. (2002). The trophic role of marine pelagic ciliates and heterotrophic dinoflagellates in Arctic and temperate coastal ecosystems: a cross-latitude comparison. *Limnology and Oceanography*, 47(2):427–439.

Lotka, A. J. (1910). Contribution to the theory of periodic reactions. *The Journal of Physical Chemistry*, 14(3):271–274.

Lotka, A. J. (1920a). Analytical note on certain rhythmic relations in organic systems. *Proceedings of the National Academy of Sciences*, 6(7):410–415.

Lotka, A. J. (1920b). Undamped oscillations derived from the law of mass action. *Journal of the American Chemical Society*, 42(8):1595–1599.

Lotka, A. J. (1925). *Elements of Physical Biology*. Williams and Wilkins Company, Baltimore.

Martínez-Garmendia, J. (1998). Simulation analysis of evolutionary response of fish populations to size-selective harvesting with the use of an individual-based model. *Ecological Modelling*, 111(1):37–60.

Matsumoto, M. and Nishimura, T. (1998). Mersenne twister: a 623-dimensionally equidistributed uniform pseudo-random number generator. *ACM Trans. Model. Comput. Simul.*, 8(1):3–30.

Maynard Smith, J. (1992). Byte-sized evolution. *Nature*, 355:772–773.

Mayzaud, P. (1976). Respiration and nitrogen excretion of zooplankton. iv. the influence of starvation on the metabolism and the biochemical composition of some species. *Marine Biology*, 37(1):47–58.

McDonald-Gibson, J., Dyke, J. G., Di Paolo, E., and Harvey, I. R. (2008). Environmental regulation can arise under minimal assumptions. *Journal of Theoretical Biology*, 251(4):653–666.

Menge, D. N. L., Levin, S. A., and Hedin, L. O. (2008). Evolutionary tradeoffs can select against nitrogen fixation and thereby maintain nitrogen limitation. *Proceedings of the National Academy of Sciences*, 105(5):1573–1578.

Menge, D. N. L., Levin, S. A., and Hedin, L. O. (2009). Facultative versus obligate nitrogen fixation strategies and their ecosystem consequences. *The American Naturalist*, 174(4):465–477.

Moloney, C. L. and Field, J. G. (1991). The size-based dynamics of plankton food webs. I. A simulation model of carbon and nitrogen flows. *Journal of Plankton Research*, 13(5):1003–1038.

Moore, J., Doney, S. C., Kleypas, J. A., Glover, D. M., and Fung, I. Y. (2002). An intermediate complexity marine ecosystem model for the global domain. *Deep Sea Research Part II: Topical Studies in Oceanography*, 49:403–462. The US JGOFS Synthesis and Modeling Project: Phase 1.

Omori, M. and Ikeda, T. (1984). *Methods in Marine Zooplankton Ecology*. John Wiley & Sons Inc.

Pattee, H. H. (1995). Artificial life needs a real epistemology. In Moran, F., Moreno, A., Merelo, J., and Chacon, P., editors, *Advances in Artificial Life*, pages 23–38. Springer-Verlag, Berlin.

Peters, R. H. (1983). *The Ecological Implications of Body Size*. Cambridge University Press.

Phillimore, A. B., Proios, K., O'Mahony, N., Bernard, R., Lord, A. M., Atkinson, S., and Smithers, R. J. (2013). Inferring local processes from macro-scale phenological pattern: a comparison of two methods. *Journal of Ecology*, 101(3):774–783.

Pimm, S. L. and Lawton, J. H. (1977). Number of trophic levels in ecological communities. *Nature*, 268(5618):329–331.

Platt, T. and Denman, K. (1977). Organisation in the pelagic ecosystem. *Helgoländer wissenschaftliche Meeresuntersuchungen*, 30(1-4):575–581.

Quéré, C. L., Harrison, S. P., Prentice, I. C., Buitenhuis, E. T., Aumont, O., Bopp, L., Claustre, H., Cunha, L. C. D., Geider, R. J., Giraud, X., Klaas, C., Kohfeld, K. E., Legendre, L., Manizza, M., Platt, T., Rivkin, R. B., Sathyendranath, S., Uitz, J., Watson, A. J., and Wolf-Gladrow, D. (2005). Ecosystem dynamics based on plankton functional types for global ocean biogeochemistry models. *Global Change Biology*, 11(11):2016–2040.

Quinones, R. A., Platt, T., and Rodríguez, J. (2003). Patterns of biomass-size spectra from oligotrophic waters of the Northwest Atlantic. *Progress in Oceanography*, 57(3-4):405–427.

Ray, T. S. (1991). An approach to the synthesis of life. In Langton, C. G., Taylor, C., Farmer, J. D., and Rasmussen, S., editors, *Artificial Life II, SFI Studies in the Sciences of Complexity*, volume 10, pages 371–408. Addison-Wesley.

Reznick, D. (1982a). Genetic determination of offspring size in the guppy (*Poecilia reticulata*). *The American Naturalist*, 120(2):181–188.

Reznick, D. (1982b). The impact of predation on life history evolution in Trinidadian guppies: genetic basis of observed life history patterns. *Evolution*, 36(6):1236–1250.

Reznick, D. (1985). Costs of reproduction: an evaluation of the empirical evidence. *Oikos*, 44(2):257–267.

Reznick, D. and Endler, J. A. (1982). The impact of predation on life history evolution in Trinidadian guppies (*Poecilia reticulata*). *Evolution*, 36(1):160–177.

Reznick, D. A., Bryga, H., and Endler, J. A. (1990). Experimentally induced life-history evolution in a natural population. *Nature*, 346(6282):357–359.

Ricklefs, R. E. (1970). Clutch size in birds: outcome of opposing predator and prey adaptations. *Science*, 168(3931):599–600.

Riley, G. A. (1941a). Plankton studies. III. Long Island Sound. *Bulletin of the Bingham Oceanographic Collection*, 7(3):1–93.

Riley, G. A. (1941b). Plankton studies. IV. Georges Bank. *Bulletin of the Bingham Oceanographic Collection*, 7(4):1–73.

Riley, G. A. (1942). The relationship of vertical turbulence and spring diatom flowerings. *Journal of Marine Research*, 5(1):67–87.

Riley, G. A. (1943). Physiological aspects of spring diatom flowerings. *Bulletin of the Bingham Oceanographic Collection*, 8(4):1–53.

Riley, G. A. (1963). Theory of food-chain relations in the ocean. In Hill, M. N., editor, *The sea: ideas and observations on progress in the study of the seas*, volume 2, pages 438–463. Interscience Publishers.

Riley, G. A. and Bumpus, D. F. (1946). Phytoplankton-zooplankton relationships on Georges Bank. *Journal of Marine Research*, 6(1):33–47.

Rockman, M. V. (2008). Reverse engineering the genotype-phenotype map with natural genetic variation. *Nature*, 456(7223):738–744.

Roff, D. A. (1992). *The Evolution of Life Histories*. Chapman & Hall, Inc.

Rose, K. A., Christensen, S. W., and DeAngelis, D. L. (1993). Individual-based modeling of populations with high mortality: a new method based on following a fixed number of model individuals. *Ecological Modelling*, 68:273–292.

Rossberg, A. G. (2012). 6 - A complete analytic theory for structure and dynamics of populations and communities spanning wide ranges in body size. In Jacob, U. and Woodward, G., editors, *Global Change in Multispecies Systems Part 1*, volume 46 of *Advances in Ecological Research*, pages 427–521. Academic Press.

Sailley, S. M., Buitenhuis, E., Klaas, C., Quéré, C. L., and Wolf-Gladrow, D. (2009). Microprotozooplankton representation in model: comparison of pelagic ciliates and heterotrophic dinoflagellates. Work not included in final thesis.

Sarmiento, J. L. and Quéré, C. L. (1996). Oceanic carbon dioxide uptake in a model of century-scale global warming. *Science*, 274(5291):1346–1350.

Sarmiento, J. L., Slater, R. D., Fasham, M. J. R., Ducklow, H. W., Toggweiler, J. R., and Evans, G. T. (1993). A seasonal three-dimensional ecosystem model of nitrogen cycling in the North Atlantic euphotic zone. *Global Biogeochemical Cycles*, 7(2):417–450.

Sheldon, R. W., Prakash, A., and Sutcliffe, W. H. J. (1972). The size distribution of particles in the ocean. *Limnology and Oceanography*, 17(3):327–340.

Sherr, E. B. and Sherr, B. F. (2007). Heterotrophic dinoflagellates: a significant component of microzooplankton biomass and major grazers of diatoms in the sea. *Marine Ecology Progress Series*, 352:187–197.

Shin, Y.-J. and Cury, P. (2001). Exploring fish community dynamics through size-dependent trophic interactions using a spatialized individual-based model. *Aquatic Living Resources*, 14(2):65–80.

Shurin, J. B., Gruner, D. S., and Hillebrand, H. (2006). All wet or dried up? Real differences between aquatic and terrestrial food webs. *Proceedings of the Royal Society B: Biological Sciences*, 273(1582):1–9.

Stearns, S. C. (1977). The evolution of life history traits: a critique of the theory and a review of the data. *Annual Review of Ecology and Systematics*, 8:145–171.

Stearns, S. C. (1989). Trade-offs in life-history evolution. *Functional Ecology*, 3(3):259–268.

Stearns, S. C. (1992). *The Evolution of Life Histories*. Oxford University Press.

Stearns, S. C. and Koella, J. C. (1986). The evolution of phenotypic plasticity in life-history traits: predictions of reaction norms for age and size at maturity. *Evolution*, 40(5):893–913.

Steele, J. H. (1974). *The Structure of Marine Ecosystems*. Blackwell Publishing, Oxford, UK.

Stergiou, K. I. (1999). Intraspecific variations in size- and age-at-maturity for red bandfish, *Cepola macrophthalma*. *Environmental Biology of Fishes*, 54(2):151–160.

Threlkeld, S. T. (1976). Starvation and the size structure of zooplankton communities*. *Freshwater Biology*, 6(6):489–96.

Vijendravarma, R. K., Narasimha, S., and Kawecki, T. J. (2013). Predatory cannibalism in *Drosophila melanogaster* larvae. *Nature Communications*, 4:1789–1797.

Volterra, V. (1926a). Fluctuations in the abundance of a species considered mathematically. *Nature*, 118:558–560.

Volterra, V. (1926b). Variazioni e fluttuazioni del numero d'individui in specie animali conviventi. *Mem. Acad. Lincei Roma*, 2:31–113.

Werner, E. E. and Gilliam, J. F. (1984). The ontogenetic niche and species interactions in size-structured populations. *Annual Review of Ecology and Systematics*, 15:393–425.

Woods, J., Perilli, A., and Barkmann, W. (2005). Stability and predictability of a virtual plankton ecosystem created with an individual-based model. *Progress in Oceanography*, 67(1-2):43–83.

Woods, J. D. (2005). The lagrangian ensemble metamodel for simulating plankton ecosystems. *Progress In Oceanography*, 67(1-2):84–159.

Yin, X., Goudriaan, J., Lantinga, E. A., Vos, J., and Spiertz, H. J. (2003). A flexible sigmoid function of determinate growth. *Annals of Botany*, 91(3):361–371.